A NMR-STUDY ON $Nd_2CuO_{4-x}F_x$
&
BUILDING A VARIABLE TEMPERATURE AND FREQUENCY NMR-PROBE

by

BERND CTORTECKA

THESIS

Presented to the Department of Physics and Astronomy of

The University of St. Andrews

in Partial Fulfillment

of the Requirements

for the Degree of

MASTER OF PHILOSOPHY

THE UNIVERSITY OF ST. ANDREWS

April, 1994

I, Bernd Ctortecka, hereby certify that this thesis, which is approximately 25,000 words in length, has been written by me, that it is a record of work carried out by me and that is has not been submitted in any previous application for a higher degree.

In submitting this thesis to the University of St. Andrews I understand that I am giving permission for it to be made available for us in accordance with the regulations of the University Library for the time being in force, subject to any copyright vested in the work not being affected thereby. I also understand that the title and abstract will be published, and that a copy of the work may be made and supplied to any bona fide library or research worker.

I was admitted as a research student under Ordinance No. 12 in September 1992 and as a candidate for the degree of Master of Philosophy in September 1992; the higher study for which this is a record was carried out in the University of St. Andrews between 1992 and 1993.

Date Signed

A NMR-STUDY ON $Nd_2CuO_{4-x}F_x$
&
BUILDING A VARIABLE TEMPERATURE AND FREQUENCY NMR-PROBE

I hereby certify that the canditate has fulfilled the conditions of the Resolution and Regulations appropriate for the degree of Master of Philosophy in the University of St. Andrews and that the candidate is qualified to submit this thesis in application for that degree.

Supervisor: _
David P. Tunstall

15.4.94
Date

Gewidmet meinen Eltern und Freunden.

Acknowledgements

First of all I have to acknowledge the Friedrich-Ebert-Foundation, Bonn, for enabling my one year stay at St. Andrews University by providing me with a generous scholarship. Furthermore I have to thank my supervisor Dr D. P. Tunstall for introducing me to Nuclear Magnetic Resonance (NMR), low temperature physics, superconductivity and his guidance throughout the work. Dr M. Jones of the School of Chemistry of the University of Birmingham supplied me with the samples as well his own neutron and AC-susceptibility measurements. The workshop, especially J. Clark, showed great understanding when bits and pieces needed to be made up at short notice. A great thank you to the cryogenics, R. C. Gavine and A. G. P. Barman, who provided the huge amounts of liquid helium and nitrogen. Dr J. Nowinski of the Department of Chemistry who showed me how to use an argon glove-box and let me use his own one. The X-Ray spectra were elaborately done by A. Calder of the Department of Geology. Of our own group I am indebted to Dr P. Mason for his ideas and never-ending support whilst the hardware was being set up and the superconducting magnet was in use. Furthermore G. Dai for his help with the Bruker MSL-500 and the assistance in acquiring and interpreting the ^{63}Cu NMR data. Very warm thanks to Heather, Geoff and Wendy for proof-reading my thesis and cheering me up every time things went a different way than expected. Last but not least I have to thank Susanne Reinhardt for lending me her PC and Martin Fischer for introducing me to the nitty-gritties of LaTeX.

Abstract

A study of the $Nd_2CuO_{4-x}F_x$ electron-doped high-T_c superconductor has been carried out, using ^{19}F and ^{63}Cu NMR techniques as well as X-ray diffraction. In order to do ^{19}F NMR a spectrometer was set up and a home-made NMR-probe was used, allowing for variable temperature and frequency studies. Both were extensively tested. Pseudo-single-crystals with identical grain orientations were obtained at room temperature by an alignment procedure in a strong external field. The alignment quality was confirmed by X-ray diffraction spectra which showed that the crystallites are aligning with the c-axis perpendicular to the external field (unlike YBCO and its derivatives). Extensive angle dependent ^{63}Cu NMR studies were done at room temperature. The spectra obtained appeared to be unusual, and a hypothesis concerning the uncommon alignment was formulated. However combining the alignment with an electric field gradient failed to explain the NMR spectra. Next a model was developed to explain them. When combining the alignment with a strong shift anisotropy plus a small or even zero quadrupole interaction, a good agreement with the NMR spectra was found. Fluorine-NMR studies were done on two out of four samples, finding resonances in both of them. Furthermore a transferred magnetic field onto the fluorine sites was found and last but not least a dependency of the applied field strength on the resonance $\frac{MHz}{T}$ could be established.

Table of Contents

List of Tables

List of Figures

Chapter 1

Introduction to NMR

1.1 Introduction to Nuclear Magnetic Resonance

The nuclear magnetic resonance (NMR) technique is a powerful tool for obtaining microscopic information on magnetic and electronic properties of solids and is extensively employed in this work on the electron-doped superconductor $Nd_2CuO_{4-x}F_x$, i.e. ^{63}Cu and ^{19}F NMR are performed. Since the pioneering work of Bloch [1], Purcell [2] and Gorter [3] in the 1940's, the field of NMR has grown extensively and become a versatile tool for both chemists and physicists.

Only a short summary of NMR is given, merely to provide a general basis for the experiments performed. More detailed information can be found in a number of articles [1–5] and textbooks [6–9,17].

1.2 Basic Concepts of NMR

NMR is based upon the existance of the nuclear spin and its classical characteristic frequency of gyroscopic precession in an applied external field. Nuclei having an odd mass number possess a spin ($\mathbf{I}$: 'nuclear spin') and an intrinsic spin angular momentum denoted by $\mathbf{I}\hbar$. The relationship between the angular momentum $\mathbf{I}\hbar$ and its magnetic moment (μ) is the gyromagnetic

ratio γ), i.e.

$$\mu = \gamma \mathbf{I} \hbar \tag{1.1}$$

When an isolated magnetic moment (μ) is exposed to an external magnetic field ($\mathbf{B}$), the interaction energy is described by the Zeeman splitting, which is given by a simple Hamiltonian ($\mathcal{H}_z = \gamma \cdot \mathbf{B}$). For simplicity the field $\mathbf{B_0}$ is commonly defined to be along the z-direction (Cartesian coordinates), i.e. $\mathbf{B} = \mathbf{B_0} \cdot \mathbf{z}$.

$$\mathcal{H}_z = -\gamma_z \mathrm{B_0} = -\gamma \hbar \mathrm{B_0} \mathrm{I}_z \tag{1.2}$$

According to quantum mechanics the nuclear spin states are quantised, i.e. $\mathbf{I}_z$ is limited to a discrete number of values $\mathbf{m_I}$, defined by the selection rule (2I+1).

$$\mathcal{H}_z = -\mathrm{m_I} \gamma \hbar \mathrm{B_0} \qquad (\mathrm{m_I} = \mathrm{I}, \mathrm{I}-1, ..., -\mathrm{I}) \tag{1.3}$$

The energies given by equation 1.3 lead to equally spaced Zeeman energy levels (spacing: $\gamma \hbar \mathrm{B_0}$). Perturbation of such levels through the application an oscillating magnetic field ($\mathbf{B_1}$) perpendicular to the static field ($\mathbf{B_0}$) induces transitions between two spin states, allowing the detection of such levels. The Bohr frequency requirement $\hbar \omega_0 = \gamma \hbar \mathrm{B_0}$ leads to the resonance condition (equation 1.4), where ω_0 is the Larmor frequency.

$$\omega_0 = \gamma \cdot \mathrm{B} \tag{1.4}$$

Only when the frequency of the oscillating field satisfies equation 1.4 is energy absorbed and a state transition obtained.

As can be seen from equation 1.4 the resonance condition is achieved either by varying the field ($\mathbf{B_1}$) or the applied frequency.

1.3 Basics of Pulsed NMR

In order to understand pulsed NMR, a macroscopic assembly of identical, spin 1/2 nuclei in a magnetic field shall be considered. For each individual spin there are two possible energy levels ($m_I = \pm 1/2$). It can be shown that Boltzmann statistics govern the population of any energy state whereby the population of the lower level ($m_I = +1/2$) is greater than that of the upper level ($m_I = -1/2$).

Two different kinds of temperature systems are involved: the spin temperature (T_S) and the lattice temperature (T_L). Thermal equilibrium is maintained via weak spin-spin interactions, keeping T_S constant and equal to T_L.

The exposure of the spin system to a pulse with the right combination of frequency and B_1 field causes the absorption of energy quanta. These energy quanta perturbe the spin system, causing some spins to 'flip' from the lower energy level to the higher one (obeying the selection rule $\Delta m = \pm 1$) and resulting in $T_S \geq T_L$. Once perturbed the equilibrium ($T_S = T_L$) is regained through some 'heat' loss or transfer to the lattice[1]. As a consequence the perturbed spins flip back to their equilibrium state giving up energy equal to the difference between adjacent levels. In a NMR experiment these changes in energy are detected by a tuned receiver coil. After the elapse of a characteristic time T_1 (spin-lattice relaxation time) the equilibrium is exponentially approached.

So far the description has been a quantum mechanical one. In 1946

[1]Lattice means any kind of surrounding.

Bloch [1] gave a macroscopic approach which was purely classical but fully sufficient for the understanding of experiments. Individual magnetic moments (μ_I) of a macroscopic sample make up the magnetisation **M** which is equivalent to the magnetic moment. When in thermal equilibrium the μ_I precess randomly, resulting in a static value $\mathbf{M_0}$ along the z-direction. The pulsed application of an field ($\mathbf{B_1}$) at the resonance frequency forces $\mathbf{M_0}$ to rotate away from $\mathbf{B_0}$. As a result $\mathbf{M_0}$ starts to precess at a tip angle Θ about the static field $\mathbf{B_0}$. The projection of $\mathbf{M_0}$ onto the x and z axes gives:

$$M_x = M_0 \sin\Theta$$

$$M_z = M_0 \cos\Theta$$

The perturbed spin system undergoes a relaxation process back to the original configuration (thermal equilibrium). To do so individual spins must relax to equilibrium with their neighbours. In this process two time constants are present:

- **'spin-spin'** or **transverse** relaxation time ($\mathbf{T_2}$): it means the steady reduction of the transverse magnetization M_x, known as 'free induction decay'(FID). This process does not affect the total magnetic moment along B_0.
- **'spin-lattice'** or **longitudinal** relaxation time ($\mathbf{T_1}$): it is understood as the remagnetisation of M_0 along B_0 due to energy exchange between the spins and the lattice.

There are a great number of pulsed NMR experiments employing special pulse sequences, some of them are very well described in [17]. Here just

two are stated, the 90° pulse and the 90°–180° pulse sequence whereby the first one is the most simple of all. Through a 90° pulse the magnetization M_0 is rotated by $\Theta = 90°$. Now the transverse magnetization M_x is equal to M_0 and rotates at the Larmor frequency ω_0 about B_0. The precessing magnetic moment induces an oscillatory magnetic flux in the receiver coil of the NMR probe. The magnetic flux decays due to the previously described T_2 relaxation process. When a Fourier transformation is performed on the resulting exponential FID the absorption lineshape is given by the real part. An additional 180° pulse would cause the formerly dephasing spins to refocus. By measuring the magnetic flux change a so called 'spin-echo' will be obtained.

Chapter 2

Devices for NMR Studies – Hardware

2.1 Introduction

The actual hardware which makes up a NMR experiment is as follows: basically there are three major components, the transmitter, the sample and the receiver.

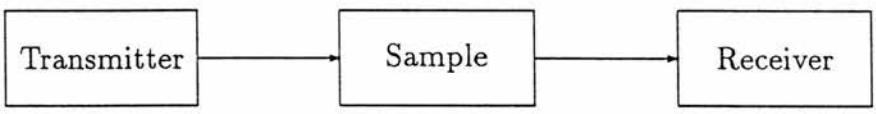

Using the arrangement given in the block diagram above and putting in a transient signal one can obtain the 'transfer function' of the sample. In NMR it is a called spectrum which allows us to deduce various qualities of the sample used. We only obtain a spectrum when the sample is exposed to high magnetic field B_0 and the angular velocity of the applied rf (radio frequency) field B_1 satisfies $\omega_0 = \gamma \cdot B_0$. Due to this, the corresponding frequency $\nu_0 = \frac{\gamma \cdot B_0}{2\pi}$ is in the rf region (kHz). This frequency is the Larmor frequency and acts as carrier frequency for the modulation caused by the sample. A modulation by the sample occurs only close to the Larmor frequency. It is this modulation which is the desired effect both in pulse and cw NMR.

Further devices are needed to couple the excitation energy to the sample and to extract the resulting signal from the sample. This is done by the

probe and associated networks. The ratio of output to input signal is always small. Necessarily the output stage consists of preamplifier, amplifier, and a detector; in other words a spectrometer or radio receiver.

2.1.1 Different Concepts

The historically first performed NMR experiments were **continuous wave** (cw) experiments. They were done by Bloch [1], Purcell [2] and Gorter [3]. Shortly thereafter, in 1950, Hahn [4] published his paper on spin echoes obtained by **pulse** experiments. Pulsed NMR at this stage was merely used for the determination of relaxation times T_1 and T_2. Later Lowe and Norberg [5] discovered that a free induction decay (FID) is related to the NMR frequency spectrum by Fourier transform. From then on multiline high resolution spectra were possible. Later Andrew [10,11] (1958) developed line narrowing experiments with solid samples. Today magic angle spinning (MAS) is a common technique in NMR laboratories.

Depending on what data one is interested from NMR, the hardware has to have certain properties, e.g. variable or fixed temperature, phase sensitive or none phase sensitive. The magnetic field can be either static or variable. In the case of a static field the frequency has to be variable in order to get resonance conditions for different nuclei. Therefore the arrangement of the hardware differs a lot. The next sections will show differences and capabilities of three different arrangements.

2.1.2 MAS – Variable frequency and temperature

Originally a very sophisticated NMR probe built by DOTY SCIENTIFIC, USA, was supposed to be used for all the planned NMR studies. According to the manual the probe should have been capable of a broad range of tasks. It was tunable without any difficulty in the frequency range of 14.5 up to 218 MHz. By putting either wands with capacitors or coils into the slots of the probe circuit, the tuning range could be lowered or rised. Both tuning and match capacitors were situated close to the coil at the bottom of the probe. The capacitance could be changed by turning knobs at the probe head.

The whole outer body of the probe and the probe circuit were kept at room temperature by flushing at a high rate with dry nitrogen gas. Once the probe was tuned to a frequency it was stable and decoupled from temperature changes in the sample region.

The probe could be run in a static or spinning mode. A cryogen reservoir of 0.5 l was located in the middle of the probe. The filling level was controlled by level sensors and automatically kept above a certain level. In order to get cryogen from a pressurized external reservoir/dewar across to the internal dewar the filling valve at the probe head was opened and a pressure gradient established. Once calibrated the whole procedure was run by a personal computer.

In MAS mode the spinning speed was adjusted through two valves. To do so the liquid cryogen, nitrogen or helium, had to be vaporized by moderate heat input. The heater was connected to a computer which kept the temperature stable. Connecting a vacuum pump to the exhaust port increased

the pressure gradient as well as the spinning speed. Spinning frequencies up to 3 kHz were mentioned in the manual. Tests with nitrogen showed a maximum stable frequency of 1.8 kHz. In static mode the sample was simply jammed and cooled with gas or liquid.

The sapphire sample holder (stator) had a rotor cap on one end and was neatly surrounded by a ceramic holder with gas jets at the same end. The complete assembly including a silver coil was embedded in PTFE and mounted on a 5 mm stainless steel plate at the bottom end of the probe.

Extended tests at temperatures as low as 77 Kelvin showed substantial failures. The automatic filling was not very reliable. Even with a vacuum insulated transfer tube this problem could not be cured. The above mentioned stainless steel plate had several passages for wires, rods and the cryogen supply tube. They were all sealed with silicone rubber which, it was later found, in the end could not withstand liquid nitrogen temperature. In the course of a number of test runs, substantial leaks developed around the tube and wires. Due to the vacuum in the region below the plate (inside the dewar), gas was sucked into the sample region which was not at all acceptable. The effects would have been even worse with helium as the coolant. The nitrogen gas would have entered the cold region and frozen out, surely resulting in blockages of the outlet. Furthermore the same metal plate was not properly insulated causing a heat leak, and hence impurities in the flushing gas were freezing out at its top. There was no way of modifying the probe to make it work.

In spite of the tremendous cost of the probe, it was decided unfit for use in NMR experiments. By this time about **3 months of intense work**

had already been spent. A suitable replacement had to be planned, built and tested. Consequently all experiments had to be altered in one way or another.

2.2 The Bruker MSL–500 System

2.2.1 Description

The MSL–500 system is commercially built and sold by Bruker. It is capable of performing pulse NMR spectroscopy over a frequency range of 17 to 203 MHz with low frequency transmitters or at 500 MHz with the proton frequency transmitter. The experiments are done at a constant magnetic field of 11.74 Tesla which is supplied by a superconducting cryomagnet from Oxford Instruments. The overall spectrometer is controlled by an Aspect 3000 computer, run by standard Bruker DISMSL software. The programme has three independent channels, allowing data acquisition and data manipulation at the same time. A well structured Bruker-specific programming language can be used to program any form of complex pulse routine. An in-built system process controller (SPC) manages transmitter and receiver simultaneously.

The spectrometer setup is as follows: continuous frequencies with 1 Hz resolution are generated by a frequency synthesizer, gated by the pulses from the SPC and firstly fed through a low power (~100 W) broadband amplifier, secondly through a high power (~1000 W max.) transmitter. Subsequently, the voltage is further amplified by a 50 dB preamplifier. By inserting the so-called plug-in units which also act as rf filters the preamplifier can be tuned to the desired frequency. In order to cover the interval 17 - 203 MHz several plug-in units are available. The variable output pulses enter a simple tuning

circuit and finally the rf coil surrounding the sample. Multi-nuclear solenoid probeheads are available to plug in at the probehead, each having a solenoid coil and a simple tuning circuit fixed to a PTFE former. In the probeheads for ^{63}Cu NMR, the size of the silver coil is such that a 5 mm diameter by 40 mm long sample is required. The tuning circuit, coil and sample are all enclosed in an NMR probe and loaded into the bore of the magnet from the underside.

Afterwards the signal is passed to a broadband receiver, whose gain and phase are controlled by the above mentioned SPC. Once the signal is detected it is amplified and passed through low pass filters to get rid of noise produced by the detection system itself. The data is collected and averaged by the computer in the time domain resulting in a FID which then is digitised by a multiplexed analogue to digital converter. The digitisation is then done by sampling the FID at discrete points. These points are separated by a certain time interval, the dwell time (DW), whereby 1/DW is called the sampling rate. The whole lot of digitised signals are saved to the hard disk. The procedure of data processing and manipulation will be decribed in the subsequent sections.

2.2.2 The Pulse Program

Usually modern pulse programs include an extensive 'phase cycling' sequence, which improves the performance of quadrature detection schemes by eliminating any mismatch between the two phase sensitive detectors (PSD). Phase cycling means repeated changes of the phase of the applied rf pulses. A simple phase cycle may consist of four stages in which the applied pulses are consecutively phase shifted by 0° (+X), 90° (+Y), 180° (−X) and 270° (−Y).

The receiver reference phase is changed correspondingly and the appropriate addition or subtraction of the signals along +X, +Y, −X or −Y proves particularly useful at reducing baseline artifacts and ringdown effects. The ^{63}Cu NMR data was gathered using a standard Hahn two pulse spin-echo sequence of the form 90°–τ–180°–τ'–(acquire). A listing of the above pulse program can be found in the appendix A.

2.2.3 Data Acquisition and Manipulation

A great number (50,000 shots) of FID signals were acquired and averaged at the appropriate spectrometer frequency (SF). The Hahn pulse sequence consisting of a 90° pulse of width 5 μs (D1) followed by a τ-delay (D6) of 10 μs, then a 180^0 pulse of width 10 μs (D2), followed by a deadtime delay (D3) of 2.5 μs, was employed to produce a ^{63}Cu spin-echo at a given frequency.

The spectrometer was timed so that only the second half of the echo was displayed on the monitor. This portion of the echo in the time domain was then Fourier transformed to obtain the corresponding frequency domain signal. If necessary, baseline and phase corrections were carried out. Next the signal was integrated and the integration area recorded. Point by point frequency sweeps through the spectral region of interest, acquired spin echo signals at the corresponding frequencies, lead to ^{63}Cu spectra. The step width of kHz was dependent on the region of interest. Each time the frequency was changed the preamplifier was retuned to the new one. Finally, plotting the area vs spectrometer frequency gave the required frequency spectrum. This procedure was repeated at room temperature for all samples at different orientations of

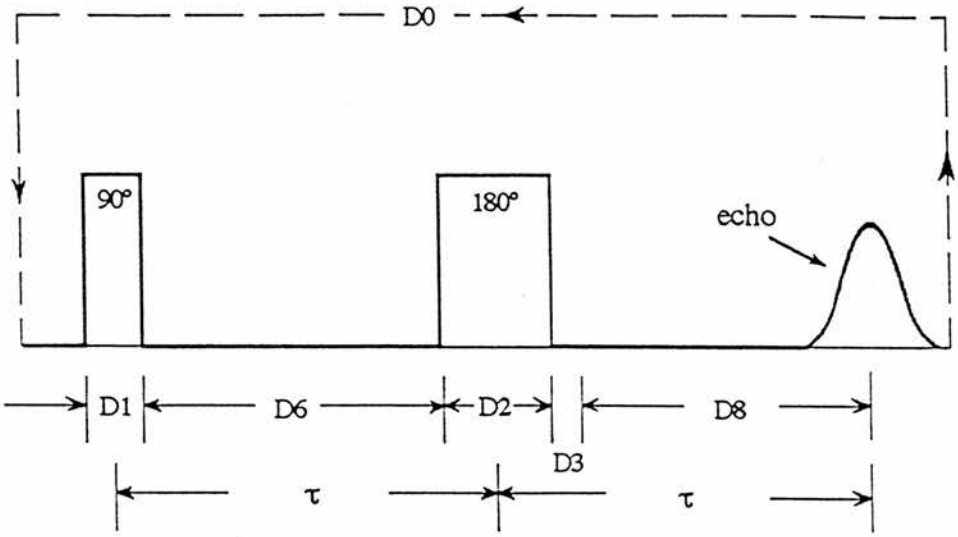

Figure 2.1: Pulse cycle

the marked axis of alignment to the field.

2.3 Setting up a Spectrometer and the Building of a Variable Frequency and Temperature NMR Probe

2.3.1 Introduction

Because of the total failure of the DOTY SCIENTIFIC MAS-probe, a new NMR probe had to be designed, built and tested. The different probe diameters necessitated the use of another superconducting magnet with a smaller bore. Only the spectrometer needed to be altered slightly by replacing a number of components in order to fit it to the different probe circuit.

The probe was designed according to the demands of the experiments. It was required to be capable of doing pulsed ^{19}F and ^{63}Cu NMR at variable

frequencies and temperatures. A high rf power across the sample coil was desired. The probe circuit should be tuned for 50 Ω to match the spectrometer which is already a 50 Ω system. Lastly the probe should fit into a vacuum sleeve and have a filling plus pump port for use when filled with liquid helium.

2.3.2 Spectrometer Design and Magnet

Spectrometer The block diagram together with the commercial specification of this variable frequency and temperature spectrometer can be found in appendix B.

It should be noted that the spectrometer can be subdivided into a transmitter and receiver branch. A rf signal of chosen frequency is generated and split. One part of it travels along the transmitter branch to the Relcom switch which is driven by amplified pulses. These are generated by the Tektronics unit (see block diagram in appendix B). The purpose of the Tektronics is to produce multi-pulse sequences. More detail will be presented later on. Once the switch is opened the rf pulses are amplified through a linear pulse amplifier (LPA) which itself is synchronized to the small opening pulse via the TTL box. Switching the LPA on and off according to the initial pulses prevents any undesired feedthrough from entering the probe. As soon as the pulse sequence is finished and the rf shut off, the far smaller NMR signal detected by the probe coil is amplified by a series of preamplifiers. The next stage is made up by a double balanced mixer (DBM), a compact broadband device. Here it acts as a mixer of the low level rf and the high level signal with the difference frequency appearing at the output. This difference is fed through a low band

pass filter and recorded on a digitizing scope. The recorded data is stored on the HP 54502 digitizing oscilloscope which is connected to a COMPAQ 286 personal computer. Stored data can be read from the memory and processed with the computer. A fast Fourier transform (FFT) written in Quick Basic was applied to the aquired data. FID's were transformed from the time domain to the frequency domain. To prevent rf leakage, many of the coaxial cables linking the main units of the spectrometer were double shielded.

The TEKTRONICS PG is a mainframe, housing modules connectable via an interconnection board. A number of different modules are available: 1 rate/ramp generator, 2 ramp and 2 pulse generators. In addition an external pulse generator is hooked up to the Tektronics mainframe. They are set up to produce different pulse sequences.

For the following description please see the drawing of appendix B.2. The rate/ramp generator module is set to gate mode, making gates of desired width at a chosen repetition rate. While the gate is open the subsequent ramp generator is producing ramps of chosen length. A first pulse module is triggered to the start of the ramp, resulting in a number of pulses, the number depending on the gate width as well as the ramp and pulse length. The spacing between the pulses depends on the ramp length. Now a ramp module is triggered to the start of the gate, its end triggers a second pulse generator.

The output of the Tektronics can be displayed on the second channel of the scope which gives a good control of the number of pulses, their width and height and the spacing between them.

By varying the ramp duration, the time delay between the end of

Settings for a Pulse Sequence

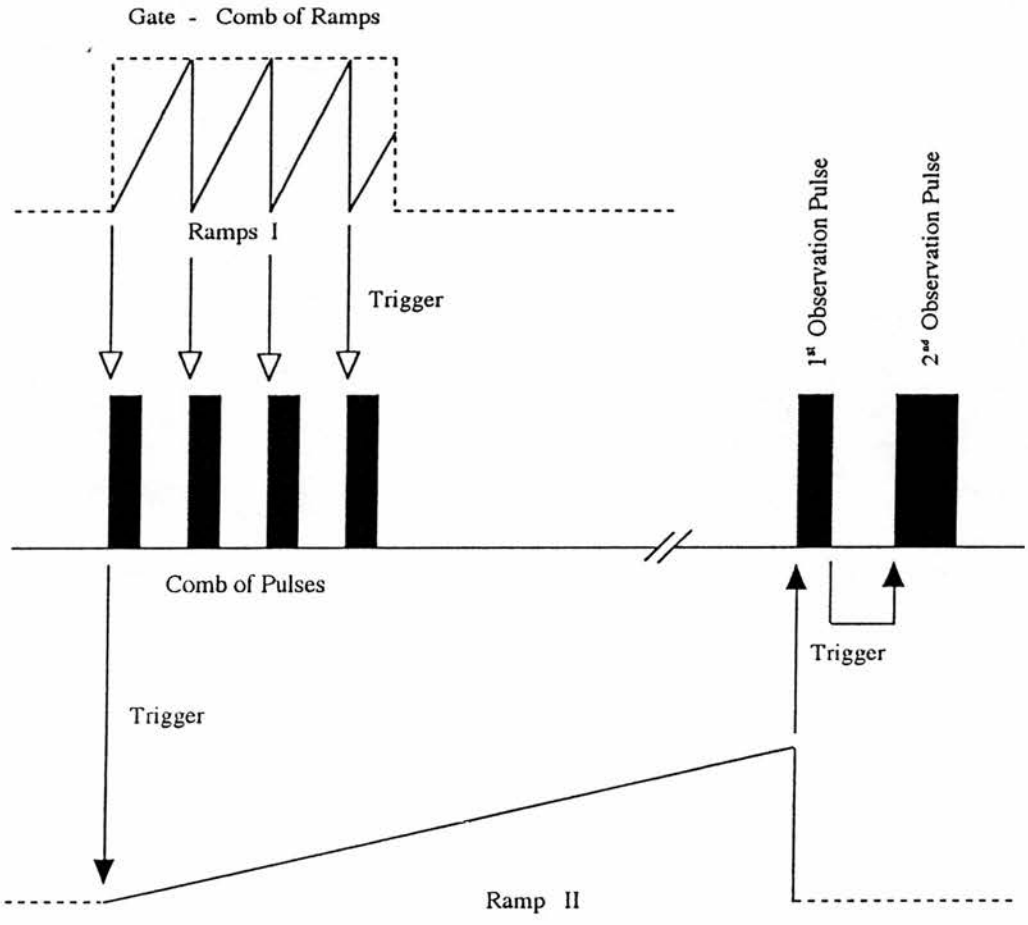

Figure 2.2: Settings for a pulse sequence

the preparation pulse(s) and the 1st observation pulse can be changed. Consequently the time between the end of the preparation sequence, either single or comb, is obtained by subtracting the first ramp length multiplied by the number of ramp starts within the gate from the duration of the second ramp. Finally if needed, e.g. for a short T_2, a 2nd observation pulse triggered to the 1st observation pulse can be used to obtain spin echoes. Spin echo sequences for the measurement of T_2 and spectra point by point as well, as a comb of pulses for T_1 studies can be easily handled.

Magnet The cryomagnet system consists of an Oxford Instruments 12.7 T superconducting magnet housed in a liquid helium/nitrogen cryostat. The helium boil off gas is fed via a return line into a closed helium recovery system. A copper magnetoresistance probe (magprobe) is used to measure the magnetic field during each experiment. It consists of a non-inductively wound coil of Cu wire, which is placed close to the centre of the field and linked to an external measuring circuit.

2.3.3 The Probe

General Considerations Before building a NMR probe several things need to be considered. As already stated in the introduction of this section the probe circuit should be matched to the 50 Ohms of the previously built spectrometer. All components should be capable of withstanding liquid helium temperature and even lower when the probe is filled with and pumped on liquid. A helium dipstick has to be included. Some kind of temperature control has to be located close to the sample. In order to vary the sample temperature a heater system

has to be designed and situated in an appropriate place. None of the employed components should be ferromagnetic least of all those close to the sample region, so special care has to be taken. In order to carry out ^{19}F and ^{63}Cu NMR on a sample, any form of fluorine and copper is banned from the region around the sample coil. The probe enclosure has to be rigid to avoid microphonics, e.g. mechanical oscillations which affect the signal by modulating the capacitance between the enclosure and the coil. Finally the probe has to be wired and its performance tested. The final probe design is shown in the drawings and black and white (b/w) photographs in appendix C.4.

2.3.4 Probe Circuit

The tank circuit is necessary to match the impedance of the coil to the electronic devices outside the tank. The easiest way to do impedance matching between spectrometer and probe is to engineer every component so they will have a common value, e.g. 50 Ω, then there is no need to worry about changing single components. Basically the probe circuit is made up of a coil, capacitors, wires and coaxial cables.

First of all some short explanations [12,13] of frequently used terms are given.

Impedance (Z): generally speaking it is an indication of the opposition offered by a circuit to a flow of alternating current, e.g., rf, in it. Actually it is the ratio of the alternating EMF applied to the circuit to the resultant current flowing in it. The impedance is complex because usually there is a phase difference

between the voltage and current. It can be written

$$Z = R + iX \tag{2.1}$$

where R is the *resistance* and X the *reactance* of the circuit. The numerical value is given by

$$|Z| = \sqrt{R^2 + X^2} \tag{2.2}$$

Reactance (X): in an alternating-current circuit it is due to *inductance* and/or *capacitance*. They are given by:

$$X_L = \omega L \tag{2.3}$$

$$X_C = -\frac{1}{\omega C} \tag{2.4}$$

In case of a circuit containing inductance and capacitance in series the net reactance is as follows $(\omega L - 1/\omega C)$.

Transformer coupling: the conductance of the probe circuit has to be 50 Ω to have effective power transfer from the signal source to the load. Therefore source and load resistances must be matched. This can be shown in a brief calculation. Let R_S be the source and R_L be the load resistance. The power in the load is

$$P = R_L I^2 = \frac{R_L}{(R_S + R_L)^2} U^2 \tag{2.5}$$

Hence P is a maximum when

$$\frac{\mathrm{d}P}{\mathrm{d}R_L} = \left(\frac{U_S}{R_S + R_L}\right)^2 \left(1 - \frac{2R_L}{R_S + R_L}\right) = 0 \tag{2.6}$$

that is, when $R_L = R_S$. Using the circuit below the above not considered reactive components of loads can be 'tuned out' by incorporating other reactive components of the appropriate, either conductive or capacitive, type and magnitude.

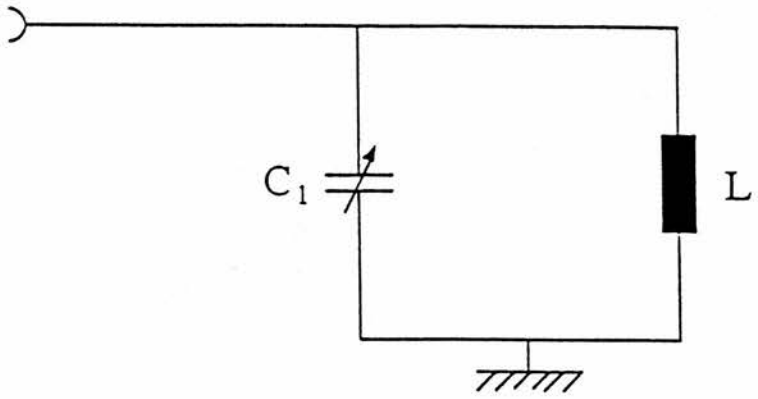

Figure 2.3: Parallel circuit

By adding a single component to the load, i.e. the probe coil, a parallel resonant circuit is established. Such circuits can be analysed by distinguishing between components which are added in series or parallel, see table 2.1.

Considering table 2.1 the reactance **X** for L and C in parallel, then, is

$$R = \left(\frac{1}{i\omega L} + i\omega C\right)^{-1} = \frac{i\omega L}{1 - \omega^2 LC} \tag{2.7}$$

which becomes infinite when $\omega^2 LC = 1$. That is the resonance condition with a resonance frequency of

$$\nu = \frac{1}{2\pi}\sqrt{\frac{1}{LC}} \tag{2.8}$$

Component	X	$Y = -\frac{1}{X}$
Resistor $U = RI$	R	$\frac{1}{R}$
Conductor $U = L\dot{I} = i\omega L$	$i\omega L$	$\frac{1}{i\omega L}$
Capacitor $I = C\dot{U} = i\omega CU$	$\frac{1}{i\omega C}$	$i\omega C$
Circuit	Series	Parallel

Table 2.1: Network analysis

Of course, the impedance at resonance can be changed by changing the L-C combination while satisfying the resonance condition (equation 2.8) but with a given coil the tank circuit can have specific impedance only at one frequency. This drawback can be overcome by adding a *match capacitor* in series to the parallel circuit of coil and *tuning capacitor*. Now the impedance can be transformed with smaller limitations to the frequency desired while keeping the circuit at nominally 50 Ohms. The circuit actually used is shown in figure 2.4.

Impedance and resonance frequency are obtained as followed:

$$\begin{aligned} Y &= i\omega C_1 + \frac{1}{i\omega L} \\ Y^{-1} &= Z_1 = \left(i\omega C_1 + \frac{1}{i\omega L}\right)^{-1} \\ Z_2 &= \frac{1}{i\omega C_2} + \left(i\omega C_1 + \frac{1}{i\omega L}\right)^{-1} \end{aligned} \tag{2.9}$$

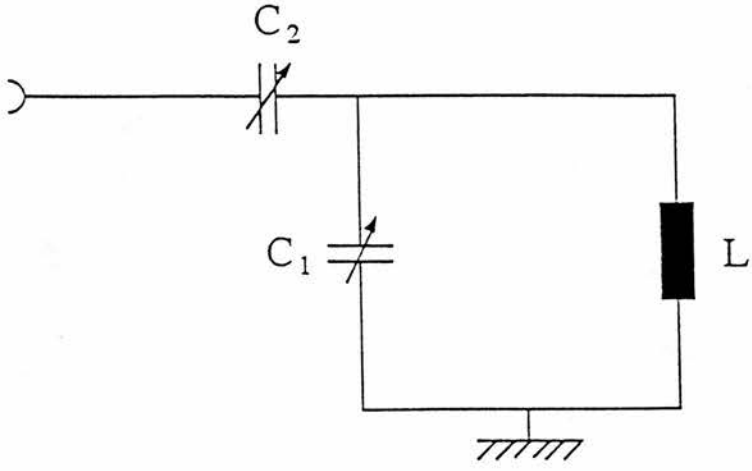

Figure 2.4: Series-parallel LC-circuit

$$\begin{aligned} \omega^2 &= \frac{1}{L(C_1 + C_2)} \\ \nu &= \frac{1}{2\pi}\sqrt{\frac{1}{L(C_1 + C_2)}} \end{aligned} \tag{2.10}$$

Technical Specifications : for a good filling factor, the **coil** is directly wound on the sample and affixed either by friction or jammed with a tiny sheet of paper. It is a free standing coil with one end soldered to the probe stem and thereby connected to earth, see figure 2.5, appendix C.1.3 and the photographs in appendix C.4. The other end is soldered to an insulated wire which connects it to the series-parallel circuit. In the final setup the coil is wound of silver wire, diameter 1 mm, according to the rule of thumb [17] ('The rule of thumb is to

is to wind a solenoidal coil with its length approximately equal to its diameter with the wire diameter equal to the spacing between the turns'), resulting in a good quality factor. The actual sizes are, inner diameter 5 mm, outer diameter 5.2 mm, length 8.1 mm and 6 turns. Using the formula 2.11 given by [14] the inductance can be roughly calculated to 0.078 μH:

$$L = \frac{(n^2 a^2)}{(23a + 25b)} \tag{2.11}$$

whereby n is the number of turns, a the radius and b the length of the coil.

The VOLTRONIC trimmer **capacitors** are of variable capacitance, non-magnetic and of high breakdown voltage. Variable capacitors of sufficient range are necessary to make a multinuclear probe. Details concerning the capacitors used are given below

	Dielectric	Capacitance	Peak RF Voltage
V 2268	quartz	0.9 - 12 pF	1,200 V
V 2270	quartz	8.5 -24 pF	1,000 V
V 2145D	teflon	1.0 - 10 pF	3,000 V

Table 2.2: Data capacitors

In the final setup V 2268 is used as the tuning (C_1) and V 2155D as the match capacitor (C_2).

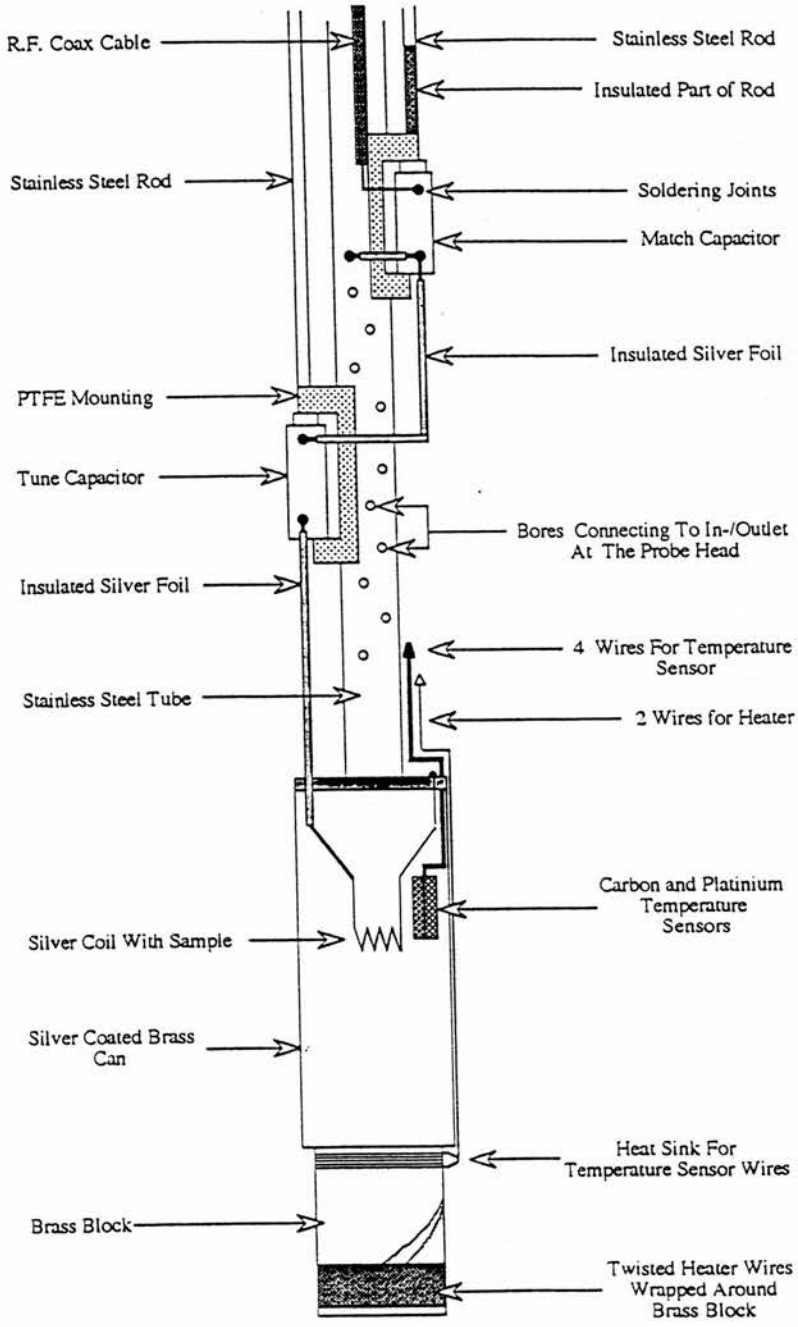

Figure 2.5: Probe design – Bottom end

2.3.5 Wiring

All wire diameters are kept small to reduce heat input from the probe head into the cold region. Great care is taken to get the wires from the socket at the top down to the bottom end of the probe. They are fixed with soft PTFE tape to the stainless steel tube of the probe. For connecting the temperature sensors, thin Eureka wire is chosen, whereas copper is sufficient for the dipstick and heater system. A copper coaxial cable connects the spectrometer and the match capacitor. The remaining bits are wired up with homemade silver strips in order to keep any copper away from the sample region. About 4 mm wide strips are cut from a 1 mm thick silver foil, inserted into shrinking sleeve (PVC) and subsequently heated to fit neatly.

2.3.6 Temperature Sensors

Firstly a thermocouple was used for temperature measurement. It was made of thin enamelled copper and Eureka wire (gauge 30 or a diameter of 0.315 mm). The soldering joint was placed close to the sample. As a reference a mixture of ice and water was employed. The connection of different metals results in the occurrence of an EMF whose magnitude is commonly measured in mV. Looking up these values in existing tables gives the temperature [15].

Secondly a combination of two resistors was chosen to give more accurate data over a wider range. They are taken from the DOTY SCIENTIFIC variable temperature system, ex-sample gas sensors. A platinium RTD (100 Ω) is suitable for temperatures above 37 Kelvin and a carbon composition resistor (27 Ω) below 37 Kelvin. The calibration points are taken from the software

supplied with the MAS probe, one curve for each resistor, and a Quick Basic program was written around them. The resistors and a mutual inductance bridge are hooked up to a switch box. Readings from the inductance bridge are taken and typed into the personal computer. Afterwards the processed data is displayed on the screen.

For good thermal insulation from room temperature (RT), 40 cm of two copper wires, gauge 36 / diameter 0.193 mm, are firstly wound around the brass block (heat sink) and then soldered to the temperature sensors. They are placed outside the sample can and protected against mechanical damage with one layer of PVC tape. Furthermore 3 Eureka wires (gauge 44 / diameter 0.0813 mm) for resistance respectively temperature measurement are connected directly to the sensors which are set up in series.

2.3.7 Heater System

The heater looks as follows: Eureka wire (gauge 30/0.315 mm diameter) is folded in the middle, carefully twisted and wrapped around a brass block at the bottom end of the sample enclosure. The block is soldered onto the sample can and has the function of a heat sink. For good electrical insulation a layer of PVC tape is wrapped around it. The heater spiral is fixed with a second tape layer. Why twist the heater wires? The magnetic field[1] of two opposing currents in both branches of the heater will cancel each other out. Eureka has a resitance of 6.29 Ohm per metre compared to copper of

[1]The nonexistance of any field is been tested over the whole range of heater current settings and in different orientations with a GM1A micropower gaussmeter.

0.221 Ohm per metre and is more suitable for making a heater. Feeding 3.31 m or 20.82 Ω of wire with a maximum current of 0.5 A produces 5.21 W of heater power; $P = RI^2$. The drawings and photos in the appendix C illustrates the above in more detail.

2.3.8 Helium Dipstick

A helium dipstick is necessary to know about the filling level when pumping the probe on liquid helium. The homemade dipstick is situated above the probe circuit, see appendix C, and connected with thin copper wires to a 10 pin glass-to-metal seal at the probe head. In order to mount a fragile superconducting wire, a small strip of veroboard is cut and insulated by wrapping it with PTFE tape. The wires are soldered together and the dipstick fixed to the probe tube. Dipping the superconducting wire in liquid helium results in a change of resistance which can be measured by an external level meter. Each time a reading is taken the meter is swiched on only for an instant to avoid extended heat input caused by flowing current.

2.3.9 Matching Network – Quarter Wave Cable

The basic function of the matching network [17] (see duplexer in figure 2.6) is to deliver the full transmitter power to the sample coil. Then to pick up the NMR signal from the sample and couple it to the receiver branch of the spectrometer. The NMR signal is in the microvolts range whereas the transmitter pulse is hundreds of volts, resulting in the difficulty to decouple the receiver from the transmitter, i.e. to attenuate the strong tansmitter signal

before entering the receiver branch. A device is needed for switching between the transmit and receive mode.

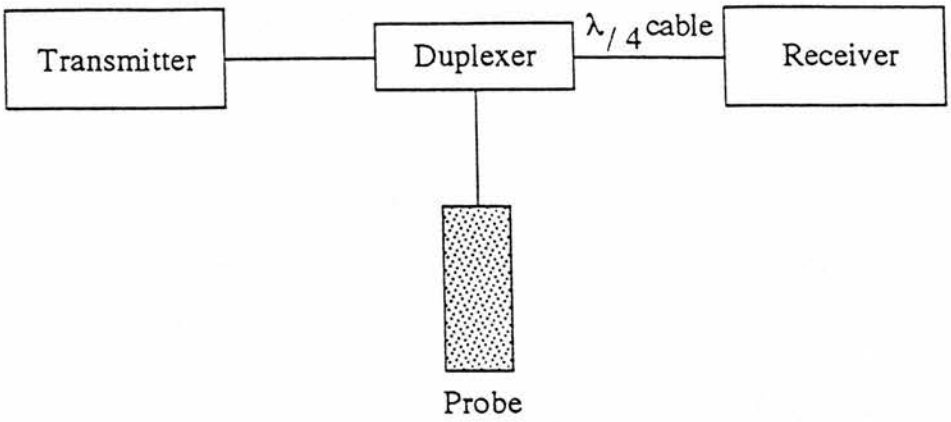

Figure 2.6: Setting up

For the setup experiment a duplexer is used to let the rf travel through an attenuated path into the tank circuit. This is done using crossed silicon diodes which will close for large signals but not for small ones. By the use of a quarter wave or $\lambda/4$ coaxial cable between the duplexer and the 1st preamplifier (see figure 2.7) plus crossed diodes at the preamplifier (LN-20), the applied rf power only goes to the tank circuit, whilst still allowing the small nuclear signal to get to the preamplifier.

With the transmitter switched on, see figure 2.8, the low impedance of the diode switch gets transformed to a high value by the $\lambda/4$–cable so that, the transmitter only sees the tank circuit.

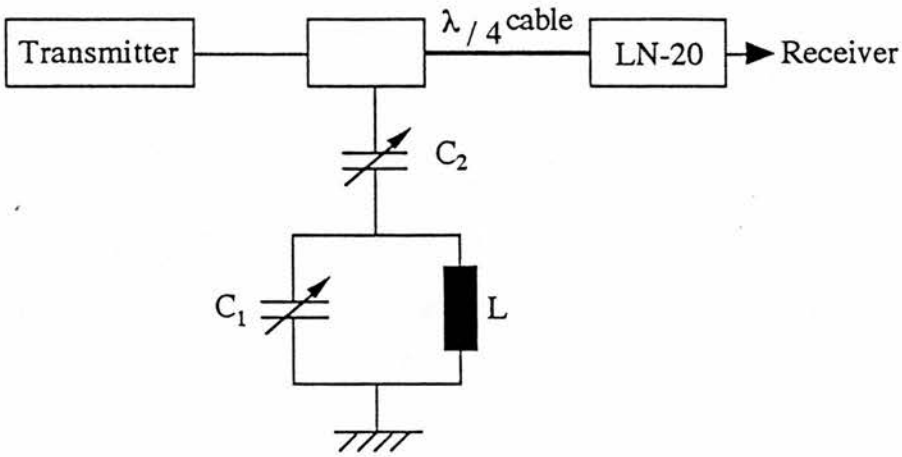

Figure 2.7: Matching network

2.3.10 Tests and Performance

Spectrometer The spectrometer was originally built to suit the DOTY MAS probe. Basically it remained the same: changes were merely done at the preamplifier stage. A Polaron amplifier capable only of lower frequencies was replaced by two amplifiers in series with the second one of adjustable gain. The amplification could be turned down until the first visible saturation of the FID (flat top, non-exponential decay) vanished. For usage in the cryomagnet, i.e. in much higher fields than in the electromagnet, the resonance frequency for the same nuclei is higher as well. Therefore the previously used linear pulse amplifier needed to be replaced. The proper function of the spectrometer and the probe was tested with ^{27}Al as the sample. Ordinary wax was melted and aluminum powder mixed into it. Then a sample of the right size was formed. Finally a T_1 measurement was done at ~100 Kelvin (see figure 2.10), to show

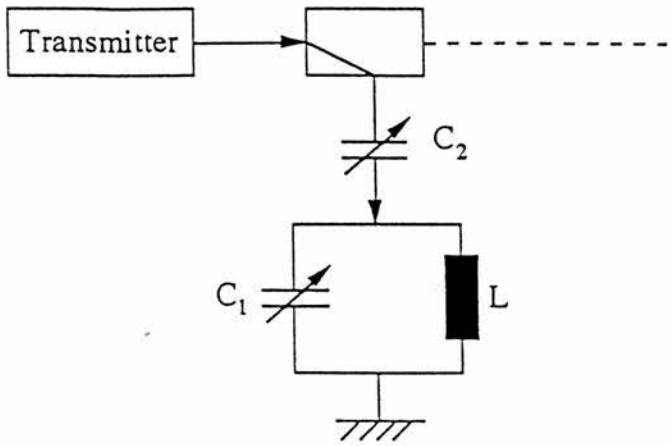

Figure 2.8: Transmitter on

that the recovery time after pulses was very short.

Probe Circuit The first circuit has been designed with a copper coil, 7.5 turns, and copper coax cables. The accessible frequency range at room temperature was determined by hooking the probe cirucit via a hybrid up to a RF generator and an analogue scope (see table 2.3[2] for the results obtained by changing the capacitance of both the tuning capacitors to its appropriate values).

While probing the tuning range it was noticed that even slightly touching and turning the drive rod of the match capcaitor caused the tuned

[2]The table shows the technical specifications of the two tuning capacitors available. In the last two columns the maximum and minimum frequency to which the probe could be tuned to at RT are given.

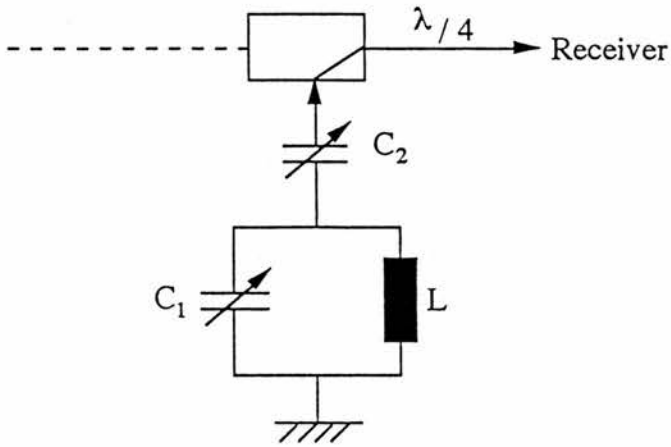

Figure 2.9: Transmitter off

	Capacitance	ν_{min}	ν_{max}
V 2270	8.5 - 24 pF	56 MHz	81.5 MHz
V 2268	0.9 - 12 pF	60 MHz	100 MHz

Table 2.3: Frequency range with different capacitors

state to disappear immediately. It was observed that in some positions of the rod, the match capacitor became earthed. An insulated joint was made up of Tufnol. A watercooled electromagnet with a maximum field of 1 T was available for testing the performance when used with pulsed RF power. Fluorine, i.e. PTFE tape, provided a good sample. It was necessary to put an extra capacitor of 12 pF in parallel with the tune capacitor in order to raise the capacitance and lower the frequency down to about 40 MHz, $\nu \sim \sqrt{1/LC}$, to match the low field. In addition to fluorine, a copper sample was used at

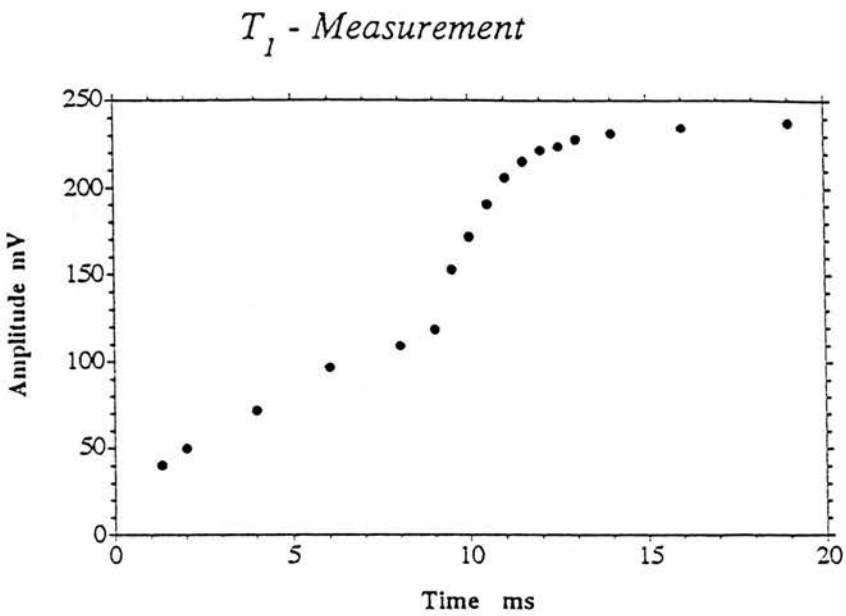

Figure 2.10: Measurement on aluminium

room temperature. Without any averaging strong FID's with low noise were obtained. The possiblity of using low temperature by filling the probe with liquid nitrogen had to be soon abandoned, since the nitrogen boil off affected the tuning considerably by causing the capacitances to change due to pressure changes in the liquid.

Now the copper coil and cables were replaced with silver as decribed in subsection 'Technical Specifications'. Once again the frequency range at room temperature was determined, see table 2.4[3]. Notice that the tuning range changes to lower values at low temperatures.

[3]The table gives the tuning range (maximum and minimum frequency) of the final setup at RT, when the Voltronic (V2268) capacitor was used.

	Capacitance	ν_{min}	ν_{max}
V 2268	0.9 - 12 pF	79.63 MHz	112.45 MHz

Table 2.4: Frequency range at RT

Next the probe was exposed to thermal cycling. It was cooled down to 77 K, taken out, warmed up with a hairdryer and cooled again. The whole cycle was repeated several times. The probe circuit withstood the thermal cycling very well, especially the tune capacitor with an inbuilt glass/quartz dielectric. Nonetheless when the probe was used in heavy duty, pulsed RF at helium temperature the PVC insulation of the homemade silver wire showed cracks twice, maybe due to the neat fit together with the sharp edges of the homemade silver strips. When not used as a ^{19}F NMR probe this problem could be overcome by wrapping the strips in many layers of PTFE tape. Last but not least the coil enclosure, brass can, was coated with silver for shielding likely impurities from the RF. The RF power across the coil was measured to ~1000 V enabling very short pulses and hence a broad range of resonance frequencies.

Heater System Extended tests were done on the heater system. The amenable temperature range was determined first with a pure vacuum in the sleeve, then exchange gas was introduced in order to lower the overall range into the regime of the phase transition temperature of $Nd_2CuO_{4-x}F_x$, which is at about 27 K. NMR studies through this transition are of great interest, as mentioned in subsequent chapters.

First of all the vacuum in the sleeve was improved, i.e. it was pumped for 8.5 hours before starting the test runs. After the probe was inserted into the helium chamber of the superconducting cryomagnet, temperature readings (shown in figure 2.11) were taken to get a rough idea of the cooling rate.

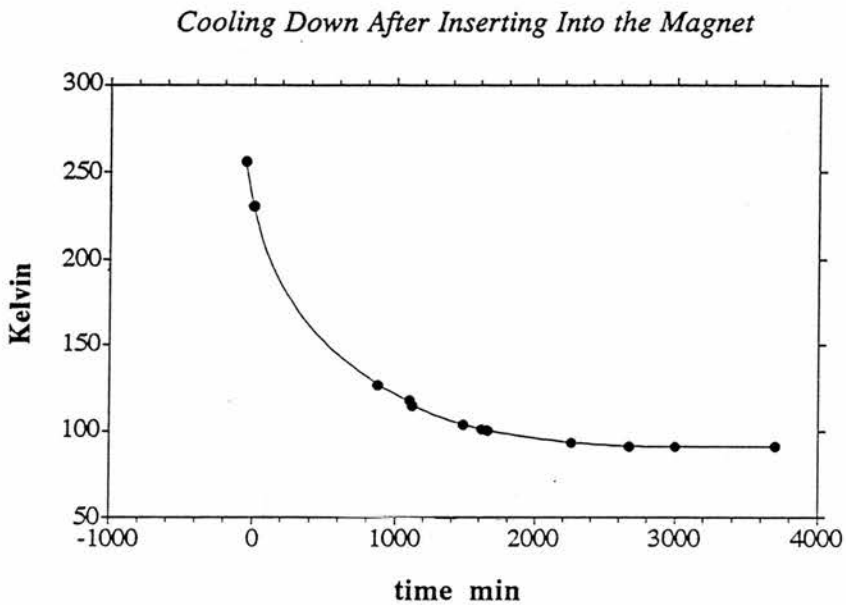

Figure 2.11: Cooling down

The curve starts when the probe was fully inserted at zero minutes at ~230 K and equilibriated within 3000 min or 50 hours down to ~91 K. A remarkably long time constant and well above T_c. Assuming the temperature could be stabilized at some temperature above 91 K the heater current was first set to 490 mA for about ten minutes (see figure 2.12) cranked down to 200 mA and finally switched off. As can be seen from the graph there was no tendency to reach an equilibrium state.

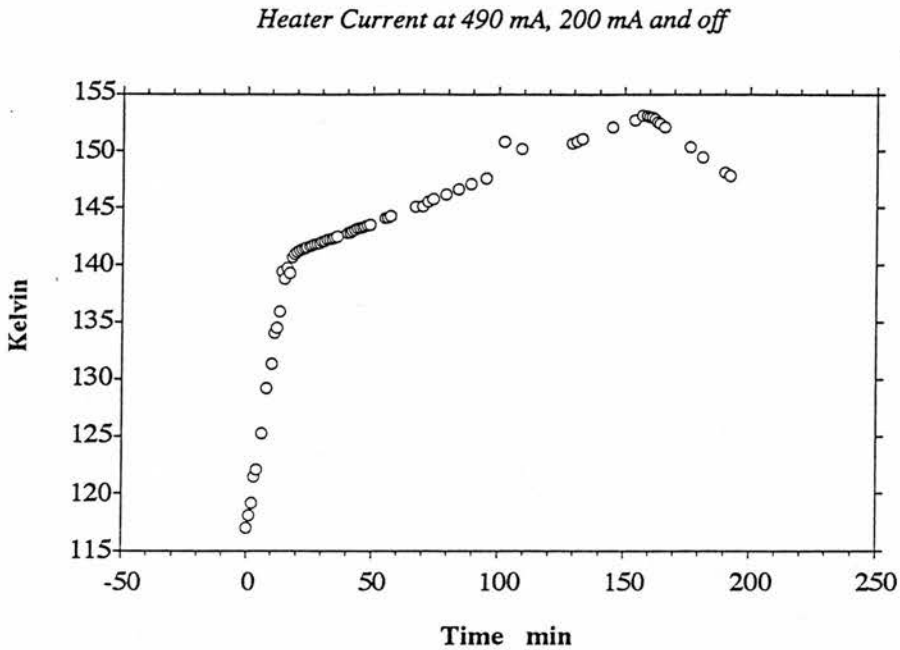

Figure 2.12: Heater current at 490 mA, 200 mA and off

Now a limited amount of helium was introduced stepwise into the vacuum. Here it acted as an exchange gas between the inside of the sleeve (probe) and the surroundings (liquid helium). For the amount of helium see table 2.5.

Filling	Pressure [mmHg]	Volume [cm^3]	Mass [mg]	Mol
1st	760	2.907	$0.520 \cdot 10^{-4}$	$4.337 \cdot 10^{-5}$
2nd	20	0.015	$0.003 \cdot 10^{-6}$	$2.238 \cdot 10^{-7}$
3rd	720	1.278	$0.229 \cdot 10^{-4}$	$1.907 \cdot 10^{-5}$

Table 2.5: Amount of exchange gas

The density of helium gas [16] is given as $\rho = 0.179 \frac{kg}{m^3}$ at 0 °C and 760 torr. Equation 2.12 is used to calculate the overall amount of exchange gas

per filling as given in the table 2.5. All together about 4.2 cm^3 or 0.752 mg or $6.266 \cdot 10^{-5}$ mol of Helium, each referenced to 0 °C and 760 torr, were introduced into the vaccum.

$$pV = NkT$$

$$\frac{pV}{T} = Nk = constant$$

$$\frac{p_n V_n}{T_n} = \frac{pV}{T}$$

$$V_n = V \frac{T_n p}{p_n T} \tag{2.12}$$

V_n : volume at 0 °C and 760 torr

p_n : pressure at 0 °C and 760 torr

T_n : temperature at 0 °C and 760 torr

Again temperature readings were taken, this time already while inserting the probe, see figure 2.13. The observed time constant for reaching an equilibrium value was many times smaller compared to figure 2.11 when no exchange gas was used. Within about one hour the lowest temperature of 4.5 K was reached. The temperature did not alter when the valve which connects the probe to the helium return line was opened.

Subsequently different heater currents were probed and ample time was given to let each temperature curve flatten out. In addition the heater was switched off at each setting, giving a rough idea about the cooling power. The data points in figures 2.14 & 2.15.

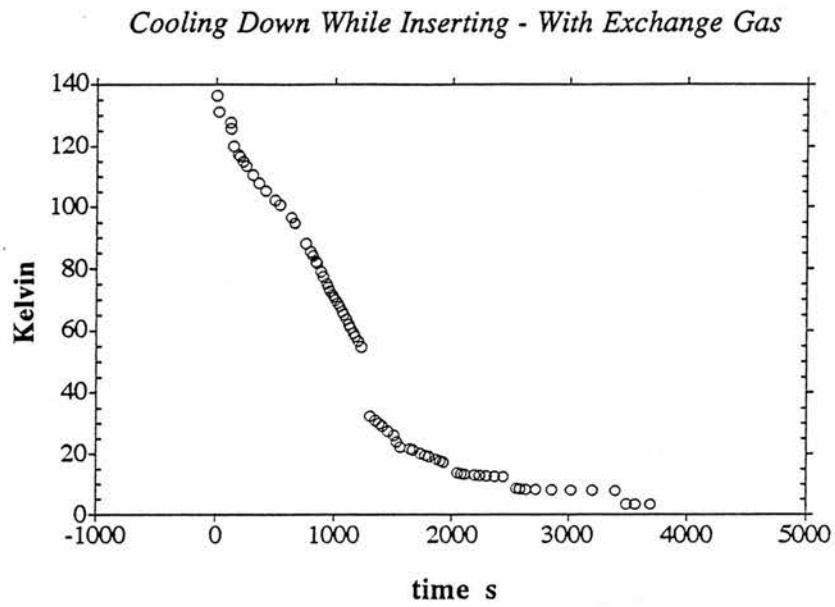

Figure 2.13: Inserting the probe

The data points obtained for several current setting are plotted in figure 2.16. An exponential curve has been fitted to them.

Finally thermal cycling was carried out and is shown in figure 2.17. The more the heater current was increased beyond 200 mA the longer it took to reach equilibrium. At higher heater currents the timescale distorted the equilibrium, it was noticed that the helium boil off was considerable. The amount of liquid helium evaporated in 1 hour by 1 Watt was 1.38 litre. Assuming most of the heat enters the cryogen reservoir, the boil off rate given in table 2.3.10 could be calculated.

The helium comsumption at 300 mA is alreay very high and at 500 mA it is no longer acceptable. The high boil off can be lowered by using less

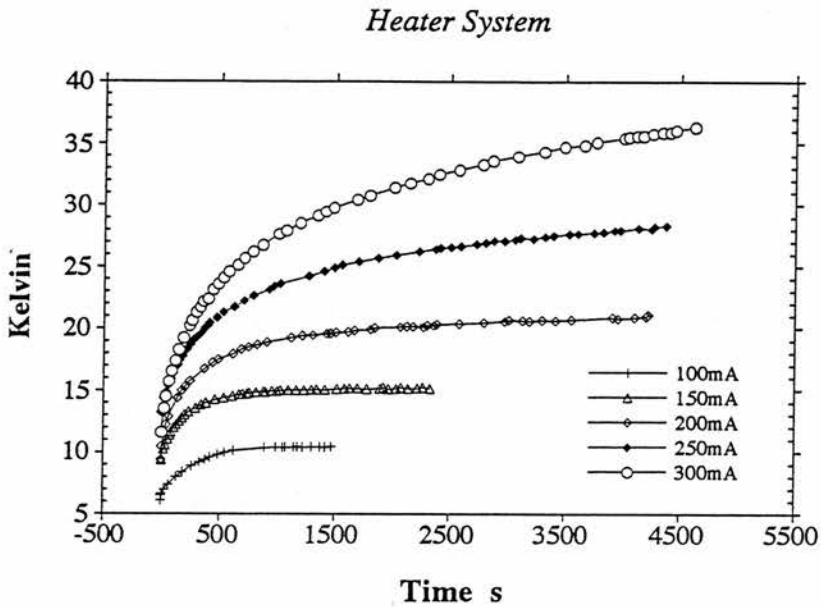

Figure 2.14: Different heater settings

mA	50	100	150	200	250	300	400	500
litre/h	0.07	0.29	0.64	1.15	1.8	2.59	4.59	5.21

Table 2.6: Helium boil off

exchange gas while keeping the temperature range approximately the same. Less heater power would be needed to get the same temperatures below and above T_c. Finally, it was necessary to search for a more efficient method of establishing and maintaining a temperature by automatic control. Another heater test with a stabilizer was carried out but failed. Overshoots in both directions happened regularly due to passive cooling, unlike the DOTY MAS where both components were active and therefore better to regulate.

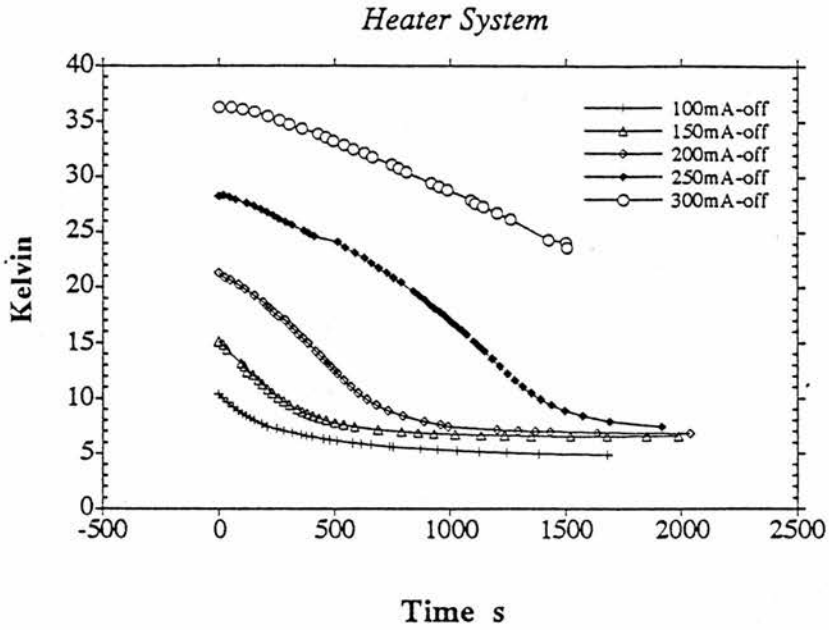

Figure 2.15: Heater off

Dipstick The dipstick performed very well when exposed to liquid helium. It was easily calibrated and had a reliable reading. Care was needed when taking the probe out of the vacuum sleeve so as to not damage it, due to its tight fit. Switching it on for a brief period of time caused the vacuum gauge to rise, a good function control.

Temperature Sensors Initially a thermocouple with room temperature as a reference was used. For more accuracy a reference made of ice and water was chosen. Nonetheless, thermocouples have certain limits, especially in that the tables available have a large step width. Exposed to a magnetic field they give false readings, unless a very tedious calibration is done. Furthermore their materials are mostly magnetic and need to be kept away from the centre field

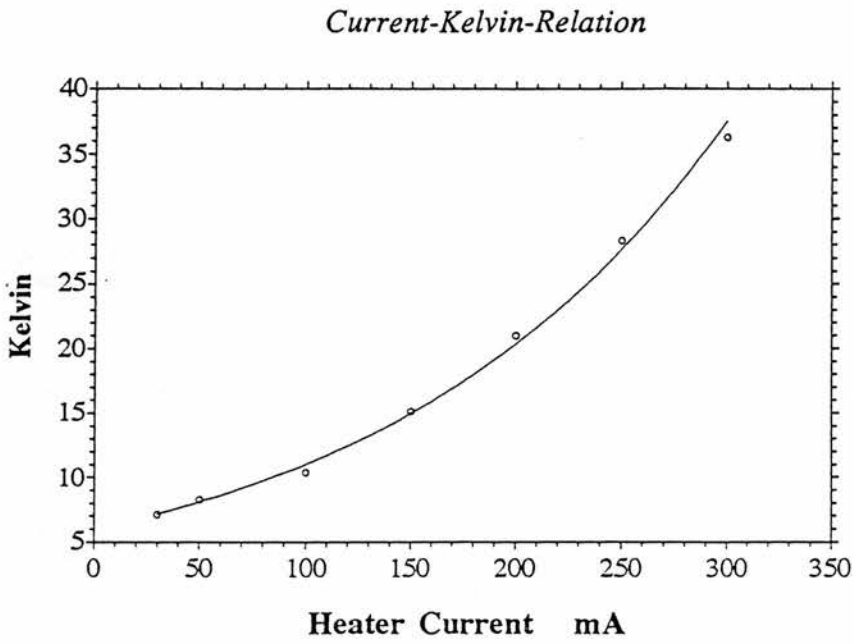

Figure 2.16: Current-Kelvin-Relation

region. That could be overcome by two thermocouples and the calculation of the temperature gradient inbetween them.

Despite of their expense, the platinum and carbon resistors are prefered because they are much easier to handle. They were placed close to the sample just inside the can. During tests a ^{63}Cu NMR signal was seen. When the sensors were taken out of the can no signal was detected, i.e. it could be traced back to the temperature sensors. Shielding the sensors and wires with very thin silver foil cured the problem. Their calibration has been tested at liquid nitrogen and helium temperature. The measured temperature is between 77.89 - 77.91 Kelvin when placed in liquid nitrogen. It should be noted that the lowest possible temperature to be measured was determined as 2.52 K. Only

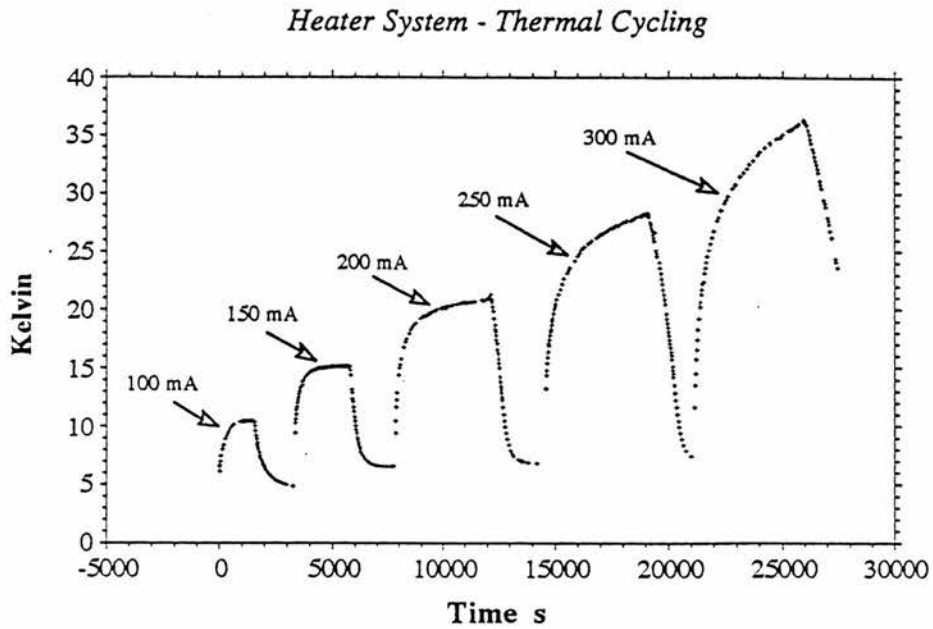

Figure 2.17: Thermal cycling

small deviation from the actual reading are to be taken into account. The lowest temperature accessible when pumping on liquid helium was ~1.4 Kelvin at ~2.8 mmHg vacuum.

2.4 Conclusions

Except for the failure of the MAS probe everything else performed very well. The spectrometer in its final set up had a good S/N ratio, a short recovery time and various pulse sequences could easily be set up. The home-made variable temperature and frequency NMR probe was tunable over a broad range of frequencies enabling high field NMR. The tuning with the hybrid was very good, making extremely short pulses possible, equivalent to many reso-

nance frequencies per pulse. The accessible temperature ranged from as low as 1.4 Kelvin to the point where helium ceased to be a superfluid. The temperature when using the built-in heater ranged from 4.2 Kelvin up to about 37 Kelvin or more with considerable helium boil-off, well above T_c. By inserting less exchange gas the maximum temperature can surely be rised to higher temperatures. Further tests will need to be done. The temperature sensors were found to cover the range from 2.5 Kelvin up to room temperature.

Chapter 3

Superconductivity

3.1 Brief Introduction to Superconductivity

3.1.1 Conventional Superconductivity

In 1908 Heike Kamerlingh Onnes [18] liquified helium (4.2 K) for the first time, enabling him to undertake a systematic study of the electrical resistance of various metals at very low temperatures. Few years later, in 1911, Onnes [19] made the remarkable observation that certain materials, when cooled to 4.2 K and lower, exhibit a drop in resistivity from a finite value to zero. The drop in resistivity occurs at a well defined **'critical'** or **'transition'** temperature $\mathbf{T_c}$. It was firstly reported for a number of pure[1] metals, e.g. lead, tin and mercury. Only at the critical temperature $\mathbf{T_c}$ the specimen undergoes a phase transition from normal electrical resistivity (normal state, $T \geq T_c$) to a resitanceless superconducting state.

In 1914, Onnes [20] discoverecd that the superconducting state can be destroyed by a sufficiently strong external magnetic field (critical magnetic field $\mathbf{H_c}$(T)). The critical field depends on the temperature, it increases as the temperature is lowered and reaches a maximal value $\mathbf{H_c}$(O) as T $\rightarrow$ 0. In

[1]It was later found that superconductivity is an intrinsic property of the material which is independent of purity.

addition, the superconducting property of a wire carrying a current can be destroyed [21,22], if the current exceeds a critical current ($\mathbf{J}_c$). Furthermore it became evident that the superconductivity is a surface property, i.e. outside a surface of certain thickness a sample turns back to its 'normal' state properties.

Years later, in 1933, Meissner and Ochsenfeld [23] found that if a superconductor is cooled below T_c a magnetic field is expelled (diamagnetism) from its interior, regardless of the conditions under which the field was turned on, i.e. before or after the transition to the superconducting state. Unlike perfect conductors, a material in the superconducting state never allows magnetic flux to exist inside its interior.

According to their behaviour during the phase transition from a superconducting to normal state or vice versa, whilst applying a field exceeding $H_c(O)$, they are divided into **type I** and **type II** superconductors (see figure 3.1). Type I or 'soft' superconductors show perfect diamagnetism below $H_c(O)$. The entire sample enters the normal state almost instantaneously while the applied field strength passes through $H_c(O)$ (see fig. 3.1(a)). Other materials of type II exhibit a magnetisation curve of the form of figure 3.1(b). Most of these are alloys or transiton metals with high values of electrical resistivity in the normal state. In these materials the transition to a completely normal state happens gradually. From a lower critical field $H_{c1}(T)$ onwards magnetic flux penetrates the specimen, whereas it was completely expelled before. At the higher critical field $H_{c2}(T)$, the phase transition to the normal state occurs (see figure 3.1), i.e. the flux penetrates completely. The state inbetween these two extremes is called a vortex state, and is characterised by the coexistance of superconducting and normal state due to partial flux penetration.

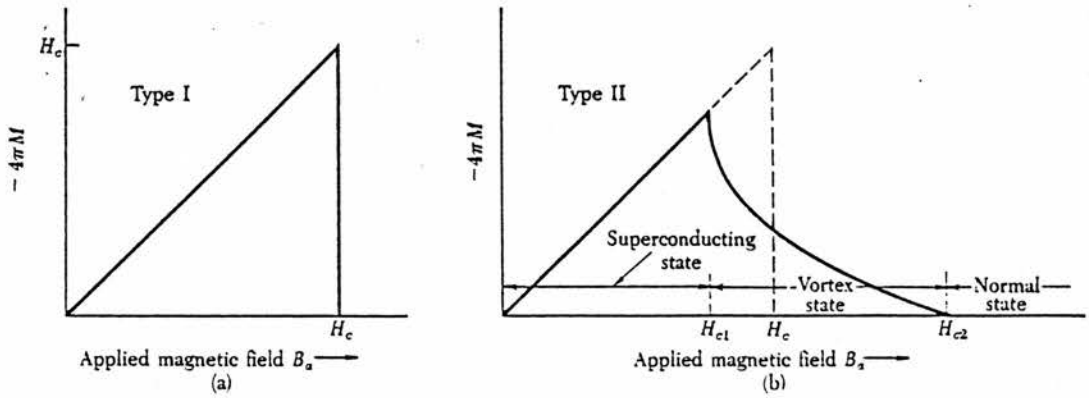

Figure 3.1: Type I and II superconductors, taken from Ch. Kittel, *Introduction to Solid State Physics*, 6th edition, John Wiley & Son, New York, 1986.

3.1.2 Theoretical Background – Abstract

One-electron quantum theory of metals was found to be incapable of explaning superconductivity. In order to reach an understanding, the electron-electron interaction had to be taken into account.

The problem was of such complexity, that it was not until 1957, when Cooper, Bardeen and Schriefer published a set of papers [24,25] which still form the basis of the understanding of the microscopic quantum theory of conventional superconductivity.

3.1.3 High Temperature Superconductivity

In 1986, Bednorz and Müller [26] announced the discovery of high-temperature (high-T_c) superconductivity in the layered barium-doped lanthanum cuprate superconductor ($La_{1.85}Ba_{0.15}CuO_4$) with a transition temperature (T_c) of 30 K. Shortly afterwards further important discoveries were made. Firstly, the transiton temperature (T_c) of $La_{2-x}Sr_xCuO_4$ could be raised by the application of pressure from 35 K to 50 K [27]. Then a major breakthrough came in January 1987 [28] when the discovery of a new compound, $YBa_2Cu_3O_{7-\delta}$ (or 123-YBCO) was made, with a T_c of 92 K, well above the temperature of liquid nitrogen (77 K or -196$_o$C).

The discovery triggered a restless search for compounds with even higher transition temperatures, leading to dramatic rises in T_c with the discovery of many novel superconductors.

So far all superconductors were hole doped. However, in 1989, Tokura et al [29] replaced the Nd^{3+} ions in Nd_2CuO_4 with electron donating Ce^{4+} (tetravalent) ions, yielding electron-doped superconductors with onset temperatures in the 20 –30 K range. Finally, James [30] doped Nd_2CuO_4 with electrons by replacing O^{2-} with F^-, and hence the $Nd_2CuO_{4-X}F_x$ samples studied here were obtained.

Later, in 1993, Asaf [31] first reported the successful combination of anion (F^-) and cation (Ce^{4+}) doping of the same compound, resulting in $Nd_{2-x}Ce_xCuO_{4-y}F_y$ with a T_c of 20–25 K. The effect of anion and cation doping was found to be additive and independent of the Ce/F ratio.

3.1.4 Properties of Layered Cuprates

The normal state and superconducting state properties of layered cuprates are believed to arise from the strongly correlated motion of the electronic charge carriers (holes or electrons) in the CuO_2 planes that essentially define these kinds of high-T_c superconductors. The other cations and oxygen atoms in the structure provide structural stability and control the number and nature of the charge carriers in the CuO_2 planes.

All cuprate high-T_c superconductors are derived from an insulating antiferromagnetic (AF) phase in which there is no charge transfer to the planes. Sufficient chemical substitution, or variation in oxygen stoichiometry of the parent compound, results in the suppression of the AF state and the system undergoes a transition from the insulating state to a metallic state which is superconducting at low temperatures. Further doping leads to a maximal T_c and finally an additonal transition to a normal metal state.

The unit cell of a layered cuprate (see chapter 4, figure 4.1) has a **c**-axis almost 3–4 times that of the **a** and **b** axes. The **a**,**b** plane corresponds to that of the CuO_2 sheets. It is these differences which produce the strong anisotropic properties of the cuprates, for example anisotropic electrical resistance. The resistance perpendicular to the CuO_2 planes is much larger than the in-plane (metallic-like) resistance, exhibiting a semiconductor-like temperature dependence. Generally speaking, the resistance in the c-direction is several magnitudes higher than in the **a**,**b**-direction.

Chapter 4

Neodymium-Copper Oxide and its Doped Compounds

4.1 Introduction

Shortly after the discovery of the first n-type superconductor $Nd_{1.85}Ce_{0.15}CuO_4$ in 1989 by Tokura [29] a new example of n-type superconductivity was reported by James [30] in the fluorine doped Nd_2CuO_4. This lead to intensive studies of their structural, magnetic and electronic properties.

4.2 Crystal Structure

Depending on the dopant, neodymium-copper oxide appears in three distinct phases of the same tetragonal crystal structure. These phases are known as T′-phase, T-phase and T*-phase [29,30]. The anion-doped Nd_2CuO_4 has the T′-phase which is composed of CuO_2 sheets having no apical oxygen atoms above or below the copper sites/planes. In contrast to the T-phase with two apical oxygens (octahedra) and the T*-phase with just one (pyramid). Unlike the other structures the superconducting copper-oxygen layers in the T′-phase are even more two-dimensional due to the absence of apical oxygen [29,30]. Figure 4.1 shows the actual structure of the parent compound as well as its fluorine doped derivative, in which there are two oxygen sites called O(1) situated in the CuO_2 plane and O(2) sitting between two Nd-planes, respectively.

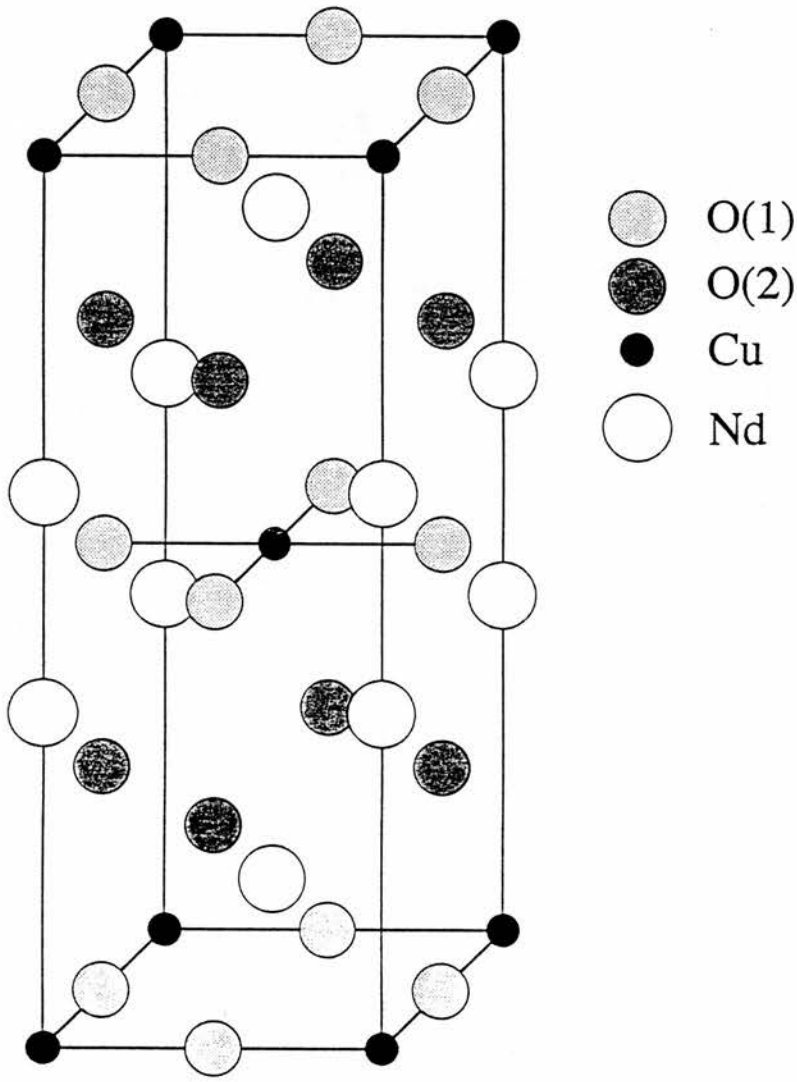

Figure 4.1: Crystal Structure

4.3 Magnetic Properties

The magnetic properties have been studied by a number of research workers [32–35] mainly by neutron scattering and antiferromagnetic resonance (AFMR). All together three phase transitions are observed at temperatures of 80 K, 30 K and ~1.7 K with an onset of long-range ordering at a Néel-temperature of $T_N = 260$ K. These transitions are due to reorientations of the Cu^{2+} spins as well as, at low temperatures, the participation of the Nd^{3+} in the three-dimensional long-range order. According to Kindo [35] the Cu spins form strong antiferromagnetic sheets in the Cu-O plane with ferromagnetic spin arrangements along the c-axis. In the Ce-doped superconducting material, with its similar crystal stucture, when F-doped the Cu-spin system does not magnetically order [33].

4.4 Doping with Fluorine

As can be seen from firgure 4.1 there are two possible sites for fluorination. Fluorine possesses nearly the same ionic atomic radius r = 0.1333 nm as the oxygen ion r = 0.140 nm. Both ions have similar electronic outer shells with p^6 configuration (see table 4.1). Krol [36] used soft-X-ray-absorption to

	Outer Shell		Outer Shell
F	$2\,s^2, 2\,p^5$	F^-	$2\,s^2, 2\,p^6$
O	$2\,s^2, 2\,p^4$	O^{2-}	$2\,s^2, 2\,p^6$

Table 4.1: Electronic configuration

investigate the local structure around the doped F atoms, finding that the ma-

jority substitutes for the O(2) sites and a minority for the O(1) site. Other researchers say there is doping only onto the O(2) site. Further investigations are necessary to determine the exact doping site. After doping, a small contraction along the c axis and expansions along the a and b axes are observed [36] (see table 5.1). The grade of doping has to obey certain lower and upper limts otherwise superconductivity is non-existent or degrades due to impurity phases [30,36,37]. The stated values vary from paper to paper.

In addition to fluorination annealing needs to be done to introduce a small oxygen deficiency, otherwise the compound would not be superconducting. This procedure may be highlighted with a **y** in the chemical formula $Nd_2CuO_{4-x-y}F_x$. Usually the nominal contents are labelled.

Chapter 5

Sample Preparation and Characterisation

5.1 Introduction

All the $Nd_2CuO_{4-x}F_x$ samples were prepared at Birmingham University, School of Chemistry, as powder samples with nominal compositions of x = 0.1, 0.25, 0.3 and 0.4. Several characterisation methods were applied to the samples, i.e. T_c measurement, neutron diffraction and X-ray diffraction. The latter was carried out three times, firstly at Birmingham University and then twice in St. Andrews. The reasons will become obvious in the subsequent sections. Finally, the powder samples were aligned to simulate single crystals for more profound NMR studies.

5.2 Preparation Procedure

The parent compound Nd_2CuO_{4-x} is fluorinated by putting it into the preparation apparatus shown in figure 5.1 and baking it together with the appropriate amount of NH_4F. The preparation conditions are as follows: first bake at 350 °C for 12 hours under nitrogen atmosphere, then subsequently at 890 °C for another 12 hours also under nitrogen gas.

Previously another preparation route, known as the bismuth reduction, was carried out but the material decomposed, even under the mild conditions used. The preparation procedure actually used still differs from the most

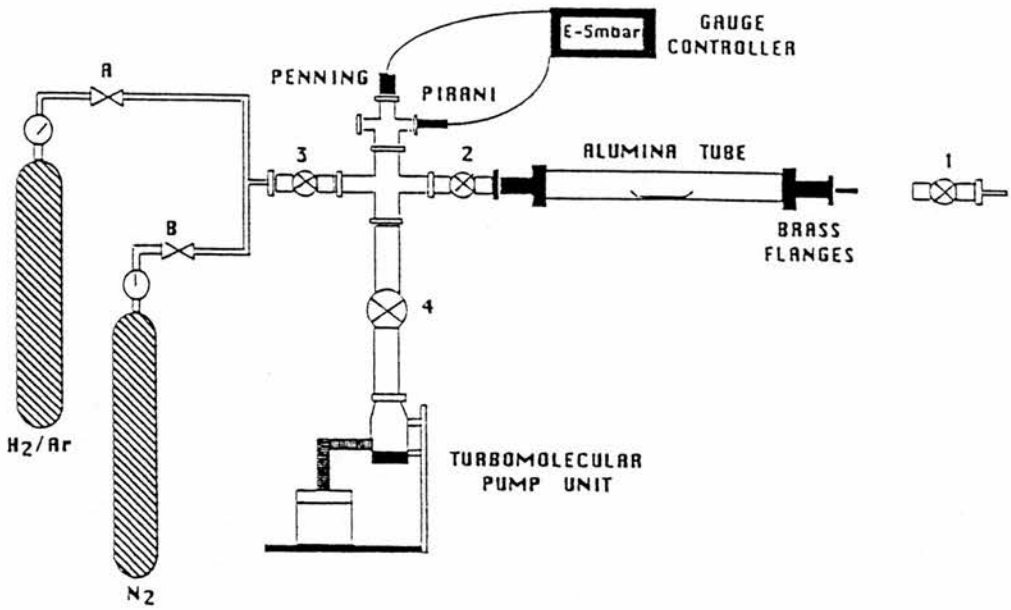

Figure 5.1: Preparation apparatus

common solid phase reaction. James et al [30] firstly reported $Nd_2CuO_{4-x}F_x$ as an electron doped superconductor. They prepared samples by heating stoichiometric mixtures of CuO, Nd_2O_3 and freshly prepared NdF_3 in air at 900 °C for 14 h followed by heating at 890 °C for 14 h in flowing N_2. Most other groups followed this preparation route with at most minor alterations. Synthesis routes and their influences on the superconducting properties are discussed by Kuentzler [38] and Tighezza [39].

5.3 Determination of the phase transition temperature

The samples have been analysed[1] for T_c, using a SQUID magnetometer. All of them, except for pure Nd_2CuO_{4-x}, were found to be superconducting, with T_c's between 22 and 23 K for allsamples. Figure 5.2, as an example, shows $Nd_2CuO_{3.6}F_{0.4}$ and the onset of the diamagnetic signal at 22 Kelvin. The other data plots can be found in appendix D.

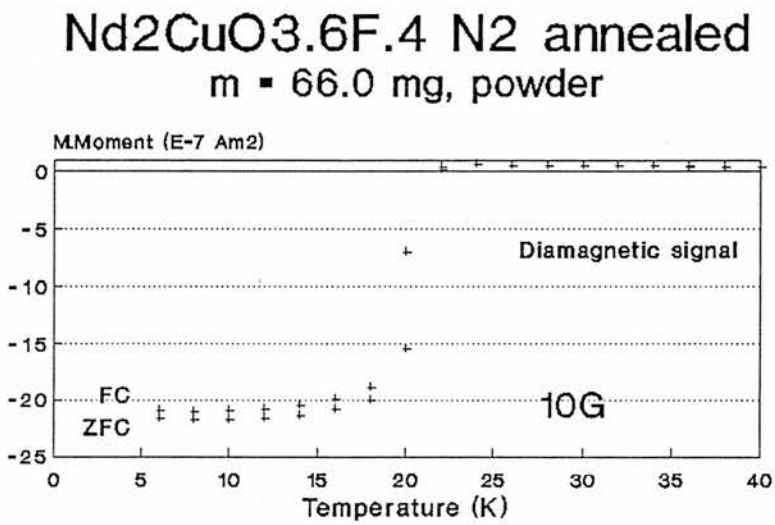

Figure 5.2: Example for T_c measurement

[1]The measurements are done at Birmingham University, School of Chemistry.

5.4 Powder Analysis

5.4.1 Neutron Diffraction

The successful fluorination of the samples has been proved at Birmingham by doing neutron diffraction on the whole set of powder samples. There are two kinds of interaction between neutrons and solids, the strong interaction with the nuclei and also the one with the magnetic atoms due to their magnetic dipolar moment. Typical neutron sources for these experiments are nuclear chain reactors and particle accelerators. Generally speaking the interference phenomena of slow or thermal neutrons are similar to those of X-rays[2] [40], since both the wavelength and the scattering cross section are comparable. Neutrons with thermal energy of 25 meV have a wavelength of $\lambda = 1.8$ Å [41]. Since the nucleus of an atom is much smaller than the wavelength of the slow neutron, the scattering amplitude shows no regular or even rapid increase with atomic number, or any variation with the diffraction angle Θ [40]. In many cases the scattering amplitudes of neighbouring elements are quite different when they occur together in a compound, enabling the distinction between them using the neutron intensity data. Unfortunately, in our case, the neutron coherent scattering amplitude of oxygen and fluorine differ only very little, preventing the direct distinction of the two nuclei. Instead the sucessful fluorination had to be deduced by comparing the relative intensity of the actual data with those generated by an atomic simulation program. By varying the sites for fluorine doping and their occupancy until the closest match with the experimental data was found, the sucessful fluorination was proved.

[2]X-ray diffraction has been described in detail in the next subsection.

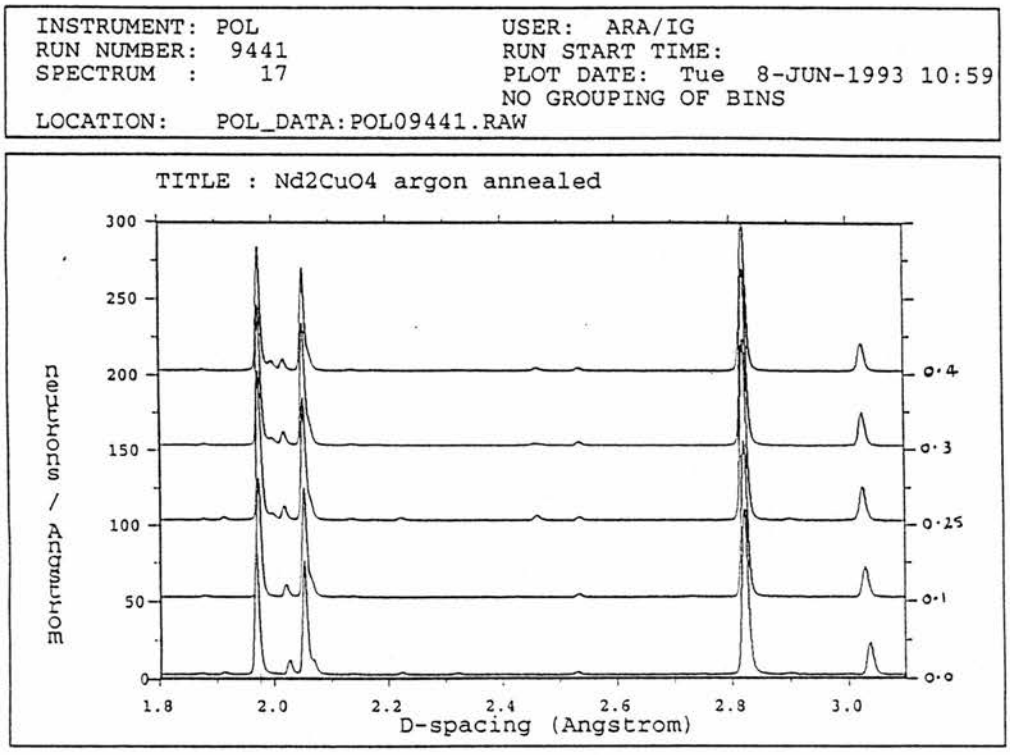

Figure 5.3: Neutron diffraction data

The neutron diffraction plot[3] (figure 5.3) obtained with the time-of-flight method shows the spectra of one set of samples. The righthand y-axis is labelled with the fluorine contents. As can be seen in the obtained data plots at a D-spacing of about 2.0 Å, a peak appears to be superposed on the right shoulder (larger D-spacing) of a peak already existing in the spectrum of the parent compound. An additional 'tiny' peak appears at about 2.46 Å, left to an already existing one. Both of these peaks appear for a fluorine content of

[3]Done at Birmingham University, School of Chemistry.

x=0.25 onwards and are not to be mistaken as replaced oxygen atoms. They are due to small impurities introduced through fluorination. Small differences of the amplitudes of the other diffraction peaks were impossible to distinguish by eye. The above mentioned simulation method had to be employed.

5.4.2 X-Ray Diffraction (XRD)

There are two equivalent formulations [42,43] of X-ray diffraction by a crystal in use: the Bragg fromulation and the Laue formulation. Both viewpoints are based on the same physical assumption but the way they approach it differs. Subsequently the still widely used Bragg approach is briefly stated in order to understand the interpretation of the X-ray spectra obtained.

The diffraction depends on the crystal structure as well as on the wave length used. One has to distinguish between the ordinary optical refraction ($\lambda \simeq 5000$ Å) where the waves are scattered by single atoms of the crystal and diffraction with lengths in the order of the lattice parameters. The latter shows diffraction totally different from the direction of the incident beam. Typically, interatomic distances in a solid are of the order of a few Ångstroms which is the wavelength of hard X-rays. This is the reason why X-rays due to interaction with the crystal electrons are used as an electromagnetic probe of the microscopic structure of solids.

In 1913 Bragg [44] demonstrated that X-rays are diffracted by crystals depending on the space lattice of the crystal and the wavelength (λ) of the rays used. He regarded the crystal as a set of parallel planes of ions, spaced a distance (d) apart. Incident beams are reflected at these parallel planes. They

behave just like lightly silvered mirrors, specularly[4] reflecting only a small fraction of the incident X-ray radiation. Sharp peaks in the intensity of scattered radiation are observed when reflected rays from successive parallel planes constructively interfere. The path difference between two adjacent X-rays is obtained from a simple geometrical consideration as $2d\sin\Theta$, where Θ is the angle of incidence[5]. The Bragg condition is given by

$$n\lambda = 2d\sin\Theta \tag{5.1}$$

where n is an integer denoting the order of the corresponding reflection.

Particular planes in a lattice are commonly specified by **Miller indices**. These are a set of three integers (hkl) by which both the position and orientation of a crystal plane are defined in relation to three mutually perpendicular crystallographic vector axes, **a**, **b** and **c**. There are two way to derive them: one uses the reciprocal lattice, the other is done geometrically and is very common among crystallographers [43].

[4]In specular reflection the angle of incidence equals the angle of refection.
[5]The angle of incidence is conventionally measured from the reflection plane.

It can be shown[6] that the interplanar spacing d_{hkl} is given in terms of the crystal lattice parameters **a, b** and **c**. The relationships for orthorhombic (a $\neq$ b $\neq$ c) and tetragonal structures (a = b $\neq$ c) are as follows

$$d_{hkl}(\text{orthorhombic}) = \frac{1}{\left[\left(\frac{h}{a}\right)^2 + \left(\frac{k}{b}\right)^2 + \left(\frac{l}{c}\right)^2\right]^{\frac{1}{2}}} \tag{5.2}$$

$$d_{hkl}(\text{tetragonal}) = \frac{a}{\left[h^2 + k^2 + \left(\frac{a}{c}\right)^2 l^2\right]^{\frac{1}{2}}} \tag{5.3}$$

$Nd_2CuO_{4-x}F_x$ has tetragonal structure where a = b $\neq$ c. First XRD's on the powder samples were done at Birmingham. The lattice parameters obtained are listed in table 5.1. They are necessary for the correct alignment procedure and further X-ray studies on the aligned samples.

Fluorine Content	Lattice Parameter[Å]	
	a = b	c
x = 0.00	3.94123	12.16530
x = 0.10	3.94962	12.13473
x = 0.25	3.95177	12.11875
x = 0.30	3.95291	12.11834
x = 0.40	3.95318	12.11823

Table 5.1: Crystal Lattice Parameter

[6]M.F.C. Ladd & R.A. Palmer, *Structure determination by X-Ray Crystallography*, Plenum (1979)

5.5 Alignment Procedure

5.5.1 Introduction

Single crystals of the diverse high-T_c superconductors are preferred for various physical measurements due to the highly anisotropic nature of these compounds. Unfortunately the growth of large single crystals presents great difficulty. Furthermore the size of one single crystals available is too small to be of use for some experiments. In NMR measurements this hindrance is overcome by producing pseudo-single-crystals, with identical grain orientation.

5.5.2 Technique

The alignment was fist accomplished by Farrell et al [45] for YBCO and later for many derivatives of YBCO as well as other high-T_c superconductors. The basic technique uniaxially aligns small portions of crystals in a high magnetic field and 'freezes' them at room temperature in a non-magnetic epoxy resin. Previously, Webster [46] performed extended studies on the alignment of a YBCO derivative, and these studies were a basis for the alignment of $Nd_2CuO_{4-x}F_x$ in the present work.

Magnetic field alignment requires each individual grain to be a single crystal. In preparation, the powder samples were thoroughly ground in a glovebox under argon atmosphere using an agate mortar and pestle. The argon prevented the building up of multicrystal clusters due to any moisture in the ambient atmosphere. Stycast 1266[7], a transparent, high impact, non-magnetic

[7]Manufacturers are Emerson & Cuming Inc..

	Unit Cell Volume [Å]	Density $\left[\frac{g}{cm^3}\right]$
Nd_2CuO_4	188.9672	3.6796
$Nd_2CuO_{3.90}F_{0.10}$	189.2957	3.6758
$Nd_2CuO_{3.75}F_{0.25}$	189.2523	3.6806
$Nd_2CuO_{3.70}F_{0.30}$	189.3551	3.6799
$Nd_2CuO_{3.60}F_{0.40}$	189.3792	3.6821

Table 5.2: Unit Cell Volume/-Density

epoxy resin, withstanding temperatures as low as 1.4 K was used. The resin part A and the volatile catalyst part B were measured out in the ratio 28 to 100 by weight. By vacuum pumping part A for about 30 min dissolved water and air was extracted. Both parts were slowly mixed together[8] and afterwards vacuum pumped for a brief time to get rid of any air bubbles trapped during the mixing process. In order to get a resin to powder ratio of 10 to 1 by volume it was necessary to know the exact volume of the sample tubes and bungs. The right mass of powder was obtained by calculating the density of each sample. This was done by firstly calculating the single crystal volume using the lattice parameters from table 5.1 and 5.2., and secondly the mass per single crystal was worked out using a perodic table. Subsequently the powders were weighed out accurately and filled into the glass tubes. Once more this is done under argon atmosphere using a balance situated in a glove box. On removal from the glove box freshly prepared stycast was added to the measured powder. First mixing was done by hand using a stirrer, then more efficient dispersion was reached

[8]The pot life is given as 30 minutes, hardening time as 8 hours.

reached by applying an ultrasonic gun for about 2 minutes. The glass tube was then sealed with a rubber bung. Almost all the air was expelled by slow removal of a fine wire between the tube wall and the bung, leaving just one little bubble at one end. Next the sample tubes were inserted into a brass former which firmly helds the sets of five samples. Two sets of samples were prepared, one of them was placed in the 12 T magnet on top of the bottom loading NMR-probe whose head was removed. The other was kept away from any magnetic field. Both sets of composites were allowed to set for 14 hours at room temperature. The crystallites align due to the torque they experience in the high magnetic field as a result of their anisotropic susceptibility. According to Livingston [47] this is a consequence of the paramagnetic anisotropy associated with the conducting CuO_2 planes. After curing the samples are taken out of the magnet, dunked into liquid nitrogen and the cracked glass was removed carefully from the sample. In the case of the aligned samples, the above mentioned air bubble acted like a spirit-level and was used to mark the axis of alignment on one top end of the sample cylinder. The samples are of 5 mm diameter and about 21 mm in length, fitting in the MSL-500 probe heads for ^{63}Cu NMR studies as well in the silver coil of the homemade NMR probe. The samples are stored at ambient pressure in a glass jar containing silica gel to extract moisture.

5.5.3 X-Ray Diffraction

In order to carry out X-ray diffraction on the aligned samples, a 1 mm thin disc, see figure 5.4(a), was cut off from the end of the sample cylinder using a diamond saw. These discs were fixed to individual sample holders in the man-

ner shown in figure 5.4(b) and were loaded into a fully computerized Philips PW1049 X-ray diffractometer [46]. The X-rays are produced by a cobalt target, $\lambda_{Co} = 1.7902$ Å, irradiating the sample disc (x-z plane), on one side. The diffraction geometry is shown in figure 5.4(b). It is as follows: the incident beam and the marked axis of alignment, here along the z-axis, are in a plane (y-z) perpendicular to the surface. With the given experimental arrangement, X-rays striking the specimen in certain points leave the sample surface along cones whose tips coincide with the very same point. The scattering makes an angle of 2Θ with the direction of the incoming beam; radiation is detected at angles of 2Θ between 5° and 90°. The number of counts at each angle are recorded on the computer, and so a spectrum of intensity versus diffraction angle (2Θ) is obtained and plotted. Scattering peaks were identified by comparing the experimental values of 2Θ with computer generated tables of 2Θ. To do so, the interplanar spacings d_{hkl} were calculated by putting in the values of the lattice constants a, b and c given by table 5.1 into equation 5.3. Subsequently the integers h, k and l are incremented and the resulting values for d_{hkl} are transformed to 2Θ using equation 5.1 and plotted. Finally, theoretical and experimental 2Θ numbers were compared and the X-ray peaks in all spectra were labeled accordingly (for example see the aligned and random powder spectra for $Nd_2CuO_{3.75}F_{0.25}$ in figures 5.5 and 5.6).

A closer inspection of the X-ray diffractometer studies on the random sample (see figure 5.5) and the aligned sample (see figure 5.6) revealed a number of interesting differences.

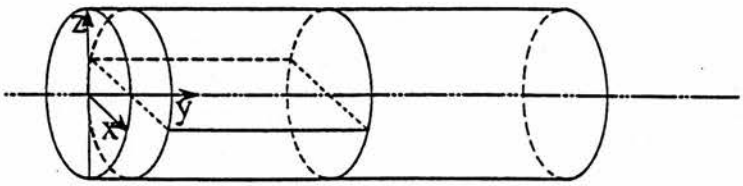

(a)

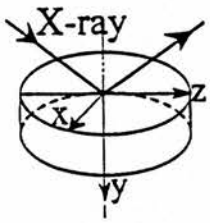

(b)

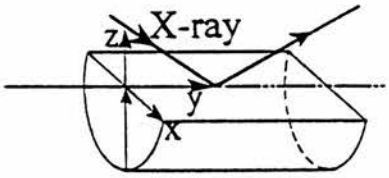

(c)

Figure 5.4: Sample cylinder–different cuttings

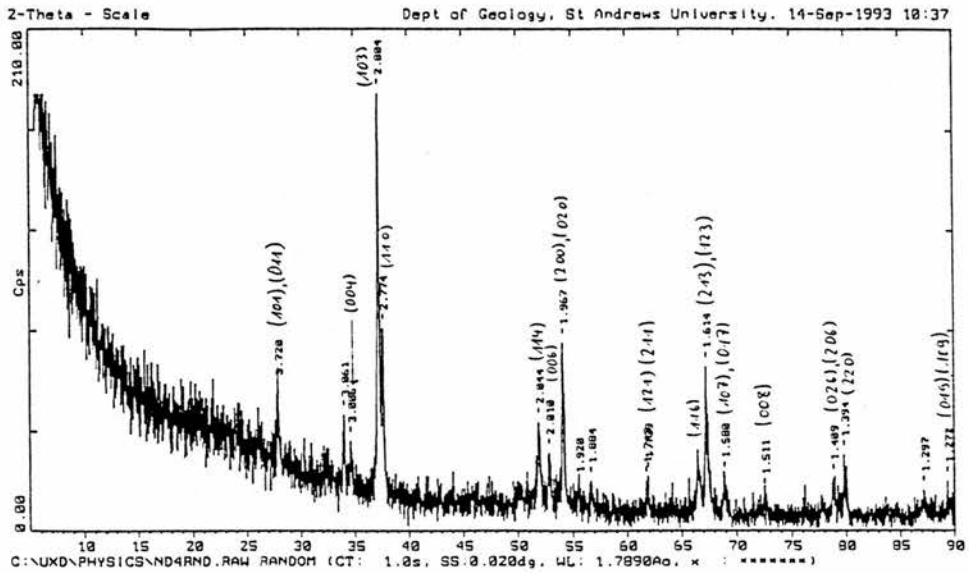

Figure 5.5: X-ray spectrum(I)–random powder sample

Comparing the random and aligned spectra shows:

- Peak (103) relative to (110) shrinks when compared to these of the aligned sample.
- Comparing (114), (006) and (200), peak (006) is enhanced relative to the other two.
- Peak (008) is almost not visible in the random spectra whereas it is enhanced in the aligned spectra (II).

Assuming that the c-axis is aligned parallel to **B**, as is commonly the case in the YBCO system [46] and the Tl-1212 system [48], then all the peaks assigned as ($hk0$) where the Miller index (l=0) should be increased in magnitude by alignment whereas all others should decrease or even disappear

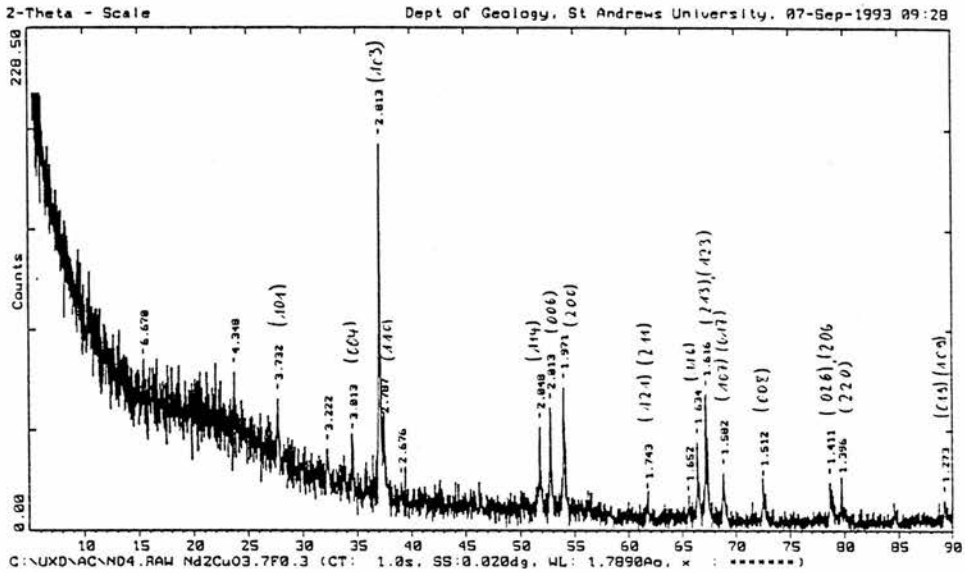

Figure 5.6: X-ray spectrum(II)–aligned sample

in perfectly aligned samples. Strikingly, the X-ray spectrum for the aligned sample, see figure 5.6, does not show increasing peaks corresponding to $(hk0)$. Instead those with indices $(00l)$ do so, showing that the c-axis of grains does not align parallel to B. Thus the c-axis is more likely to align perpendicular to the aligning magnetic field. Subsequent Cu-63 NMR, see chapter 6, supports this statement making a more datailed evaluation of the X-ray diffraction necessary. When the cylinder is sliced parallel to the x-y plane see figure 5.4 (a) (c)) and the X-ray spectra are taken on the x-y plane, the peaks corresponding to (hkl) for l=0 (crystal planes parallel to c) should enhance and the others should deminish. The X-ray spectrum for this cut is shown in figure 5.7 where the previous assumptions are proven. The remaining peaks are (110), (200)/(020) and (220), showing that a very good alignment is obtained. Nonetheless two tiny 'peaks' almost invisible in the noise are present. Presumably they are due

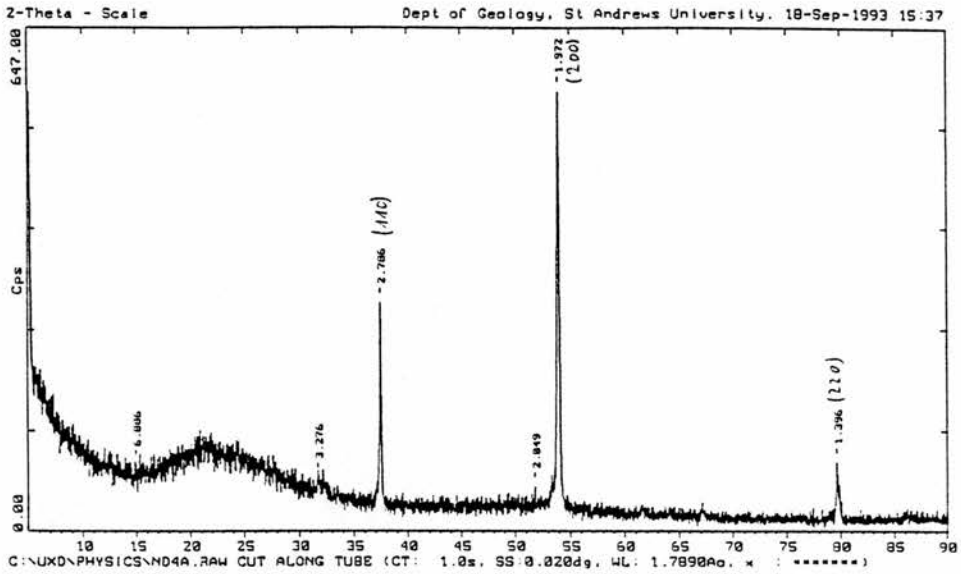

Figure 5.7: X-ray spectrum(III)–aligned sample

to impurities.

Obviously on a macroscopic spatial average there is no prefered direction of orientation in the a-b plane as a = b and the c-axis of the aligned crystallites is randomly orientated parallel to the flat surface of the new cut. Finally it should be mentioned that the X-ray spectra of the parent compound show just the same results has been described above. Therefore the kind of alignment is not due to doping.

5.5.4 Discussion

Finding that the c axis aligns parallel to the field in some compounds and perpendicular to the field in others can be explained, according to Livingston [47], with the 2nd order Stevens factor α_j of the crystalline electric field (CEF) Hamiltonian. The magnetic rare earths R^{3+} ions are the most likely source of anisotropy associated with crystal fields at the rare-earth site. A correlation with the sign of the second-order Stevens factor was assumed. Extended investigations were done e.g. by Livingston [47] on $R\mathrm{Ba_2Cu_3O_{8-\delta}}$ with R=Eu, by Ferreira [49] on $R\mathrm{Ba_2Cu_3O_{8-\delta}}$ with R = Y, Nd, Sm, Eu, Dy, Ho, Er, Tm and Yb. With a few exceptions the alignment direction correlates with the sign of the 2nd-order Stevens factor as shown in table 5.3, data is taken from [47,49]. Most investigations are based on the 123-structure which

Rare Earth R	**c** relative to to **B**	Sign of α_j
Y	$\parallel$	0
Nd	$\parallel$	−
Sm	$\parallel$	+
Eu	$\perp$	0
Dy	$\parallel$	−
Ho	$\parallel$	−
Er	$\perp$	+
Tm	$\perp$	+
Yb	$\perp$	+

Table 5.3: Stevens factor

is orthorombic or nearly tetragonal. In most of these cases $\chi_{\parallel c} > \chi_{\perp c}$ coincides with a negative α_j and vice versa $\chi_{\perp c} > \chi_{\parallel c}$ with a positive α_j. Ferreira [49]

possibility of a sign change in the paramagnetic anisotropy of Ho at elevated temperatures whereas Livingston points out the influences due to interactions among magnetic ions on the anisotropy. The latter point leads to the understanding of the alignment of $Nd_2CuO_{4-x}F_x$ which is opposite to the behaviour in Nd-123. The $Nd_2CuO_{4-x}F_x$ and $Nd_{1.85}Ce_{0.15}CuO_{4-y}$ are both electron doped superconductors having the same T′ crystal structure. Recent studies [50] of magnetic properties between 5 and 300 K on single crystal $Nd_{1.85}Ce_{0.15}CuO_{4-y}$ give evidence that the susceptibility when B || ab-plane is larger than B || c-axis. A plot of the inverse susceptibility χ^{-1} per mol Nd^{3+} shows strong anisotropy at temperatures below 125 K and more importantly there is still considerable anisotropy starting at about 200 K up to room temperature, strongly supporting the similar alignment of $Nd_2CuO_{4-x}F_x$.

Chapter 6

Copper–63 NMR on $Nd_2CuO_{4-x}F_x$

6.1 Introduction

The properties of $Nd_2CuO_{4-x}F_x$ are already stated in chapter 4 'The Neodymium-Cuprate and its doped Compounds', and chapter 5, 'Sample Preparation and Characterisation'. Features relevant for Copper–63 NMR are now briefly repeated to provide a better understanding. $Nd_2CuO_{4-x}F_x$ is an anion-doped high-T_c superconductor having the Nd_2CuO_4 (T'-phase) structure, in which there are two oxygen sites labelled O(1), situated in the CuO_2 plane, and O(2), situated between two Nd layers.

When doing copper NMR one is interested to resolve, along with other properties, the NMR frequency shift, namely the different contributions to the *Knight shift.* Unlike in non-metals there are additional corrections to the resonance frequency for metals like copper. These are due to interactions between the conduction electrons and the nucleus, which cause an extra positive or negative field at the nuclei, known as the hyperfine field. Depending on the symmetry around the copper site, different contributions to the Knight shift, as well as first and second order quadrupole interactions can occur.

So far, a few copper NMR studies have been reported in the literature and a summary shall be given here. All of them were done on the parent material or related compounds, with just one on the fluorine doped derivative [37].

Shortly after the n-type superconductor $Nd_{1-x}Ce_xCuO_{4-x}$ was first discovered by Tokura [29], a Cu NMR signal for x = 0.15, which had an anomalously small electric quadrupole ($\frac{e2qQ}{h}$) interaction was reported by Zheng [51]. Further work was done by Kohori [48], and two groups of ^{63}Cu signals were found in $(Nd_{1-x}Th_x)_2CuO_4$; one spectrum at $\nu \sim 50$ MHz and a magnetic field of about 5 Tesla, having nearly no electric quadrupole interaction, and one broad nqr spectrum distributed between 20 – 70 MHz. Finally these findings were confirmed by Abe et al [52]. Since in this compound each Cu atom sits in the centre of a two-dimensional square of O-atoms, a large electric field gradient at the copper nuclei is expected; the absence of an electric quadrupole interaction is to be regarded as anomalous.

6.2 Experimental Procedure

Copper-63 NMR spectra as a function of the angle between an orientation of the magnetically-aligned samples and the magnetic field of 11.74 Tesla have been done. As mentioned earlier in chapter 5, 'Sample Preparation and Characterisation', two sets of samples with nominal fluorine contents of x = 0.1, 0.25, 0.3, 0.4 and 0 were prepared. Four different orientations between the field and the marked axis of alignment were chosen, i.e. 0°, 22.5°, 45°, 67.5° and 90°. All the data were acquired at room temperature and processed using the Bruker MSL–500 system[1]. The copper resonance is known to be very broad, which is why each ^{63}Cu frequency spectrum needs to be constructed by per-

[1]A detailed descrition of the hardware and the pulse program can be found in chapter 2, 'Devices for NMR Studies–Hardware'.

forming a point by point sweep through the region of interest. Figure 6.1 shows as an example of the single spectra for the set of orientations, showing those of $Nd_2CuO_{3.7}F_{0.3}$. The narrow peak at 0° broadens at larger angles and finally a second peak appears. This time the spectrometer frequency increases incrementally in narrower steps than necessary. For all subsequent measurements the step-width will be moderately wider, namely 100 kHz. The spectra gathered will be discussed in the subsequent section.

In addition, the spin-spin relaxation time T_2 of each sample is measured at room temperature using the same hardware but different software. The frequency has been chosen according to the peak frequency of the previously collected spectra. No angular dependence could be seen when plotting the relaxation times versus the different orientations (see figure 6.2).

6.3 Results

The resulting angular-dependent spectra for the chosen orientations and the random spectrum are superposed and plotted together in one diagram. An example[2] for one of the samples (x = 0.3) is shown below in figure 6.3. Similar spectra are obtained for x = 0.4, 0.25 and 0.1. They can be found in appendix E. When the spectrum is broadened widely as is the case here it is necessary to make corrections to obtain a true spectrum. First attempts to deconvolute the spectra are done using the method mentioned in [48]. Based on the assumption that the spectra are generated by a second-order quadrupolar

[2]The spectra for 22.5° and 67.5° are omitted for reasons of clarity.

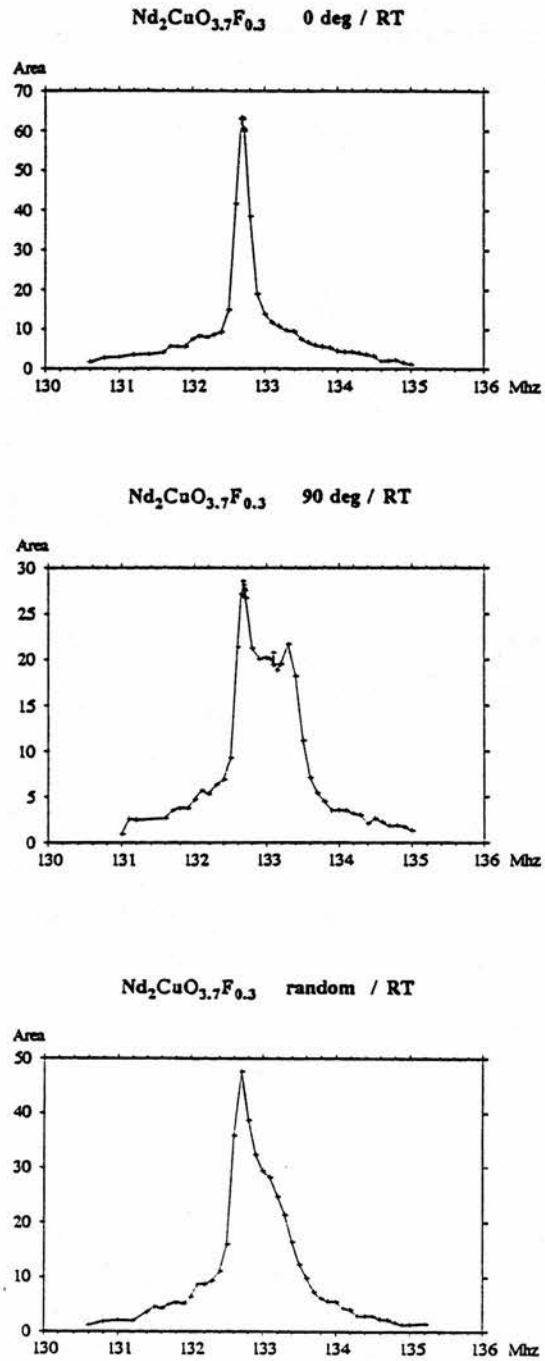

Figure 6.1: Different orientations

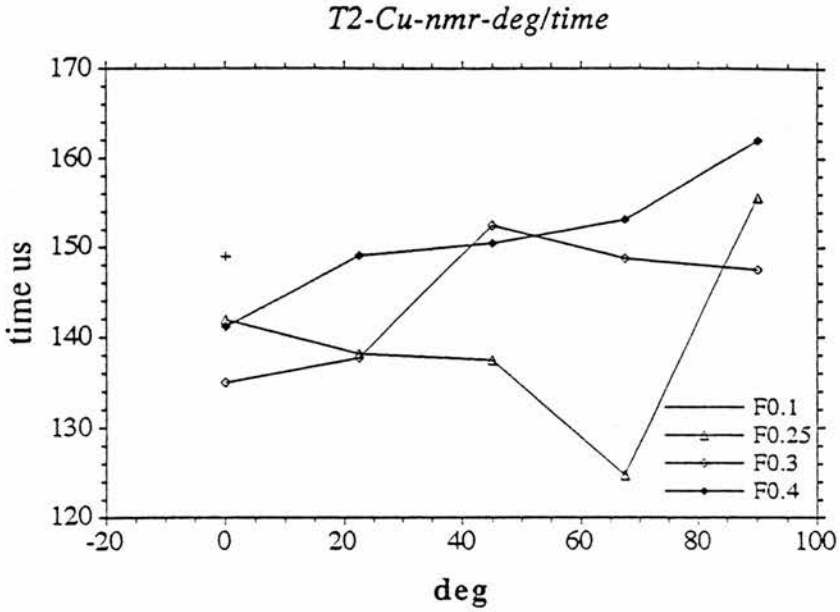

Figure 6.2: T_2 measurements

distribution plus same random fraction due to imperfect alignment, subtracting a small random fraction ρ from the partially aligned orientation dependence spectra should give the 'pure' aligned spectra. Strangely, it was not possible to obtain an orientation-independent value ρ of the random fraction. A common feature of the spectra obtained is the relatively narrow line when the axis of alignment and the applied field of the NMR experiment are parallel to each other, but which grows much broader when orientated away from the field. Reconsidering the features seen, the hypothesis is formulated that the c-axis of the crystallites were orientated perpendicular to the alignment axis. Thus a single-crystal-like spectrum was seen for **B** applied parallel to the alignment axis whereas a two-dimensional powder spectrum was obtained for **B** applied perpendicular to the alignment axis.

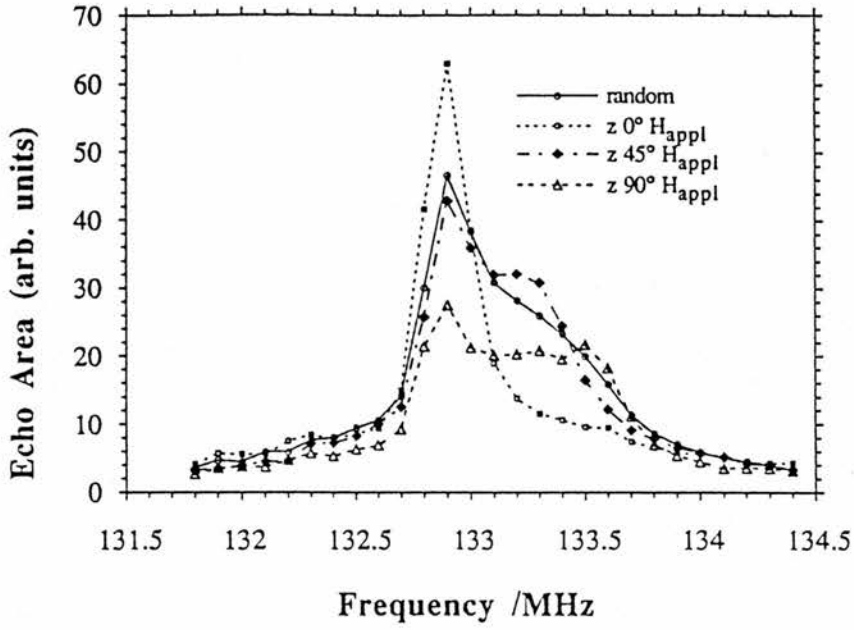

Figure 6.3: Copper-63 NMR spectra of $Nd_2CuO_{3.7}F_{0.3}$

6.4 Discussion

Given the fact that the c-axis in the aligned powder lies perpendicular to the alignment axis then the NMR spectra are expected to appear as follows:

- With the magnetic field B applied parallel to the alignment axis, meaning the electrical field gradient (efg) axis is perpendicular to the field (Θ), a sharp NMR line should be observed.

- When the field is applied perpendicular to the axis of alignment, meaning the efg axis lies anywhere along the radii of a circle of possible directions, with the magnetic field B also along a radius of this circle, a two-dimensional random powder pattern should be observed. For random powder samples the resonance line shape consists of contributions

from all the crystal orientations possible, with their intensity $I(\nu)$ proportional to $\left(\frac{\delta\nu}{\delta\theta}\right)^{-1}$, the resulting line shape is shown in Carter [54] p. 67.

- Intermediate orientations in between the two extrema should show the angular dependence of the second-order quadrupole interaction.

- For the random samples having crystallites randomly distributed, i.e. three-dimensional, a two peak spectrum as described in [54] should show up.

At first glance the experimental spectra (see figure 6.3) are qualitatively conforming to the given description. Nonetheless, they fail to follow in some crucial datails:

- When considering a series of lineshape functions with combined and weighted quadrupole and axial shift interaction as given by Carter [54], p. 91, the random powder seems to bear a much greater resemblance to the pattern from a *positive anisotropic magnetic shift distribution* than from a *quadrupolar orientation distribution.*

- The narrow spectrum (c-axis perpendicular to the applied field B) is situated at the **low** end of the frequency range from ~132–134 MHz. For second order quadrupolar distributions, the orientation where the principal axis is perpendicular to the applied magnetic field B gives the **highest** shift in frequency i.e. the narrow line would appear at the **high** end of the frequency range.

- It is noted that the narrow peak (z 0°) coincides with the large peak of the random powder distribution (see figure 6.3).

- The angular dependence of the spectra correspond to that expected from an anisotropic magnetic shift distribution, with a monotonic shift of spectral weight to higher frequency as the sample is turned from parallel to **B** to perpendicular to **B**. This is different from the expected behaviour of a second order quadrupolar distribution described in [55].

- In the frequency range of 17.5 MHz to 62.6 MHz no nuclear quadrupole resonance (NQR) spectra could be found.

From the results of the above discussion a model can be drawn, its drawings are given in figure 6.4. They are based on the presumed alignment, qualitatively modelling the spectra in relation to the angle enclosed by the crystallite c-axis and the magnetic field (z-axis). We assume that the shapes are due to an anisotropic shift pattern, rather than a second order quadrupolar pattern. Firstly the possible c-axis orientations lie in a circle (x-y plane) leading to the narrow spectrum observed. The second drawing shows the same circle, this time with the angle between the circle and z-axis as 45°. Now the crystal c-axis is distributed between 45° and 135° with respect to the magnetic field. These orientations can be described by the opening of the solid angle with its origin at the circle centre. In the random sample, assuming the crystallite c-axis is equally distributed around a unit sphere then there is a higher possibility of finding the c-axis at 90°. Therefore intensities will be larger for 90° and decline at smaller angles.

Moving on to confirm the presumed alignment scenario a second set of X-ray diffraction was done on the aligned samples by slicing them in a different manner. The whole procedure and their results are described in detail

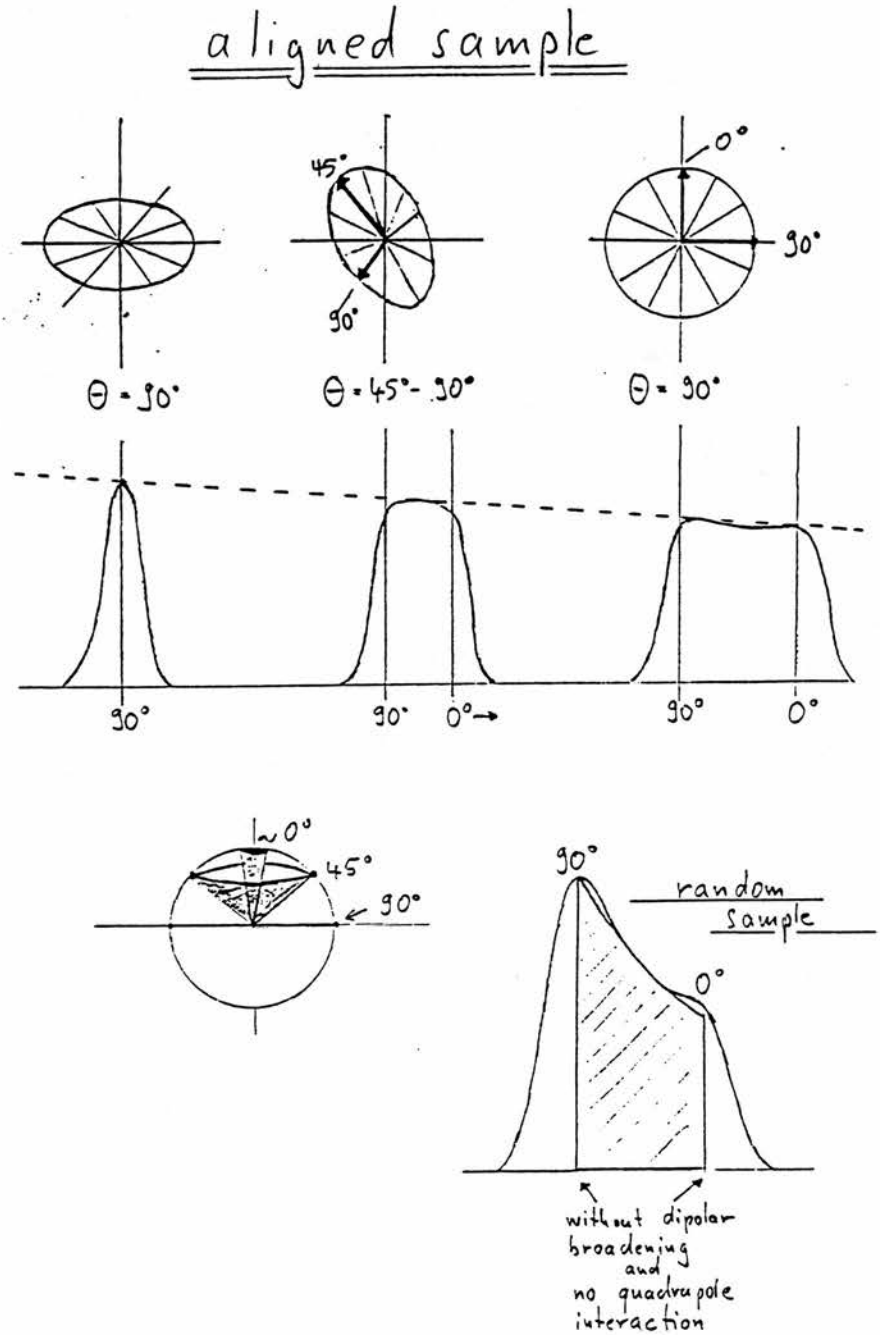

Figure 6.4: Modelling the spectra

in chapter 5. It could be confirmed that the alignment axis was not the c-axis, rather the c-axis aligns perpendicular to the field of alignment.

6.5 Conclusion

Finally, it is concluded that the spectrum is dominated by an anisotropic magnetic shift and that quadrupole interactions are to be considered minimal. Furthermore the spectra given in figure 6.3 are consistent with this hypothesis insofar as:

- In cases where the principal axis of the magnetic shift tensor and the magnetic field direction are lying in the same plane, i.e. z at 90° to **B**, the lineshape is a two-dimensional powder pattern. Such a case has line intensities proportional to $\left(\frac{d\nu}{d\Theta}\right)^{-1}$. Here the relation between resonance frequency ν and angle Θ [$\angle$ = (principal axis, **B**)] is given by the anisotropic magnetic shift from $\nu = (constant)\,(3\cos^2\Theta - 1)$. Therefore the powder pattern is easily established as involving two square root infinities at either end of the spectrum, having one when $\cos\Theta = 0$ and the other when $\sin\Theta = 0$. As can be seen in figure 6.3, two such peaks are distinguishable in the spectrum with **B** perpendicular to the z axis.

- For sample orientations where the principal axis is perpendicular to the magnetic field (z 0° **B**) everywhere a single-crystal-like spectrum (narrow line) is predicted and can be seen in figure 6.3.

- Intermediate orientations: The $\cos\Theta = 0$ singularity of the powder spectrum is predicted to remain but not the $\sin\Theta = 0$ singularity. Because of

this, the $\Theta = 0°$ contributions cease to exist, narrowing the spectrum by losing the high frequency end (see figure 6.3).

- The following shift parameters with an associated error of approximately 10%are obtained from fitting[3]:
  $K_{ax} = +1.5 \times 10^{-3}$ and $K_{iso} = +4.0 \times 10^{-3}$
  $K_{\perp} = +2.5 \times 10^{-3}$ and $K_{//} = +4.0 \times 10^{-3}$

Now the question arises as to what extent quadrupolar interactions might be hidden within the data, even though the spectra appear to show only anisotropic magnetic shifts. The random powder spectrum gives the decisive clue. The article published by Jones [55] in 1963 shows a set of powder spectra drawn for different ratios **r** of anisotropic magnetic shift to quadrupole interaction magnitudes. A comparison of those spectra to the random powder spectrum gives evidence that a spectrum dominated by anisotropic magnetic shift only appears at a ratio r of 4 and larger. The ratio **r** is given as $r = \frac{a\nu_0^2}{b}$, ν_0 is the resonance frequency, $a = \frac{K_{ax}}{(1+K_{iso})}$ and $b = \frac{3\nu_Q^2}{16}$, and ν_Q is the quadrupole resonance frequency. Using the measured K_{ax} and the critria given above, an upper limit for quadrupole interactions in the system under investigation is determined as 6 MHz.

The paper by Yu et al [56], giving theoretical calculations of quadrupole interactions via the FLAPW method[4], makes clear that very small redistribu-

[3]This data has been derived by Dr. Tunstall and G. Dai and does not form part of this thesis.

[4]FLAPW: full-potential linear augmented-plane-wave method.

tions of electron populations around 'semi core' copper states can have a dramatic influence on quadrupolar interactions. Schwarz et al [57] have demonstrated that the dominant influence in determining the electric field gradient around copper sites in high T_c materials is the valence charge distribution on-site; a $3d^{10}$ configuration would therefore have a close to zero quadrupole interaction. Thus the filling up of the 3d shell via electron doping over and above the standard Cu^{2+} of the planes in high T_c materials, would be expected to lead to a small quadrupole interaction.

Finally, when combining the results obtained for the alignment (X-ray study) with a strong shift anisotropy plus a small or even zero quadrupole interaction, a good agreement with the ^{63}Cu NMR spectra is found. A comprehensive report on the results is submitted [58].

Chapter 7

Fluorine–19 NMR on $Nd_2CuO_{4-x}F_x$

7.1 Introduction

As mentioned in chapter 4, it is still unknown whether there are one or two doping sites for fluorine in the crystal structure. Another unsolved question in the same context is the influence of the amount of doping on the occupation of the possible doping sites. Therefore it is of great interest to carry out further investigations in order to solve the questions and their implications for n-type superconductivity.

One promising way to do this is nuclear magnetic resonance on fluorine over a range of temperatures. Of interest are the temperature dependences of the spin-lattice relaxation time T_1 and the spin-spin relaxation time T_2, especially around the phase transition at the critical temperature T_c from insulator to superconductor or vice versa.

7.2 Experimental Procedure

Previous to any measurements being taken, the probe was inserted into the magnet and tuned without loading any sample. This was necessary to check for impurities whose resonances may be picked up by the sample coil. While slowly sweeping the magnetic field through the known resonance frequency of fluorine no signal was seen, proving the absence of any undesired

contaminations in the sample region.

Firstly, the sample with the highest fluorine content was chosen to work out the actual resonance frequency in this compound. A first measurement (see table 7.1) was done on aligned $Nd_2CuO_{3.6}F_{0.4}$ at a temperature of 84.4 K while the probe circuit was tuned to 104.255 MHz. External field and axis of alignment were always kept parallel to each other. When the probe was properly tuned the field strength belonging to the present frequency was calculated and the field very slowly swept through this value until the onset of resonance. The field was varied between 2.5457 T and 2.6417 T. At 2.6010 T, a resonance was seen as a free induction decay (FID) belonging to a resonance frequency of about 40.081 $\frac{MHz}{T}$, proving the existence of a slightly shifted fluorine resonance in the x = 0.4 compound. At the higher field (2.6417 T) an oscillation was superposed on the FID. It was recorded and the plot is shown in figure 7.1.

The resonance frequency of pure fluorine should be seen at 40.078 $\frac{MHz}{T}$. As a matter of interest, a T_1 measurement was done in order to get a rough idea for the next experiments, i.e. to avoid too fast pulse repetition rates in subsequent measurements. The same sample was used between temperatures of 86 – 110 K, a frequency of 104.476 Mhz and a field of 2.5937 T. Then a resonance frequency of 40.281 $\frac{MHz}{T}$ was calculated. The pulse generator was set to produce a comb of sixteen 90° pulses with a spacing of 35 μs. The marked amplitude of the FID decreased from 232 mV at the beginning to 4 mV at the end of the comb, showing a good disturbance of the magnetiziation. Afterwards the recovery of the magnetiziation was observed by an additional 90° pulse and was determined to be about 8 to 9 seconds. Trying a 90° –180° pulse sequence

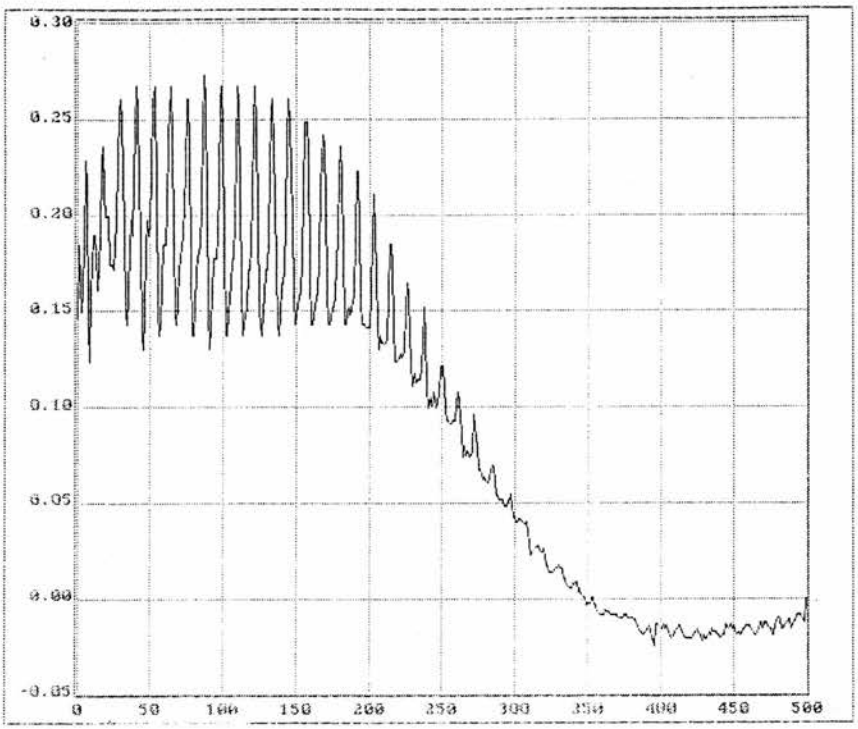

Figure 7.1: Free Induction Decay (FID)

did not lead to a spin echo.

The subsequent measurements were mostly done at lower temperatures, as shown in tables and discussed accordingly. The first two measurements in table 7.1 were done at temperatures between 84 – 110 K. When compared to measurements number 3 – 6 which were done at far lower temperatures, the resonance frequency surprisingly does not differ very much. Nonetheless, resonance frequencies between 40.124 - 40.337 $\frac{MHz}{T}$ were quite close to of pure fluorine (40.078 $\frac{MHz}{T}$).

Until measurement number 16 there is a 90° phase difference between signal and reference to the receiver. Unlike the case for no phase difference, the 'on resonance' FID does not show up in such circumstances. Instead, a flat

Number of measurement	Settings			Resonance
	Kelvin	MHz	Tesla	$\left[\frac{MHz}{T}\right]$
1	84	104.255	2.601	40.081
2	86-110	104.476	2.5937	40.281
3	1.46	101.052	2.5071	40.306
4	1.46	101.053	2.5079	40.294
5	1.46	101.059	2.5099	40.264
6	1.95	101.016	2.5043	40.333
7	1.46	101.059	2.5079	40.294
8				40.287
9	1.46	101.056	2.5086	40.279
10	1.46	101.131	2.5330	39.914
11	1.46	101.131	2.5339	39.911
12	1.46	101.131	2.5348	39.897

Table 7.1: $Nd_2CuO_{3.6}F_{0.4}$ NMR Data

line occurs at exact resonance with up and down 'FIDs' at lower and higher fields. This has been considered insofar as each time two data points are taken and the actual resonance frequency in between them is obtained by averaging.

The last data points in table 7.1 belong to the same measurement. Number 11 is taken right on resonance (flat line on the scope). When comparing the average between #10 and #12 with #11 the resonance frequency differs only by 0.005 MHz and so there is no reason to worry about the phase problem.

The superposed signal was puzzling at first because it was considered to be a second fluorine signal, shifted in frequency but broad enough to cause the pattern shown in figure 7.1. It was necessary to evaluate whether the signal was to be found at lower or higher frequency. To do so the beating was counted whilst on and off resonance, i.e. the beating frequency should be higher when

getting closer to the shifted resonance. However no clear indication of the shift direction could be obtained. Frequencies between 1.0 and 2.38 MHz were determined at a temperature of 1.46 Kelvin. Later it was determined to be a proton signal caused by the Stycast.

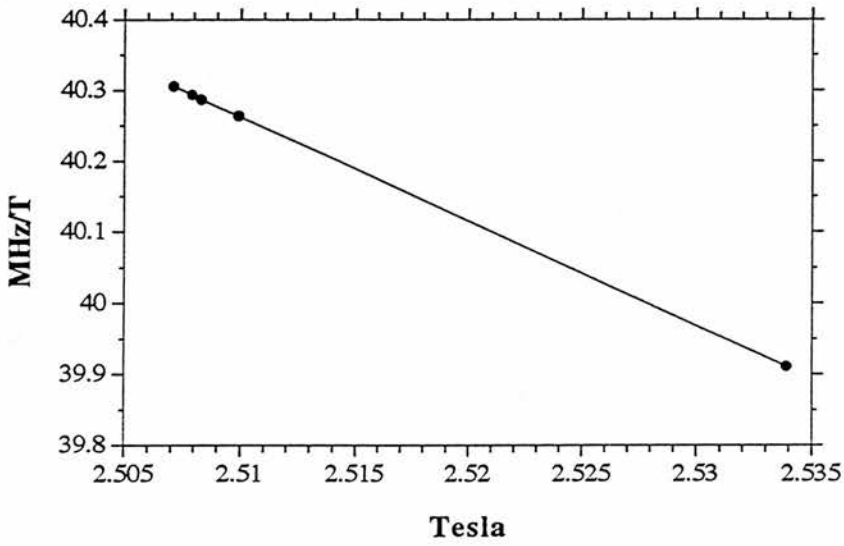

Figure 7.2: $Nd_2CuO_{3.6}F_{0.4}$ – Field dependence

From table 7.1 it can be shown that there is a dependence of the applied field strength on the resonance in $\frac{MHz}{T}$, in so far as at the same temperature (1.46 K) the actual resonance given in $\frac{MHz}{T}$ decreases whilst increasing the applied rf frequency (see figure 7.2). The higher rf frequency necessitates a higher external field strength to keep the resonance condition ($\nu \sim \mathbf{B}$). When bearing in mind the paramagnetic property of neodymium, the polarization of Nd moments obviously adds a magnetic field to the external field ($\mathbf{B}$) at the fluorine sites. Therefore, at higher field, resonance was found at a smaller $\frac{MHz}{T}$

ratio. After the completion of the experiments, it was discovered that the data should have been acquired at the same field.

Subsequently, calcium fluoride (CaF_2) was chosen as a reference sample for the fluorine NMR on $Nd_2CuO_{4-x}F_x$. Calcium fluoride powder was loaded into a quartz glass sample holder and the open end was sealed with Stycast. As can be seen in table 7.2, at 1.48 K a resonance frequency of 40.133 $\frac{MHz}{T}$ was measured. As in the previous measurements a superposed beating pattern occured. For the samples under investigation two distinct sites are likely to be doped with fluorine but there is only one site in calcium fluoride, giving clear evidence that the superposed signal is not due to fluorine nuclei.

Number of measurement	Settings			Resonance
	Kelvin	MHz	Tesla	$\left[\frac{MHz}{T}\right]$
13	1.48	99.250	2.4726	40.140
				40.133
14	1.48	99.250	2.4735	40.125

Table 7.2: CaF_2 – Reference sample

After changing the sample a third time (x = 0.1), data was acquired between temperatures of 4.3 and ~11 Kelvin (see table 7.3). A fluorine resonance (see table 7.3) was found at both temperatures. Unfortunately the given data was acquired at different fields. It therefore does not allow any statement about temperature dependent frequency shifts in this compound (x = 0.1). In order to calibrate the magnetic field, a reference signal has to be available while doing an actual measurement on the sample, therefore $Nd_2CuO_{3.7}F_{0.3}$ was wrapped with PTFE tape. Subsequently different combinations of field

Number of measurement	Settings			Resonance $\left[\frac{MHz}{T}\right]$
	Kelvin	MHz	Tesla	
15	~4.2	102.997	2.5728	40.033
				40.026
16	~4.2	102.997	2.5738	40.018
17	10.86	102.155	2.5186	40.559
18	10.86	102.150	2.5240	40.470
19	10.86	102.150	2.5272	40.420
20	10.44	102.155	2.5189	40.556

Table 7.3: $Nd_2CuO_{3.9}F_{0.1}$ NMR Data

and frequency were recorded (see table 7.4). Due to a lack of time no more measurements on $Nd_2CuO_{3.7}F_{0.3}$ could be taken.

Number of measurement	Settings			Resonance $\left[\frac{MHz}{T}\right]$
	Kelvin	MHz	Tesla	
21	6.56	99.614	2.4901	40.003
22	6.56	101.505	2.5394	39.972
23	6.56	102.905	2.5717	40.014
24	6.56	104.507	2.6147	39.969
25	6.56	105.746	2.6392	40.067
26	6.56	107.201	2.6816	39.976

Table 7.4: $Nd_2CuO_{3.7}F_{0.3}$–Calibration with PTFE

7.3 Conclusion

The constraints of a one year project have left the data presented in this chapter incomplete, i.e. the experiments could not be performed to the extent originally planned.

Two out of four fluorinated samples (x = 0.4 and 0.1) were used for ^{19}F NMR; fluorine resonances were found in both compounds. The x = 0.3 compound was prepared with PTFE as a permanent reference source. Unfortunately there was not sufficient time available to carry out tests on this sample.

A transferred magnetic field due to the polarization of the paramagnetic neodymium moments was found at the fluorine sites, causing the ratio of applied rf and external field $\frac{MHz}{T}$ to decrease whilst increasing the external field strength. Unfortunately this fact was evaluated too late to be considered in the actual measurements.

Chapter 8

Final Conclusion

8.1 Conclusion

Right at the beginning of the project it was decided to use a newly acquired Magic Angle Spinning (MAS) probe for ^{63}Cu and ^{19}F NMR measurements on the electron-doped superconductor $Nd_2CuO_{4-x}F_x$. Despite the great amount of time spent on setting it up, learning how to use it and testing its performance, it could not be used due to the failure to comply with crucial specifications. Nonetheless the previously built spectrometer could be used after some alterations had been made. Subsequently, a new NMR probe was designed, built and tested. The probe was especially designed to match the demands of the planned experiments. For the probe circuit, a series-parallel arrangement of match and tune capacitor was chosen. Calculations were done to obtain a 50 Ω system, to match the spectrometer used. The homemade probe showed very good performance during testing as well as during the actual experiments. The tuning was precise and easily done within a broad range of frequencies available. Once tuned, it remained stable for a long time. The maximum tuning frequency was found to be $\sim$112 MHz, giving access to high field NMR with all its advantages. With the capacitors close to the sample coil very good tuning obtained, enabling easy rf power transfer, making remarkably short pulses possible. When exposed to thermal cycling and heavy duty use,

the electronic equipment within the sleeve was reliable and worked well. The in-built heater system and temperature sensors covered the region of interest very well, i.e. below and above the critical temperature T_c. At higher temperatures, the helium consumption was found to be quite high. For further work an attempt should be made to use less helium as exchange gas.

The signal to noise (S/N) ratio of the spectrometer was excellent. Furthermore, the breakthrough during pulses was small and the recovery time after pulses was very short. Various pulse sequences were set up and displayed on the oscilloscope with great ease. Data could be transfered to a PC, where a fast Fourier transform algorithm (FFT) was available.

Pseudo-single-crystals with identical grain orientations were obtained by aligning the grains in a strong external magnetic field and 'freezing' the single crystals in an epoxy resin. These preparations were necessary for the performance of angle dependent copper-63 NMR studies. The quality of alignment was confirmed by comparing the X-ray spectra of random powder and aligned samples. It was found to be very good.

Extended angle dependent copper-63 NMR studies at room temperature (RT) were done on the complete set of samples. Each spectrum was constructed by performing a point by point sweep through the region of interest. The resulting angular-dependent spectra were firstly treated to be generated by a second-order quadrupolar interaction. This approach failed to explain the derived data. Next the hypothesis was formulated that the c-axis of the crystallites had orientated perpendicular to the alignment axis. Taking into account the assumed alignment and an electric field gradient perpendicular to

the axis of alignment, a qualitative description was proposed, confirming the data. However it failed to follow in very crucial details. After reconsidering the results, a model was developed using the assumption that the line shapes are due to an anisotropic shift pattern, rather than a second order quadrupolar pattern. The assumed alignment scenario was proven by cutting the samples differently and performing a second set of X-ray spectra. The alignment differed from that of YBCO and its derivatives, and could be explained by the sign of the second order Stevens factor of Neodymium. Finally, when combining the results obtained for the alignment with a strong shift anisotropy plus a small or even zero quadrupole interaction, a good agreement with the NMR spectra was found. Studies are presently in progress on the temperature dependence of the results described above.

Further NMR studies were done at low temperatures on ^{19}F. Two out of four fluorinated samples were used. In both compounds fluorine resonances were found. The comparison of data acquired at the same temperature allowed the evaluation of a transferred magnetic field onto the fluorine sites. It is found to be due to the polarization of the paramagnetic neodymium moments in the external field. A dependency of the applied field strength on the resonance in $\frac{MHz}{T}$ could be established. More measurements are desirable and the extra magnetic field should be considered in order to obtain comparable data. They therefore need to be carried out at the same field strength.

Appendix A

Pulse Program MSL 500

A.1 Spin Echo Pulse Program for ^{63}Cu

```
        - - - - FILE: SAM1ECHO.PC
; HAHNECHO:PC
; TWO PULSE SPIN-ECHO TECHNIQUE FOR REMOVING
; BASELINE DISTORTION DUE TO RINGING OF PROBE WITH
; 16 PHASE CYCLING. REF: A.C. KUNWAR ET AL.,
; JMR 69, 124--127 (1986).
PROT NONE
START,
2U [XT +T]
D1 [F1 @PLS1 XT +X RGATE]; 45 OR 90 DEG. PULSE
D6 [XT +X RGATE] ; TAU DELAY
D2 [F1 @PLS2 XT +X RGATE]; 2 TIMES D1
D3 [XT +X RGATE] ; SECOND TAU DELAY
D8 [STA RGATE] ; ACQUIRE WITH NT
DO
++PLS1
++PLS2
GOTO START
```

```
BEGIN LISTS
PLS1, +X +X +X +X
PLS2, +X +Y -X -Y
RLS, -Y +Y -Y +Y END LISTS
```

A.2 Pulse program for T_2 measurement

SATURATION PULSE RECOVERY PROGRAM

```
PROT NONE
START, 5U [XT +X]
LOOP C1 TIMES
2U [XT +X]
D5 [F1 +X XT +X]; TRAIN OF
SATURATION PULSES
D20 [XT +X]; PULSE SEPERATION
END LOOP
VD [XT +X]
D1 [F1 @PULSE1 XT +X +X RGATE]; VARIABLE RELAXATION
DELAY
D6 [ST +X RGATE]
D2 [F1 @PULSE2 XT +X RGATE]; 2 TIMES D 1
D3 [XT +X RGATE]
D8 [STA RGATE]; DEADTIME DELAY AND TRIGGER
D0
++PLS1
++PLS2
```

```
GOTO START
BEGIN LIST
PLS1 +X +X +X +X
PLS2 +X +Y -X -Y
RLS -Y +Y -Y +Y
END LIST
```

AUTOMATIC ACQUISITION PROGRAM--TONEAQ:AUM

```
FD 1
1 ZE ; CLEAR DATA
2 VD ; GET VD FROM LIST
3 GO ; AQUIRE DATA
4 WR*1 ; SAVE DATA
5 IF*1 ; NEXT
6 IN=1 ; LOOP NE TIMES & INC. VD POINTER
7 EXIT
```

Appendix B

Block Diagram Spectrometer

B.1 Technical Specifications

1. FARNELL SSG 520 Signal generator Frequency range: 10-520 MHz Output: 50 Ω
2. SPLITTER PMD8-2 EIN Rochester
3. WATKINS JOHNSON (wj) S1 Relcom switch
4. TEKTRONICS PG Mainframe with 5 modules connectable via an interconnection board: 2 Pulse generators, 1 Rate/Ramp Generator, 2 Ramp Generators
5. FARNELL PG5122 Pulse generator. Output impedance: 50 Ω
6. PULSE AMPLIFIER Home-made
7. TTL-Box Home-made
8. KALMUS 500 Watt Linear Pulse Amplifier
   Frequency range (bandwidth): 80-200 MHz. Output level: typically 5 dB
9. T-Piece

10. LOW NOISE PREAMPLIFIER (LN-2L), Doty Scientific Inc. Frequency bandwidth: 5-500 MHz. Recovery time: 4 μs. Power gain: approximately 31 dB.

11. PREAMPLIFIER Home-made preamplifier with two Avantek casscade thin film amplifiers. Frequency range: 5-400 MHz. Power gain: 13 dB.

12. VARIABLE GAIN PREAMPLIFIER Home-made variable gain amplifier with two Avantek cascade thin film amplifiers. Frequency range: 5-400 MHz. Power gain: 9 and 13 dB. Placing an Avantek series attenuator in cascade allows attenuation of 30 dB min within a frequency range of 5-400 MHz.

13. MINI CIRCUITS 15542 ZFM-2 DOUBLE BALANCED +7dBm MIXER Frequency range: 1-1000 MHz. Impedance: 50 Ω.

14. LOW BANDPASS FILTER Home-made double filter system to control signal noise and deadtime.

15. HEWLETT PACKARD 54502A DIGITIZING OSCILLOSCOPE
    A 400 MHz, 400 Msample/s digitizing scope with a signal averaging facility and the possibility of remote control by a personal computer.

16. OXFORD INSTRUMENTS 12.7 T CRYOMAGNET Field variable up to a maximum of 12.7 T. Field homogeneity: 1 in 10^5. Bore diameter: 40 mm. Superconducting three coil magnet, in which the outer coil is Niobium tin wound and the inner is niobium titanium wound. Runs from an OXFORD INSTRUMENTS high current water cooled magnet power supply.

B.2 Block Diagram

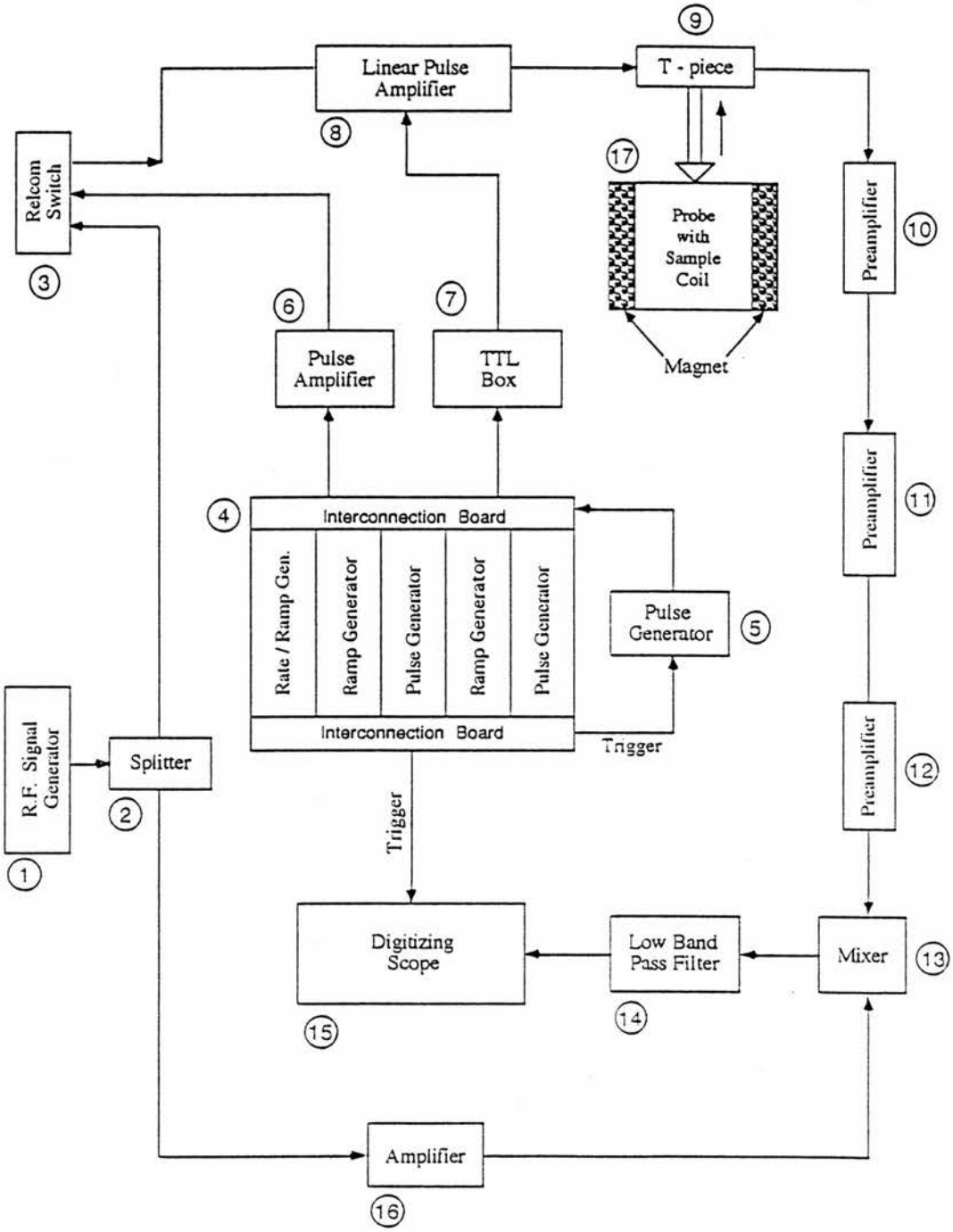

Appendix C

Drawings and Photographs of the NMR Probe

C.1 Drawings

C.1.1 Probe–Top End

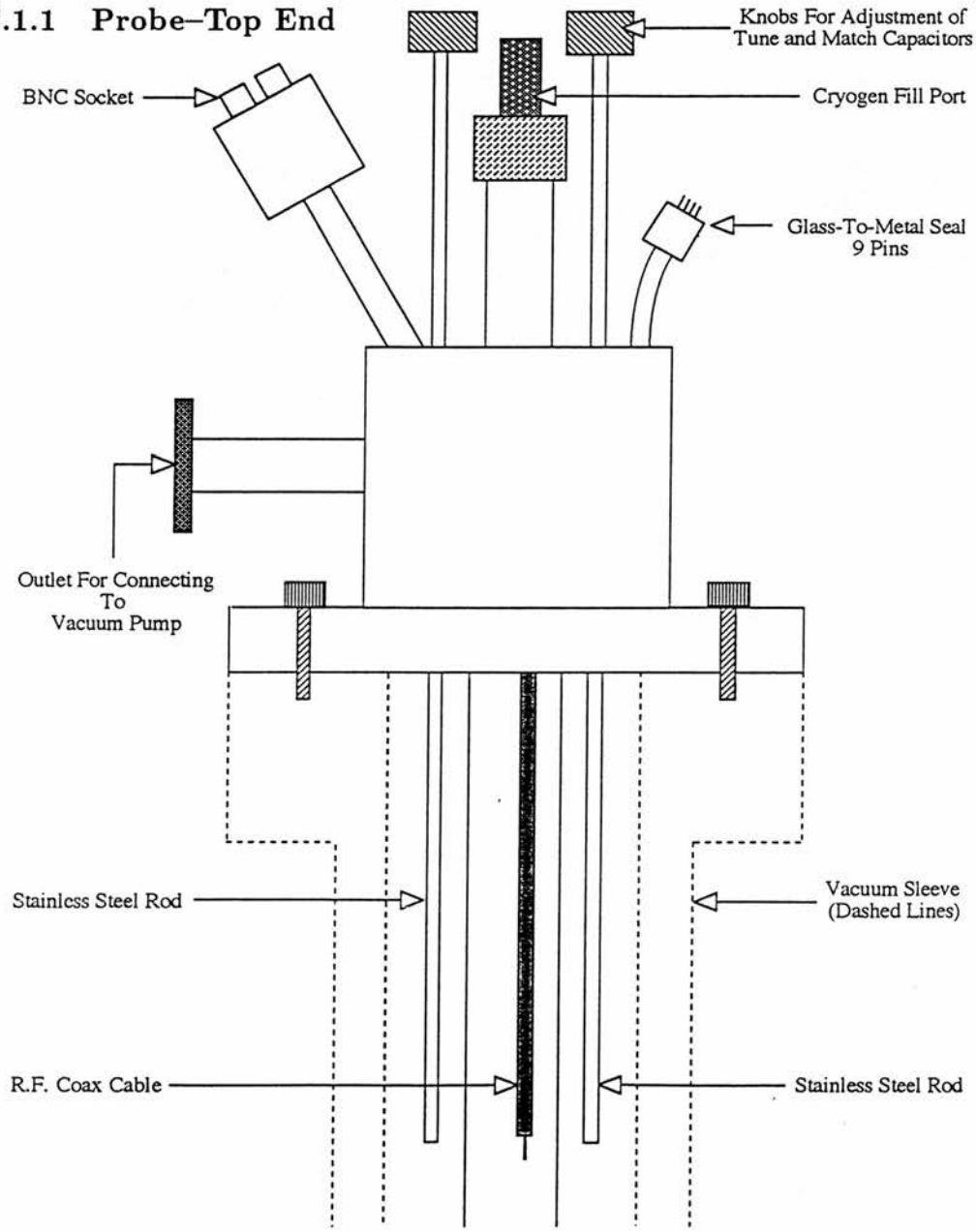

C.1.2 Dipstick

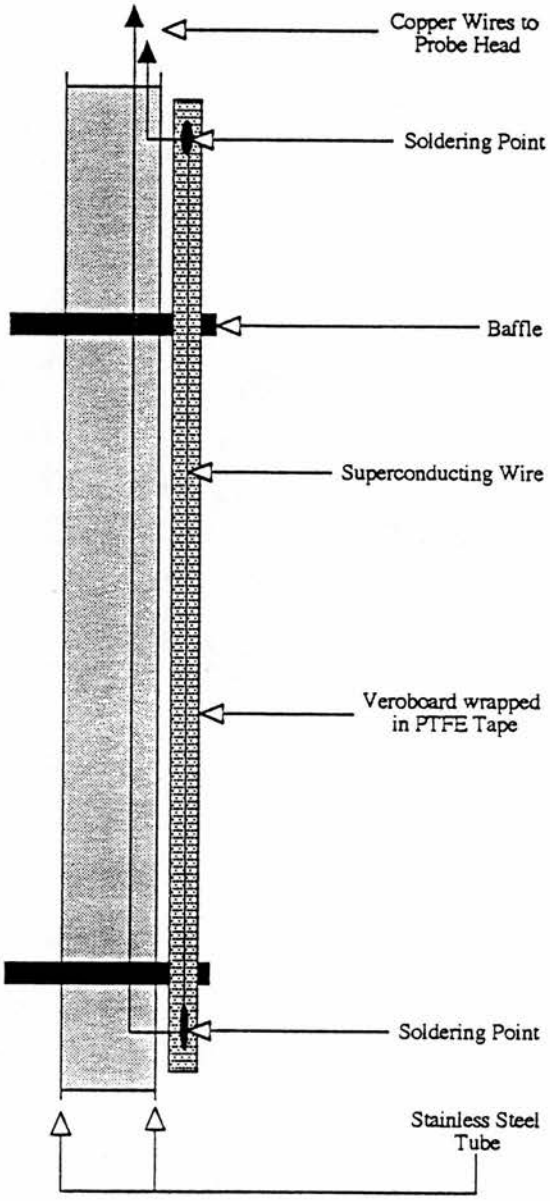

C.1.3 Probe–Bottom End

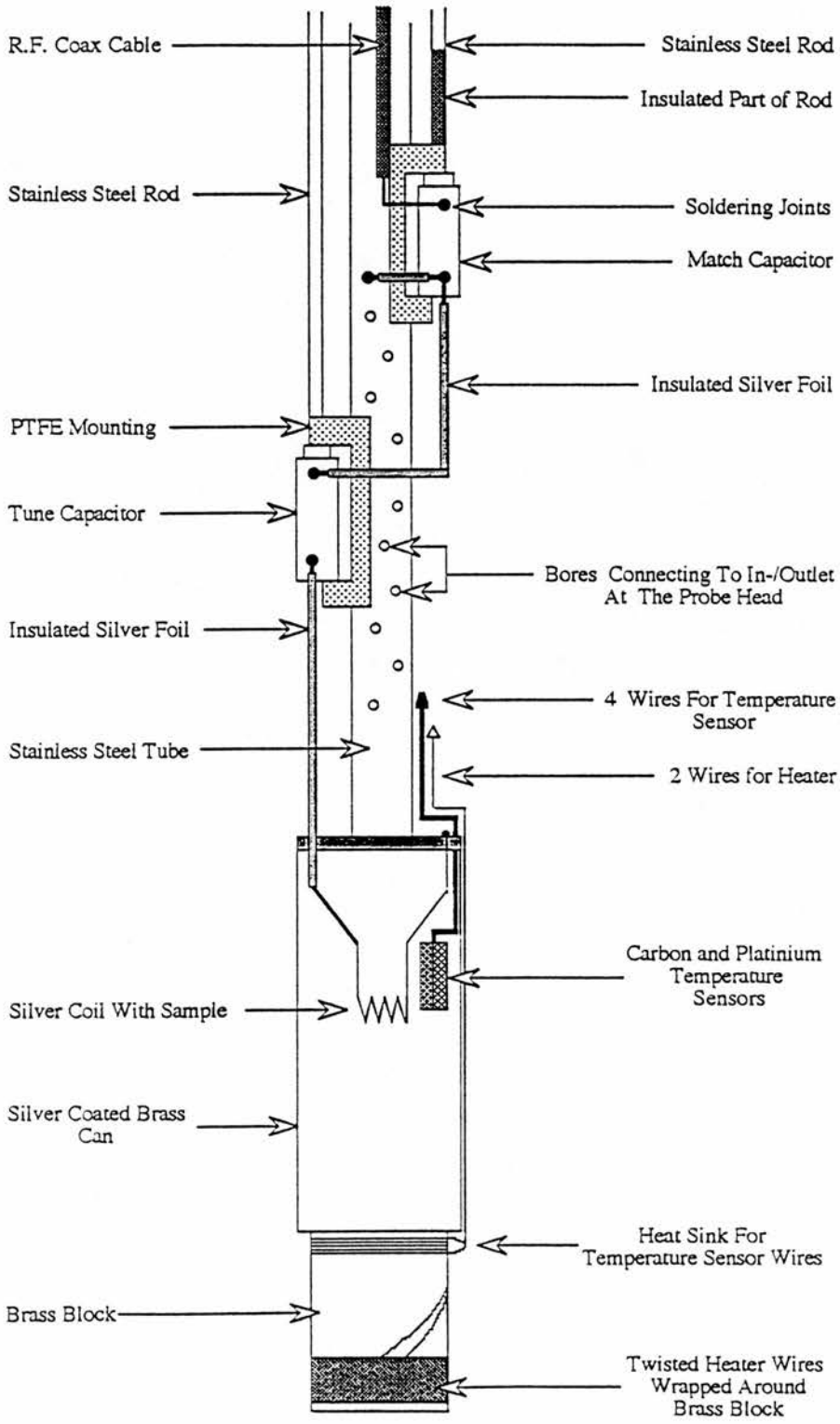

C.2 Photographs

C.2.1 Homemade Probe

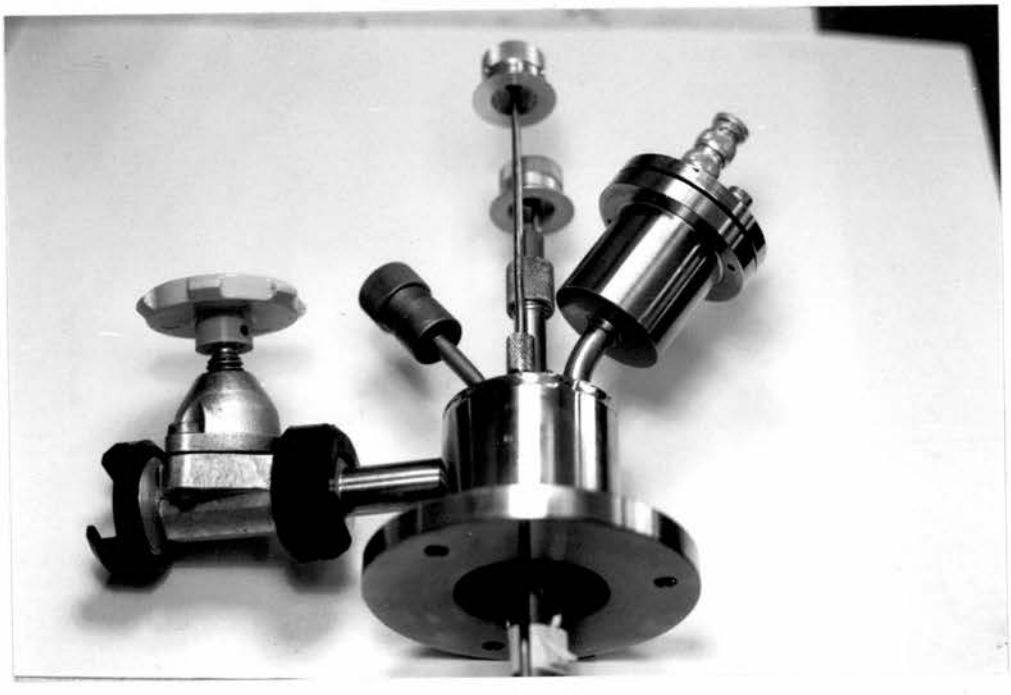

Figure C.4: Probe–Top end

Figure C.5: Probe–Bottom end

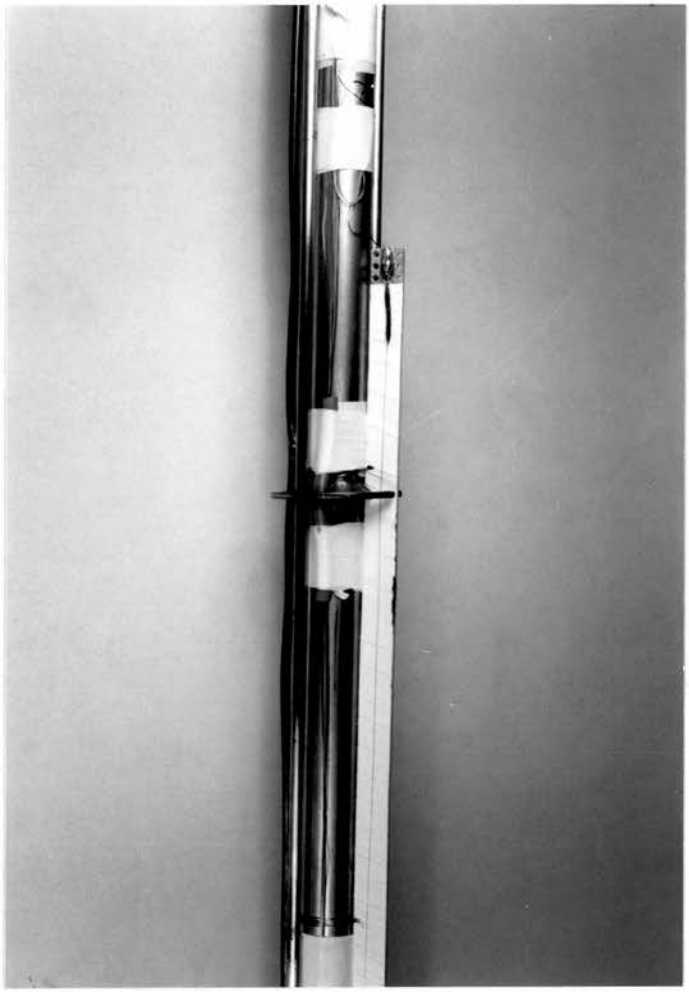

Figure C.6: Dipstick

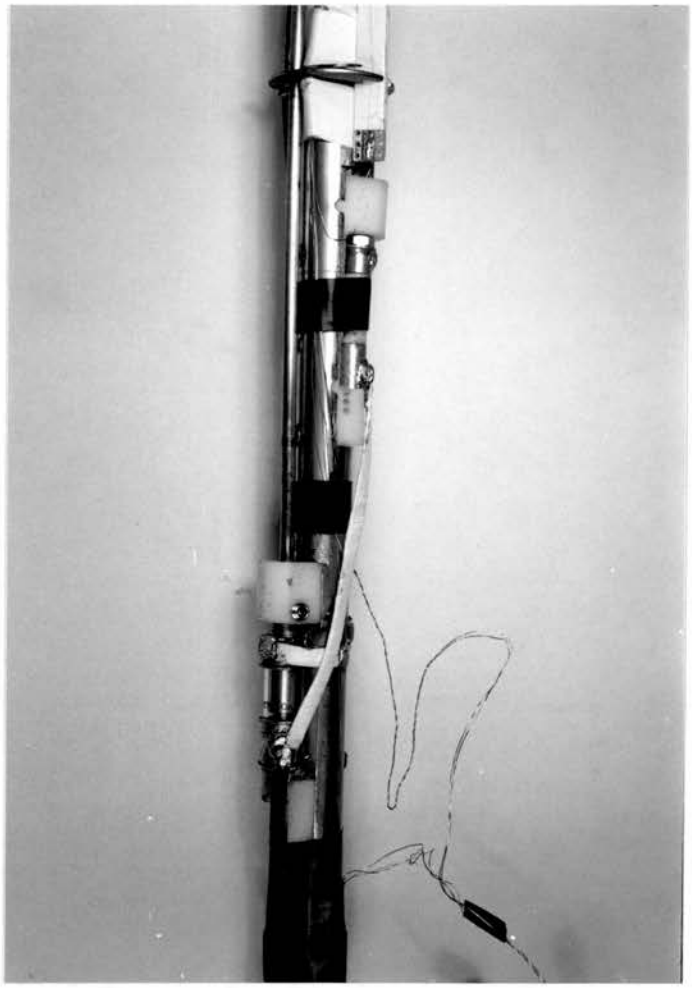

Figure C.7: Circuit

C.2.2 Doty Scientific MAS Probe

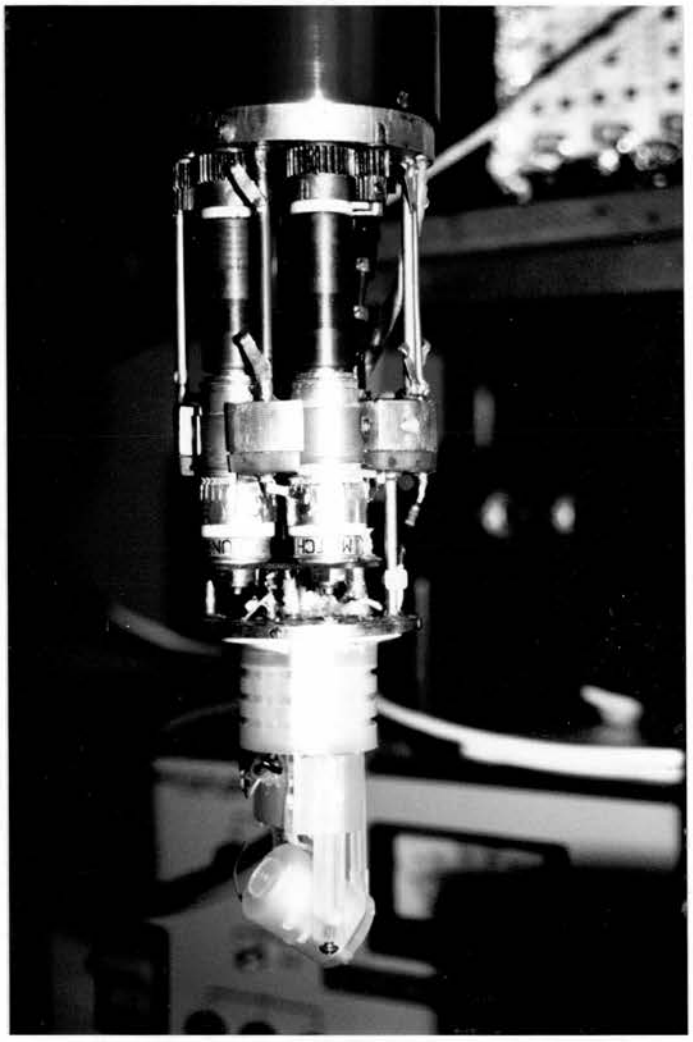

Appendix D

Data – SQUID Measurement

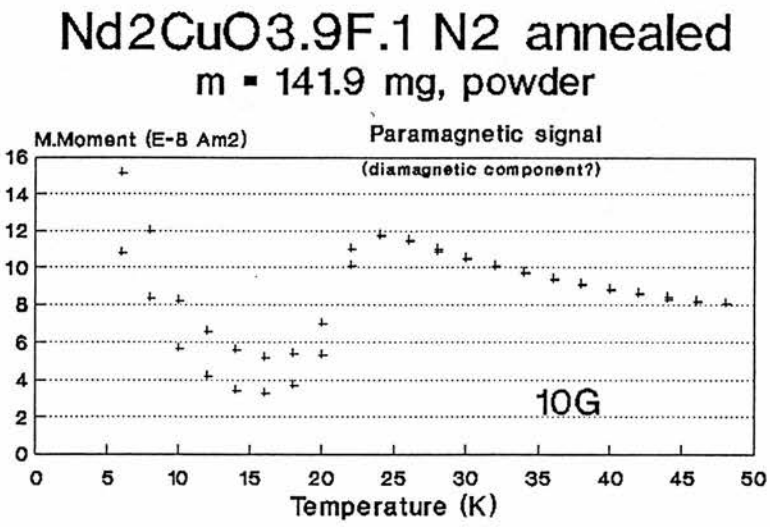

Figure D.1: $Nd_2CuO_{3.9}F_{0.1}$ –T_c measurement

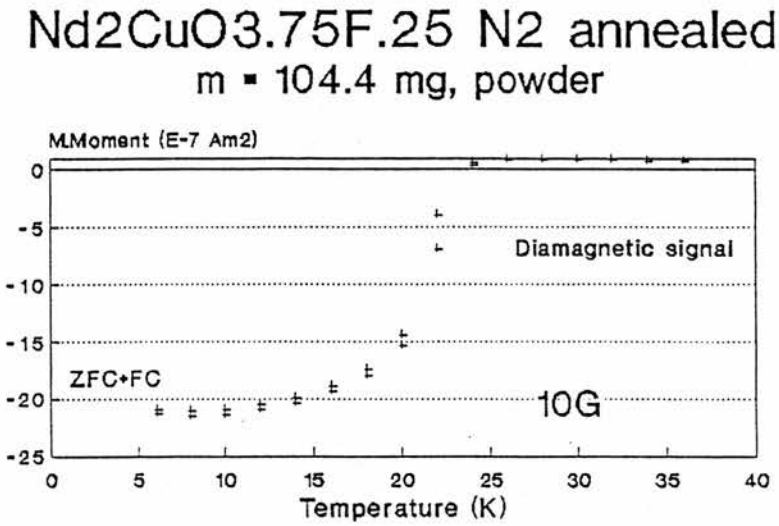

Figure D.2: $Nd_2CuO_{3.75}F_{0.25}$ $-T_c$ measurement

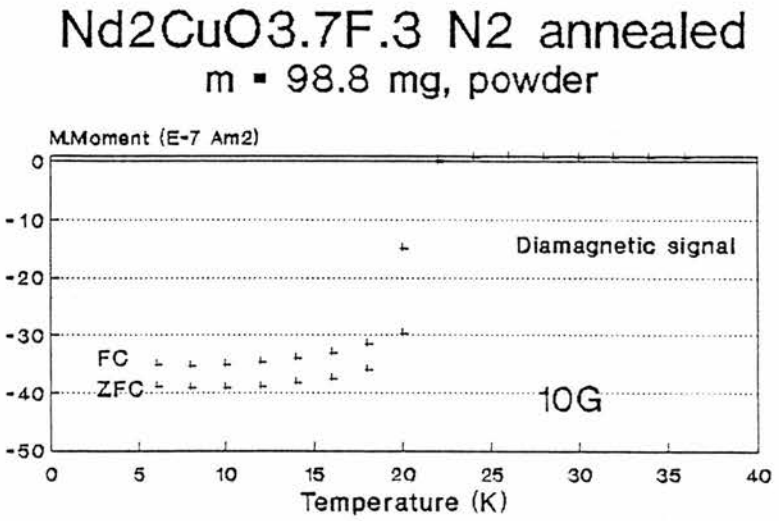

Figure D.3: $Nd_2CuO_{3.7}F_{0.3}$ $-T_c$ measurement

Appendix E

X-Ray Spectra

E.1 Nd_2CuO_4 – X-Ray Spectra

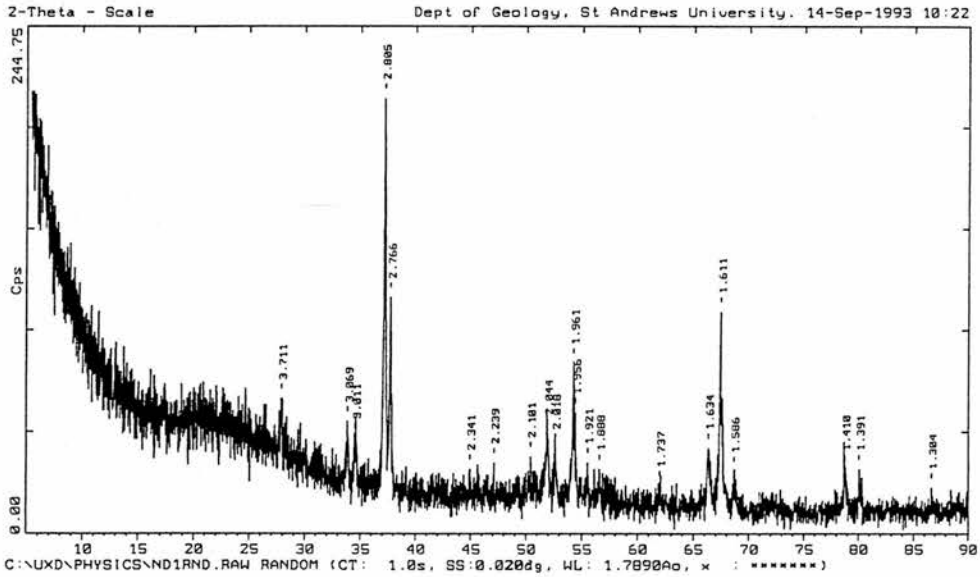

Figure E.1: Random powder – Cutting along the x-y plane

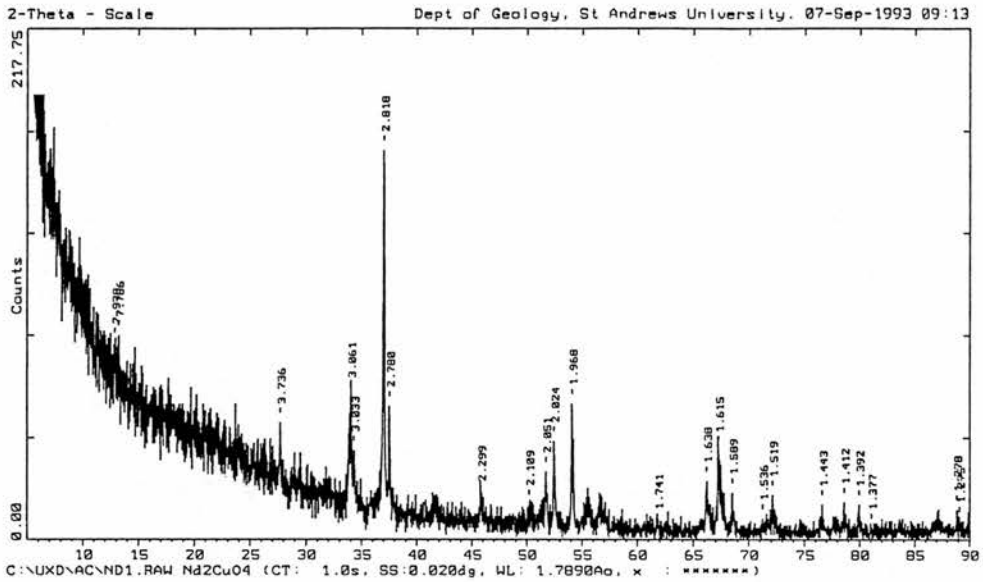

Figure E.2: Aligned sample – Cutting along the x-y plane

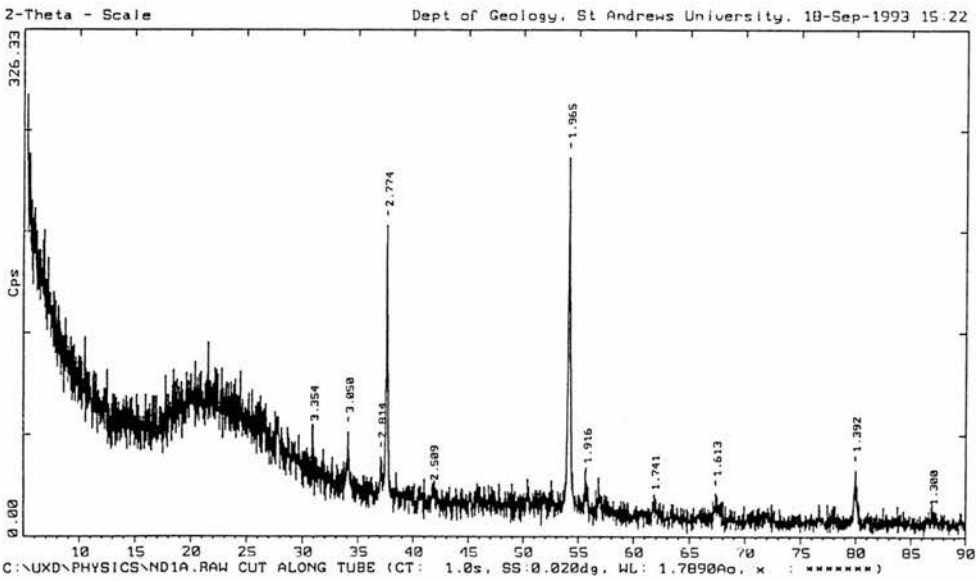

Figure E.3: Aligned sample – Cutting along the y-z plane

E.2 $Nd_2CuO_{3.9}F_{0.1}$ – X-Ray Spectra

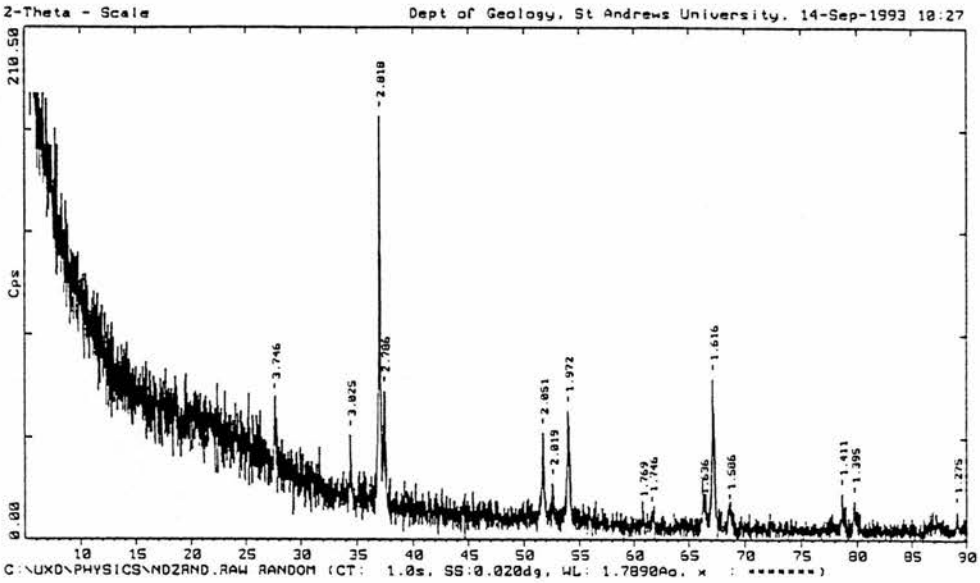

Figure E.4: Random powder – Cutting along the x-y plane

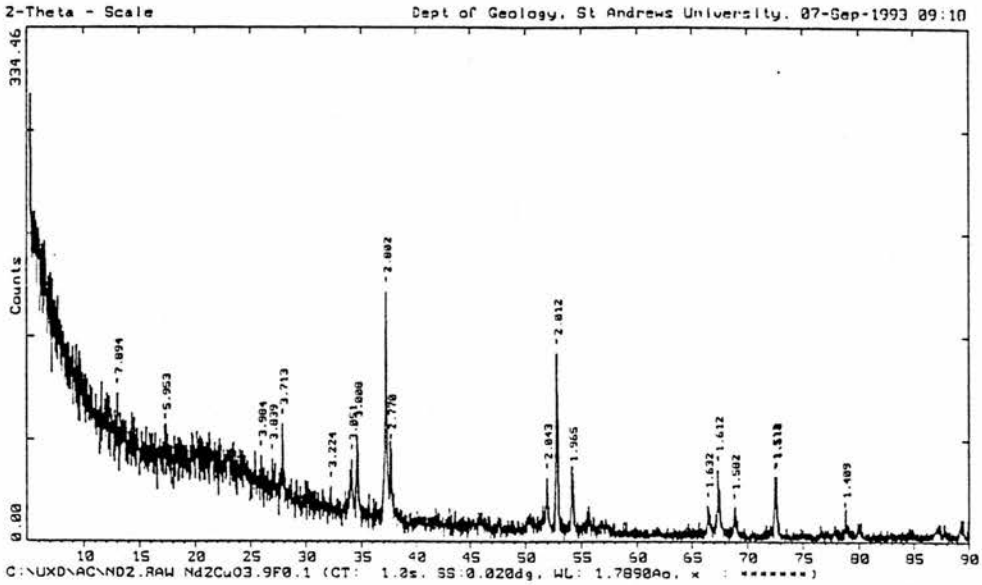

Figure E.5: Aligned sample – Cutting along the x-y plane

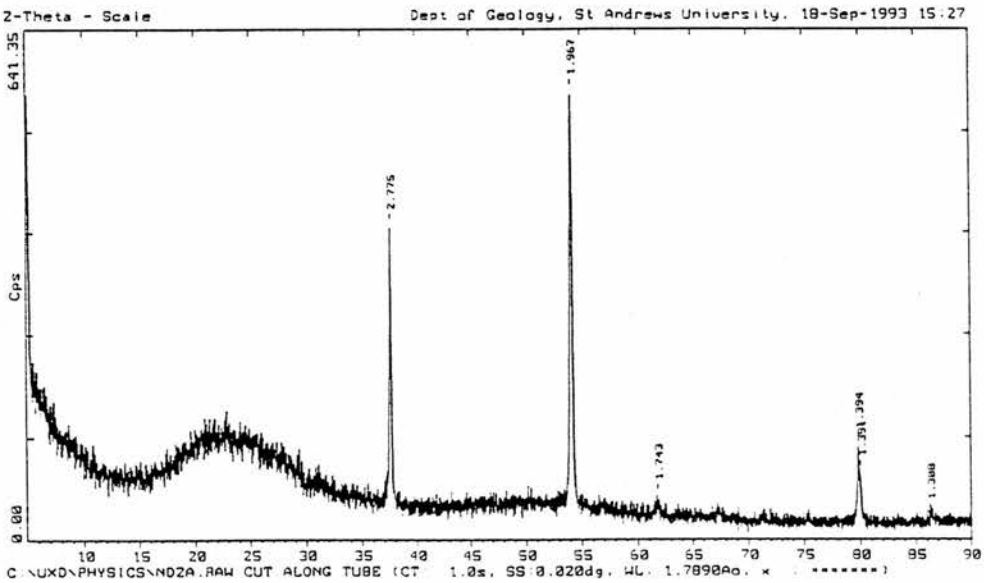

Figure E.6: Aligned sample – Cutting along the y-z plane

E.3 $Nd_2CuO_{3.75}F_{0.25}$ – X-Ray Spectra

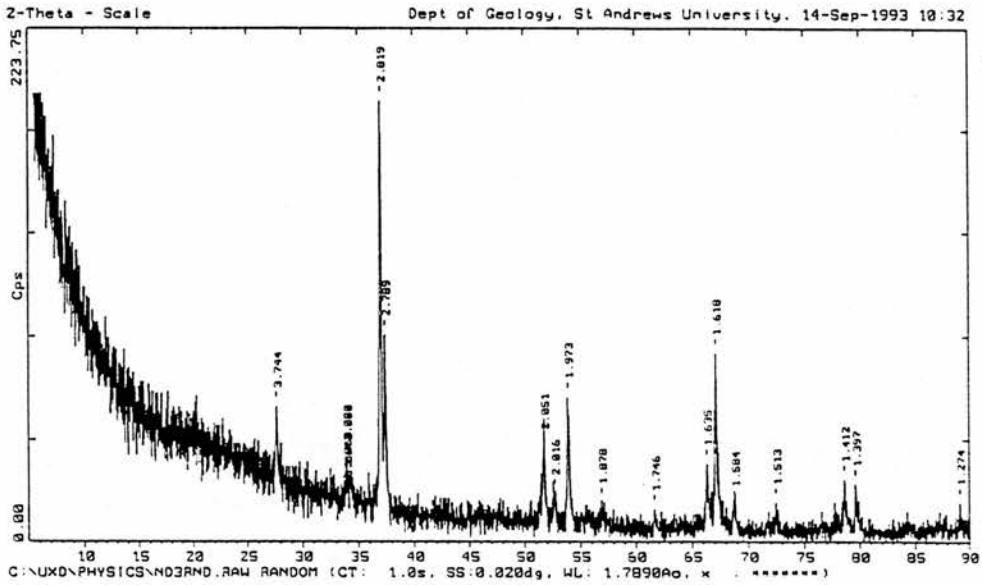

Figure E.7: Random powder – Cutting along the x-y plane

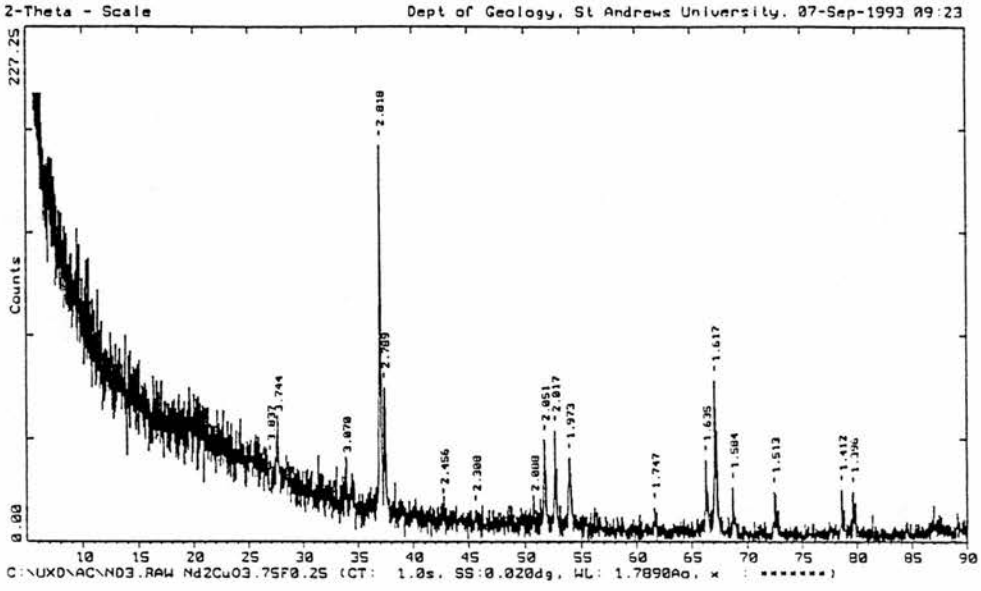

Figure E.8: Aligned sample – Cutting along the x-y plane

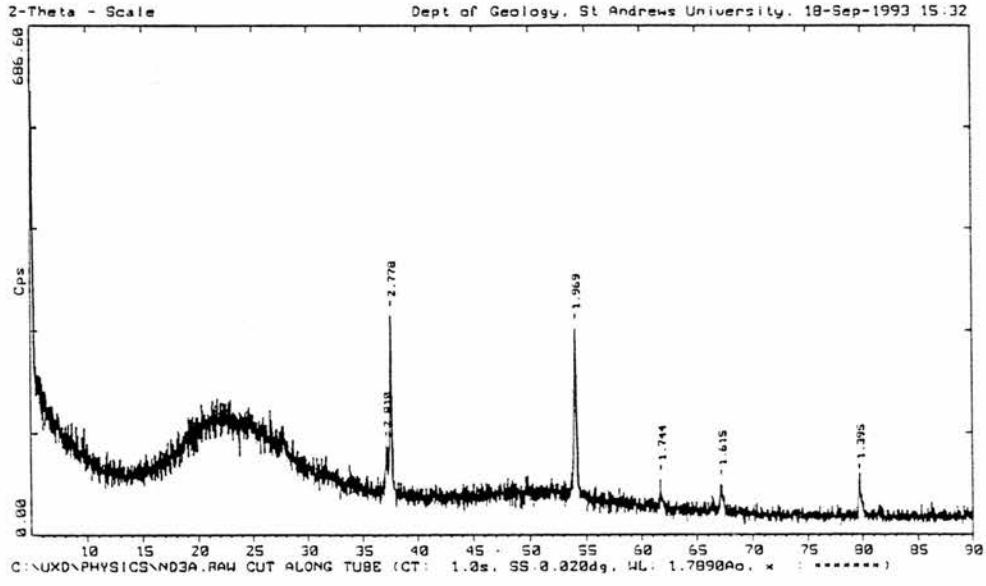

Figure E.9: Aligned sample – Cutting along the y-z plane

E.4 $Nd_2CuO_{3.6}F_{0.4}$ – X-Ray Spectra

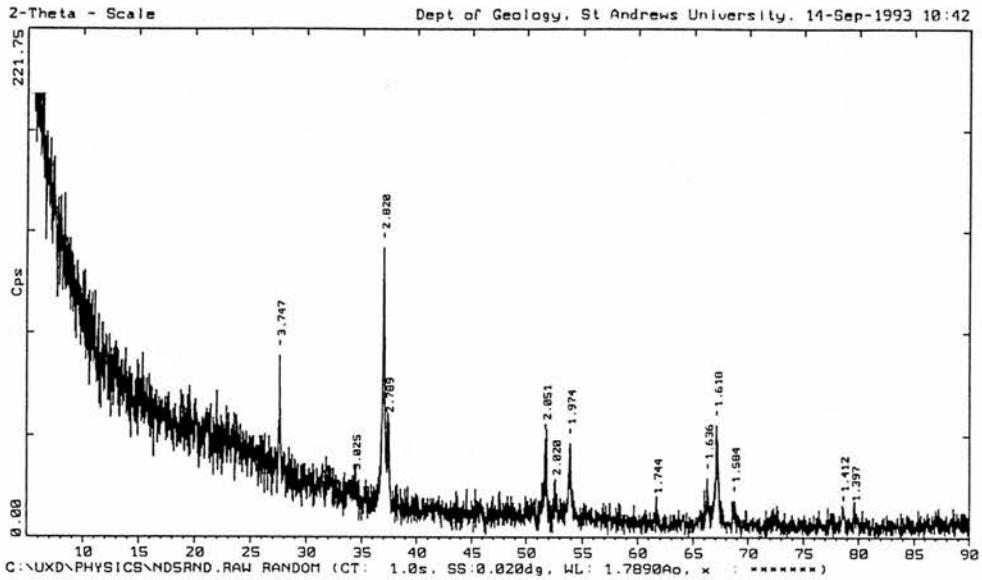

Figure E.10: Random powder – Cutting along the x-y plane

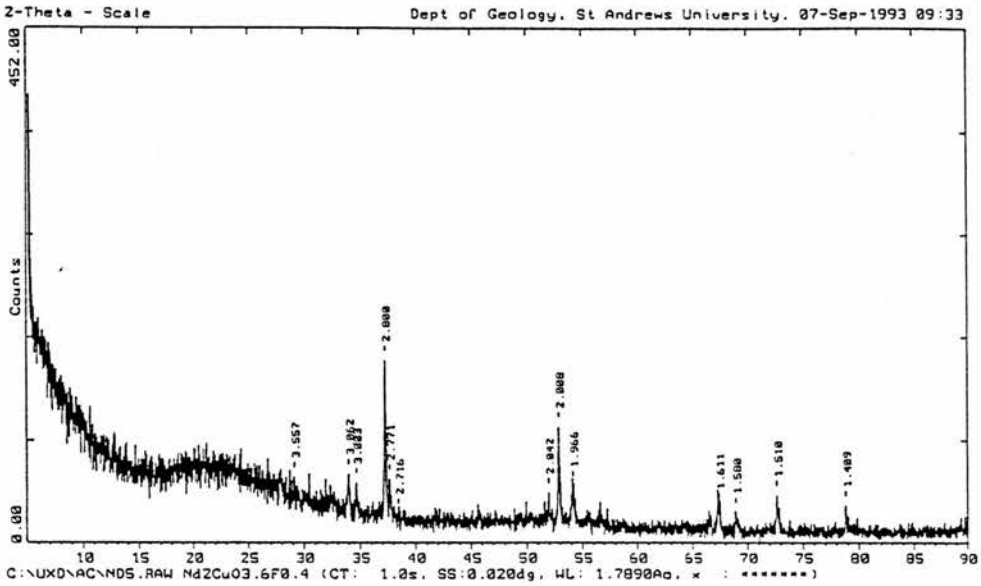

Figure E.11: Aligned sample – Cutting along the x-y plane

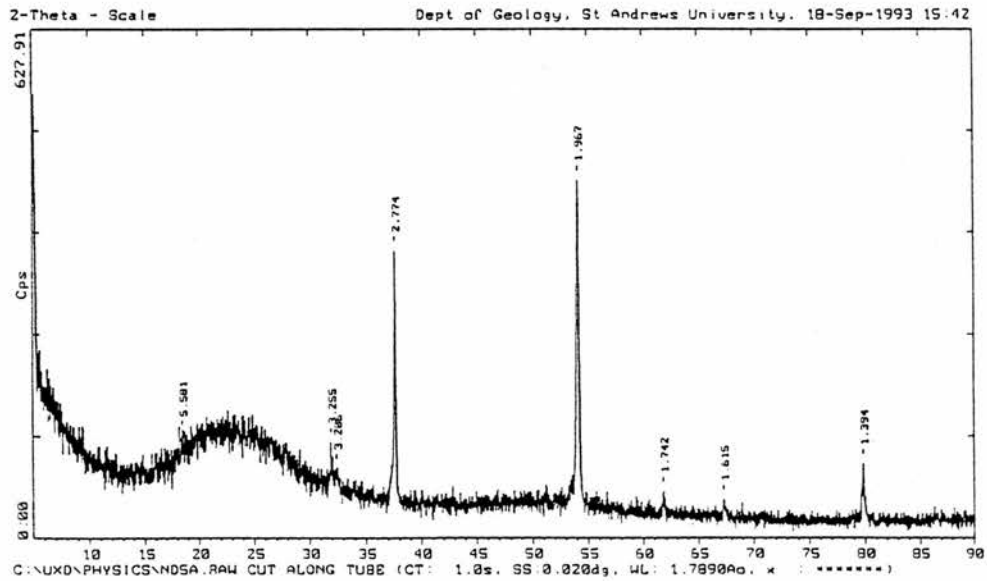

Figure E.12: Aligned sample – Cutting along the y-z plane

Appendix F

Copper–63 NMR on $Nd_2CuO_{4-x}F_x$

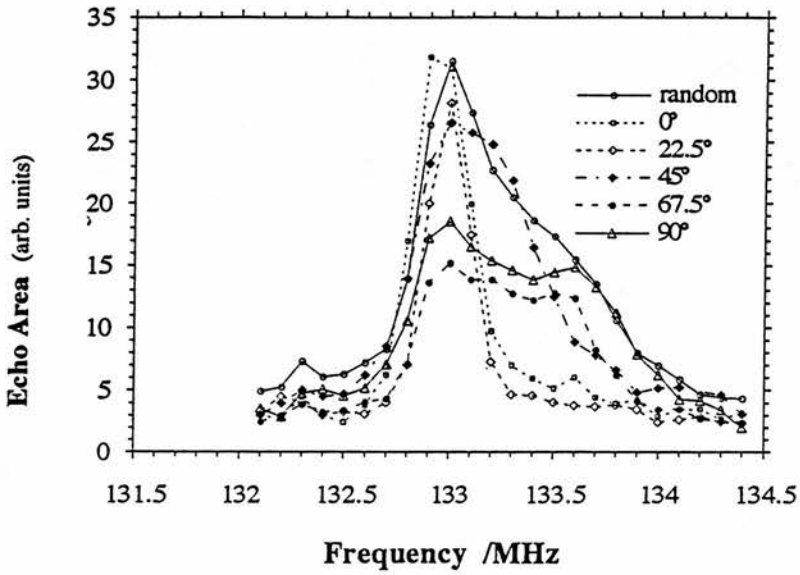

Figure F.1: $Nd_2CuO_{3.9}F_{0.1}$ – ^{63}Cu NMR

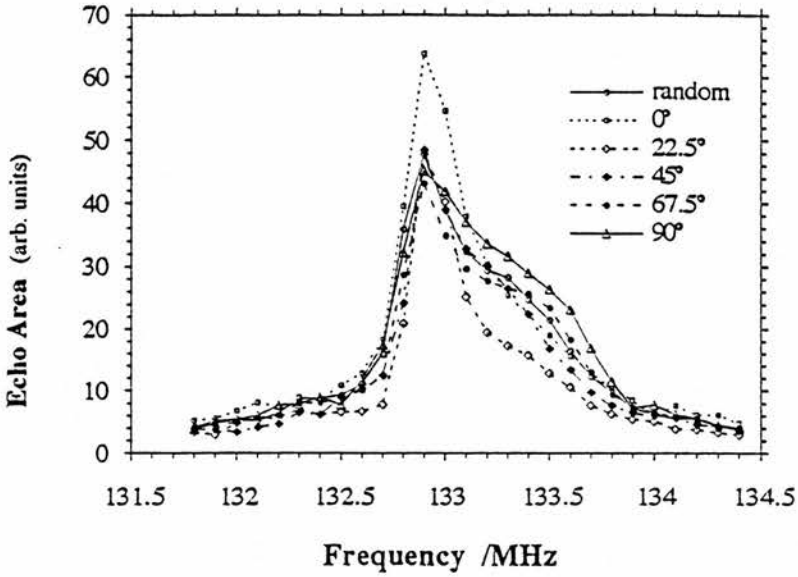

Figure F.2: $Nd_2CuO_{3.75}F_{0.25}$ – ^{63}Cu NMR

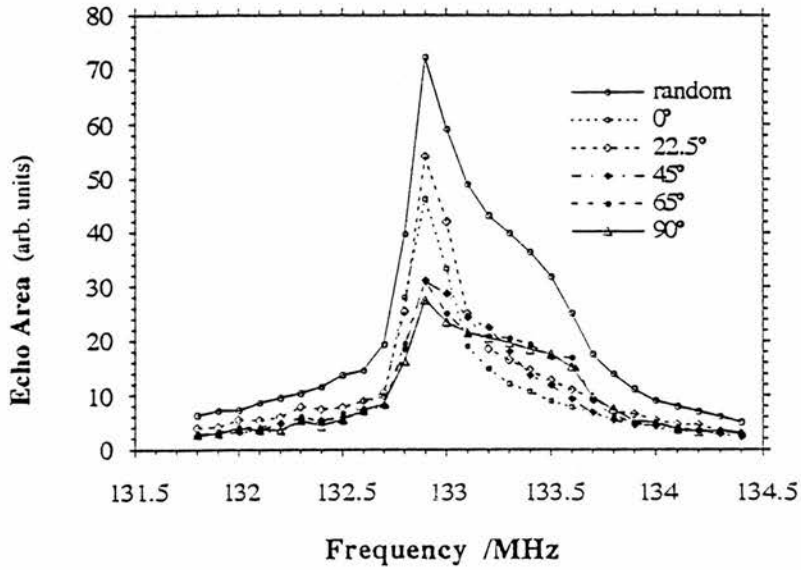

Figure F.3: $Nd_2CuO_{3.6}F_{0.4}$ – ^{63}Cu NMR

BIBLIOGRAPHY

[1] F. Bloch, W. W. Hansen & M. E. Packard, *Nuclear Induction*, *Phys. Rev.* **69** 127 (1946)

[2] E. M. Purcell, H. C. Torrey & R. V. Pound, *Resonance Absorption by Nuclear Magnetic Moments in a Solid*, *Phys. Rev.* **69** 37 (1946)

[3] C. J. Gorter & L. J. F. Broer, *Negative Result of an Attempt to observe Nuclear Magnetic Resonance in Solids*, *Physica* **9** 591 (1942)

[4] E. L. Hahn, *Spin Echos*, *Phys. Rev.* **80** 580 (1950)

[5] I. J. Lowe & R. E. Norberg, *Free-Induction Decays in Solids*, *Phys. Rev.*, **107** 46 (1957)

[6] J. W. Hennel & J. Klinowski, *Fundamentals of Nuclear Magnetic Resonance*, Longman Scientific & Technical, London, (1993)

[7] E. R. Andrew, *Nuclear Magnetic Resonance*, Cambridge University Press, (1955)

[8] F. A. Rushworth & D. P. Tunstall, *Nuclear Magnetic Resonance*, Gordon and Breach, London, (1973)

[9] C. P. Slichter, *Principles of Magnetic Resonance*, Springer-Verlag, (1990)

[10] E. R. Andrews, A. Bradbury & R. G. Eades, *Arch. Sci. Geneva* **11** 223 (1958)

[11] E. R. Andrews, A. Bradbury & R. G. Eades, *Nuclear Magnetic Resonance Spectra from a Crystal rotated at high Speed*, *Nature* **182** 1659 (1958)

[12] S.W. Amos, *Dictionary of Electronics*, Butterworth Scientific, (1981)

[13] C. Gerthsen, H. O. Kneser & H. Vogel, *Physik - Ein Lehrbuch zum Gebrauch neben Vorlesungen*, 16. Auflage, Springer-Verlag, Berlin Heidelberg, (1989)

[14] American Radio Relay League, *Radio Amateur's Handbook*, Inc., Newington, Connecticut, (1973)

[15] R. C. Weast, S. M. Selby & C. D. Hodgman, *Handbook of Chemical Physics*, 46th, The Chenmical Rubber Co., Cleveland Ohio, (1965)

[16] H. Kuchling, *Physik-Handbuch für Grundlagenfächer*, 19. Auflage, VEB Fachbuch Verlag, Leipzig, (1989)

[17] E. Fukushima & S. B. W. Roeder, *Experimental Pulse NMR - A Nuts and Bolts Approach*, Addison-Wesley (1981)

[18] H. K. Onnes, *Proc. Acad. Sci. Amst.* **11** 168 (1908)

[19] H. K. Onnes, *Leiden Comm.* **119b, 120b, 122b, 124c** (1911)

[20] H. K. Onnes, *Leiden Comm.* **139** (1914)

[21] H. K. Onnes, *Leiden Comm.* **133d** (1913)

[22] H. K. Onnes, *Leiden Comm.* **suppl. no.34** (1913)

[23] W. Meissner & R. Ochsenfeld, *Naturwissenschaften* **21** 787 (1933)

[24] J. Bardeen, L. N. Cooper & J. R. Schriefer, *Microscopic Theory of Superconductivity*, *Phys. Rev.* **106** 162 (1957)

[25] J. Bardeen, L. N. Cooper & J. R. Schriefer, *Theory of Superconductivity*, *Phys. Rev.* **108** 1175 (1957)

[26] K. A. Müller & J. G. Bednorz, *Possible High-T_c Superconductivity in the Ba-La-Cu-O System*, *Zeitschrift für Physik* **B64** 189 (1986)

[27] C. W. Chu, P. W. Hor, R. L. Meng, L. Gao, Z. J. Huang & Y. Q. Wang, *Phys. Rev. Lett.* **58** 405 (1987)

[28] M. K. Wu, J. R. Ashburn, P. H. Hor, R. L. Meng, L. Gao, Z. J. Thiang, Y. Q. Wang & C. W. Chu, *Phys. Rev. Lett.* **58** 908 (1987)

[29] Y. Tokura, H. Takagi & S. Uchida, *A superconducting copper oxide compound with electrons as the charge carriers*, *Nature*, **337** 345 (1989)

[30] A.C.W.P. James, S.M. Zahurak & D.W. Murphy, *Superconductivity at 27 K in fluorine-doped Nd_2CuO_{4-x}*, *Nature*, **338**, 240 (1989)

[31] U. Asaf, I. Felner & U. Yaron, *Combination of anion and cation doping (The $Nd_{2-x}Ce_xCuO_{4-y}F_y$)*, *Physica C*, **211** 45 (1993)

[32] Y. Endoh, M. Matsuda, K. Yamada, K. Kakurai, Y. Hidaka, G. Shirane & R. J. Birgeneau, *Two-dimensinonal spin correlations and successive magnetic phase transitions in Nd_2CuO_4*, *Phys. Rev. B*, **40** 7023 (1989)

[33] J. W. Lynn, I. W. Sumarlin, S. Skanthakumar, W. H. Li, R. N. Shelton, J. L. Peng, Z. Fisk & S. W. Cheong, *Magnetic ordering of Nd in $(Nd,Ce)_2CuO_4$*, *Phys. Rev. B*, **41** 2569 (1990)

[34] D. Petitgrand, L. Boudarène, P. Bourges & G. Galez, *Interplay of copper and neodymium magnetic moments in the magnetic structure of Nd_2CuO_4 investigated by neutron scattering*, *J. of Magnetism and Magnetic Materials*, **104-107** 583 (1992)

[35] K. Kindo, Y. Chiba, Y. Hidaka & M. Date, *Antiferromagnetic Resonance in Nd_2CuO_4*, *J. Phys. Soc. Japan*, **61** 1019 (1992)

[36] A. Krol, Y L. Soo, Z. H. Ming, S. Huang, Y. H. Kao, B. C. Smith, K. Lee, A. C. W. P. James & D. W. Murphy *Local structure around F in the fluorine-doped Nd_2CuO_4 superconductor*, *Phys. Rev. B*, **46** 443 (1992)

[37] J. Sugiyama, Y. Ojima, T. Takata, K. Sakuyama & H. Yamauchi, *Superconductivity in* $Nd_2CuO_{4-x}F_x$, *Physica C*, **173** 103 (1991)

[38] R. Kuentzler, G. Pourroy, A. Tighezza, & Y. Dossmann, *Effect of preparation method and impurities on the specific heat and magnetic susceptibility of $Nd_2CuO_{4-x}F_x$*, *Solid State Communications*, **78**, 113 (1991)

[39] A. Tighezza, J. L. Rehspringer & M. Drillon, *The Oxyfluoride $Nd_2CuO_{4-x}F_x$–Influence of synthesis routes on the superconducting properties*, *Physica C* **198** 209 (1992)

[40] G. E. Bacon, *Neutron Diffraction*, Oxford University Press, London, 1962

[41] G. Schatz & A. Weidinger, *Nukleare Festkörperphysik*, B. G. Teubner Verlag, Stuttgart, 1992

[42] C. Kittel, *Einführung in die Festkörperphysik*, R. Oldenbourg Verlag München Wien, 9. Auflage, (1991)

[43] N. W. Ashcroft & N. D. I. Mermin, *Solid state physics*, W.B. Saunders Company, int. ed., (1976)

[44] W. L. Bragg, *Proc. Cambridge Phil. Soc.* **17** 43 (1913)

[45] D. E. Farrell, *Superconducting Properties of Aligned Crystalline Grains of* $YBa_2Cu_3O_{7-\delta}$, *Phys. Rev. B*, **36** 4025 (1987)

[46] W. J. Webster, *A Study of the High Temperature Superconductor,* $YBa_2Cu_3O_{7-\delta}$ *& Its Cobalt-Doped Derivative, PhD Thesis*, University of St. Andrews, Scotland, (1993)

[47] J. D. Livingston, H. R. Hart & W. P. Wolf, *Paramagnetic anisotropy in high-*T_c *superconductors*, *J. Appl. Phys.* **64** 5806 (1988)

[48] Y. Kohori, T. Sugata, H. Takenaka, T. Kohara, Y. Yamada, J. T. Markert & B. Maple, *Cu NMR Study of Th-Doped* Nd_2Cu0_{4-y} *and* Pr_2Cu0_{4-y}, *J. Phy. Soc. Japan* **58** 3493 (1989)

[49] J. M. Ferreira, M. B. Maple, H. Zhou, R. R. Hake, B. W. Lee, C. L. Seaman, M. V. Kuric & R. P. Guertin, *Magnetic Field Alignment of High-*T_c *Superconductors* $RBa_2Cu_3O_{7-delta}$ *(R=Rare Earth)*, *Appl. Phys. A*, **47** 105 (1988)

[50] G. Balakrishanan, S. K. Malik, C. K. Subramaniam, D. McK. Paul, S. Pinol & R. Vijayaraghavan, *J. of Magnetism and Magnetic Mat.*, **104-107** 469 (1992)

[51] G. Zheng, Y. Kitaoka, Y. Oda & K. Asayama, *NMR Observation in* $Nd_{1.85}Ce_{0.15}CuO_4$, *J. Soc. Japan*, **58** 1910 (1989)

[52] M. Abe, K. Kumagai, S. Awaji & T. Fujita, *Cu-NMR Studies of* $Nd_{2-x}Ce_xCuO_{4-y}$ *Physica C*, **160** 8 (1989)

[53] S. Kambe, H. Yasuoka, H. Takagi, S. Uchida & Y. Tokura, ^{63,64}*Cu–NMR Study of Oxidized and Reduced* $Nd_{2-x}Ce_xCuO_4$, *J. Phys. Soc. Japan*, **60** 400 (1991)

[54] G. C. Carter, L. H. Bennet & D. J. Kahan, *Metallic Shifts in NMR*, Part I, Pergamon Press, 1977

[55] W. H. Jones, T. P. Graham & R. G. Barnes, *Nuclear Magnetic Resonance Line Shapes Resulting from the Combined Effects of Nuclear Quadrupole and Anisotropic Shift Interactions* , *Phys. Rev.*, **32**, 1898 (1963)

[56] J. Yu, A. J. Freeman, R. Podloucky, P. Herzig & P. Weinberger, *Origin of electric-field gradients in high-temperature superconductors:* $YBa_2Cu_3O_7$, *Phys. Rev. B*, **43** 532 (1990)

[57] K. Schwarz, C. Ambrosch-Daxel & Blaha, *Charge distribution and electric-field gradients in* $YBa_2Cu_3O_{7-x}$, *Phys. Rev. B*, **42** 2051 (1990)

[58] G. P. Dai, B. Ctortecka, D. P. Tunstall, M. Jones, I. Gameson & P. P. Edwards, *Copper NMR Studies of the* $Nd_2CuO_{4-x}F_x$ *System*, *Solid State Communications*, submitted

[59] E. F. Kukovitzkii, R. G. Mustafin & G. B. Teitelbaum, *The Fluorine NMR in Electron Doped* $Pr_2CuO_{4-x}F_x$, *Appl. Magn. Reson.*, **3**, 677 (1992)